

Inductive

Heating and Temperature Measuring System for Small Metal Objects

in the Context of RepRap

Master Thesis

published by: Krallinger Sebastian
matriculation number: 780 421
first reviewer: Prof. Dr.-Ing. Alfred Rozek
second reviewer: Prof. Dr. Sven-Hendrik Voß

Berlin, 2012

Abstract

This thesis describes the development of hardware and software for the implementation of inductive heating in a RepRap extruder, as well as the implicit temperature measuring by detecting temperature-dependent changes of physical quantities of the heated object. Different mechanical setup and hardware options are shown, and the result is verified by means of several simulations. Within a test setup including various measurements, the system is proven to be working.

Contents

Nomenclature	IV
1 Introduction	1
1.1 About the thesis and the authors	1
1.2 The Problem	1
1.3 Objective and hypothesis	2
1.3.1 Example use	2
1.4 Advantages	3
1.5 Patent research	3
2 Foundations	5
2.1 Skin effect	5
2.2 Inductive heating	6
2.2.1 Frequency	7
2.2.2 Core material	7
2.2.3 Wire coil	8
2.3 Inductive temperature sensing	9
2.4 RepRap	9
2.4.1 Extruder	10
2.4.1.1 Nozzle	11
2.4.1.2 Outlet	13
2.4.1.3 Heating zone	14
2.5 ADC oversampling	14
2.6 Direct digital synthesis	16
2.7 Impedance matching	17
3 Mechanics	20
4 Hardware	24
4.1 Power Supply	25

INDUCTIVE HEATING AND TEMPERATURE MEASURING SYSTEM

Contents

4.2	Resonator circuit	25
4.2.1	Load model	26
4.2.2	Parallel resonator circuit	28
4.2.2.1	Conclusion	34
4.2.3	Series resonator circuit	34
4.2.3.1	Conclusion	38
4.2.4	Comparison	40
4.3	Capacitor	41
4.4	Inverter	43
4.4.1	Half bridge	43
4.4.2	Full bridge	44
4.4.3	Comparison	47
4.4.4	Control circuit	47
4.5	Phase measurement	48
4.6	Tank voltage measurement	50
4.7	Setup	52
4.7.1	BM02-Modul	54
4.8	Cooling	55
4.9	EMC	56
5	Software	62
5.1	global	62
5.2	AD9833	62
5.3	adc	64
5.4	FrequencyMeasurement_raw	65
5.5	FrequencyOutput_raw	65
5.6	thermistor	67
5.7	uart	67
5.8	controller	68
5.9	main	70
6	Test and measurement	71
6.1	General circuitry measurements	71
6.2	Test runs	77
6.2.1	First test run	77
6.2.1.1	Extrusion test	80
6.2.2	Second test run	80
6.2.2.1	Extrusion test	83

INDUCTIVE HEATING AND TEMPERATURE MEASURING SYSTEM

Contents

6.2.3	Third test run	83
7	End	90
7.1	Conclusions and prospects	90
7.2	Used tools	91
7.3	Acknowledgments	92
	Bibliography	93
A	Appendix	i
A.1	Setup	i

Nomenclature

Nomenclature

ω	Radial frequency
\underline{s}	$= j \cdot \omega = j \cdot 2 \cdot \pi \cdot f$
$\underline{U}, \underline{I}, \underline{P}, \dots$	Complex value of the signal with magnitude and phase / imaginary and real part.
$\underline{x}, \underline{y}, \underline{z}$	Complex variables
\underline{Z}	Impedance
f_0, ω_0	Resonance-frequency, -radial frequency
$Im(\underline{x})$	Imaginary part of \underline{x}
$Re(\underline{x})$	Real part of \underline{x}
ABS	Acrylonitrile Butadiene Styrene
AC	Alternating current
ADC	Analog Digital Converter
CMOS	Complementary Metal Oxide Semiconductor
CPU	Central Processing Unit
DAC	Digital Analog Converter
DDS	Direct Digital Synthesis
EMC	Electromagnetic Compatibility
EMF	Electromotive force
ESR	Equivalent Series Resistance
f	Frequency
FFF	Fused Filament Fabrication
GND	Ground
I/O	Input/Output
IC	Integrated Circuit
IGBT	Insulated Gate Bipolar Transistor
ISP	In-system Programming
j	Imaginary unit ($j^2 = -1$)

INDUCTIVE HEATING AND TEMPERATURE MEASURING SYSTEM

Nomenclature

JTAG	Joint Test Action Group
K	Kelvin
LSB	Least Significant Bit
MOSFET	Metal Oxide Semiconductor Field Effect Transistor
MSB	Most Significant Bit
NTC	Negative Temperature Coefficient Thermistor
PC	Personal Computer
PCB	Printed Circuit Board
PEEK	Polyether ether ketone
PLA	Polylactic Acid
ppm	parts per million
PWM	Pulse Width Modulation
RepRap	Replicating Rapid Prototyper
RMS	Root Mean Square
ROM	Read-Only Memory
SMD	Surface-mounted Device
SPI	Serial Peripheral Interface
TTL	Transistor Transistor Logic
U, I, P,	RMS value of the signal
u, i, p,	Time-dependent values of the signal
UART	Universal Asynchronous Receiver Transmitter
USART	Universal Synchronous/Asynchronous Receiver Transmitter
XOR	eXclusive OR

1 Introduction

1 Introduction

1.1 About the thesis and the authors

This thesis is based on an idea by Jacob Bayless and has been created in cooperation with him. Jacob Bayless recently graduated as a bachelor in engineering physics at the University of British Columbia [30] in Vancouver, Canada. He was a member of the team that developed the SpoolHead [10] (and project wiki [11]) for the RepRap printer.

I, Sebastian Krallinger, made my bachelor's degree in electrical and information engineering at the Deggendorf University of Applied Sciences [14]. Currently, I am taking a master's degree in embedded systems at the Beuth University of Applied Sciences [13] in Berlin. This work is a collaborative project. As far as this is possible, the individual contributions will be marked by the authors in order to facilitate an individual grading.

(March 2012)

1.2 The Problem

In the following the term “small objects” is used, which should be considered as an object with the volume of less than one cubic centimeter. This is not a constant and it depends on a variety of factors such as type of metal, its shape, density and others. Accordingly, this definition is only an approximate value. It also should be possible to apply this to bigger objects, but this is not the objective of this thesis (cf. section “Example use” 1.3.1). This can be worked out after the process is proven to be working.

If a small metal object is put in an alternating magnetic field, it will be heated inductively. If the temperature of this object is supposed to be controlled, it will be necessary to measure the actual temperature of this object.

There are two important factors to consider. First, the temperature change will occur relatively fast because the object is relatively small. Second, if the object is also a good heat conductor (which most metals are), it can be assumed that the object has a homogeneous temperature. This means that the temperature measured on the surface is almost the

1 *Introduction*

same as inside the object.

There are different methods to measure temperature. Among them are infrared temperature measurement and resistance temperature detection. There are different disadvantages and problems associated with each of these measurement methods, given that the target temperature can exceed 240 °C. These are e.g.:

- Not all contact sensor can tolerate such high temperatures.
- Non-contact sensors usually need free line of sight with the object.
- A contact sensor needs contact to the object and in most cases wires for the transfer of information.
- The sensors can be influenced by the changing magnetic and electrical field of the inductive heating process.
- Most of them are relatively slow, because heat has to flow from the object into the sensor.

Generally speaking, it would be preferable to directly measure the temperature of the object without any additional sensors. The main topic of this thesis will be how that can be achieved. The approach how to do this will be discussed in section 2.3.

1.3 Objective and hypothesis

The objective of this work is to find a way to measure the temperature of an inductively heated small metal object. The measurement is to be carried out as accurate and as fast as needed to control the temperature of this object. This can be achieved by creating a test setup and taking different measurements. If the system works, it can be applied to a RepRap Extruder, as described below.

1.3.1 Example use

As an example use and as a prototype application for this thesis, the idea will be implemented in a RepRap Extruder (cf. section “RepRap” 2.4) to melt the plastic filament. The idea is to use a glass tube with a spool wrapped around it and metal tube inside (cf. figure 1.1). If the metal tube is heated, the temperature can be measured and controlled. There is a wide range of other applications to use this method, for example in chemical processing it could be used to run a fast temperature curve.

1 *Introduction*

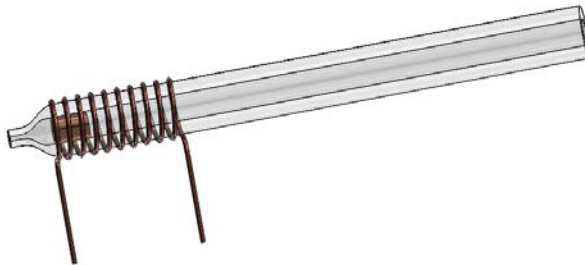


Figure 1.1: Nozzle structure (by Bayless).

1.4 Advantages

The advantages of this approach are:

- The high thermal gradient that is made possible by the inductive heating and the low mass of the object.
- Less heating of the surrounding environment via direct heating.
- The very fast direct temperature measurement.
- Better temperature control via this fast temperature measurement.
- Simpler design of the RepRap extruder nozzle, since it can be entirely enclosed and there are no wired sensors or heaters needed at the heated object.

1.5 Patent research

A background search revealed a patent by Matsumoto [23] for heating catalytic converters (which are much bigger objects than the ones described in this thesis) and temperature measurement. According to the United States Patent and Trademark Office [6], the patent is still valid in the United States. According to “Deutsches Patent- und Markenamt” [4], the German patent has expired in 2011 due to not paid license fees.

In his patent, Matsumoto states that with a change in temperature the relative permeability (μ_r) of the heated object changes. As a result, the inductance of the primary coil and by that the resonance frequency changes. The method discussed in this thesis states that a change in temperature changes the resistivity of the core material and by that the penetration depth of the core. This affects the inductance of the primary coil and the resonance frequency of the resonator circuit. It is necessary to check whether or not the approach of the setup discussed here is in fact innovative, since the penetration depth is also influenced by the permeability of the object, as shown in section 2.1. From a more

INDUCTIVE HEATING AND TEMPERATURE MEASURING SYSTEM

1 Introduction

general viewpoint, the patent only describes temperature control by means of a change in the resonance frequency. This is also the approach employed in this thesis, and it would call for a later adjustment of the used temperature measurement method, e.g. the bridge circuit Bayless describes in [12]. However, his method has the downside of a much more complex setup and since the patent has expired in Germany, this fact isn't discussed any further.

(Compare [12] by Bayless)

2 Foundations

2 Foundations

2.1 Skin effect

According to [18, p. 265, equ. 12.53], the penetration depth (δ_S) of a current can be approximated using equation 2.1. After reshaping this equation to 2.2 and with the material constants from table 2.1, δ_S can be approximated for different materials. Since the material constants also depend on the temperature and the material composition (especially μ_r for iron depends very much on the composition), this gives only a rough approximation. But since these values are only needed to estimate the necessary material dimensions, the approximation is accurate enough.

Using this information, the figure 2.1 can be plotted, visualizing the penetration depths of copper and iron against the frequency. Furthermore, it shows that the δ_S for iron is at least one decimal power lower than for copper, mainly due to the bigger μ_r of iron.

$$\delta_S = \sqrt{\frac{2}{\omega \cdot \mu \cdot \kappa}} \quad (2.1)$$

$$\delta_S = \sqrt{\frac{2 \cdot \rho}{2 \cdot \pi \cdot f \cdot \mu_r \cdot \mu_0}} \quad (2.2)$$

- δ_S : Penetration depth. In the case of a circular conductor, this represents the depth from the surface of the conductor at which the current density has declined by e^{-1} [m].
- ω : Radial frequency [rad/s]
- κ : Conductivity (the more common symbol is σ) [S/m]
- ρ : Resistivity [$\Omega \cdot \text{m}$]
- μ : Permeability [H/m]
- μ_0 : Magnetic field constant $4 \cdot \pi \cdot 10^{-7}$ (see [25, p. 1-1]) [N/A^2]
- μ_r : Relative permeability [H/m]

2 Foundations

	μ_r []	$\rho @ 100 \text{ } ^\circ\text{C}$ $[\Omega \cdot \text{mm}^2/\text{m} (= 10^{-6} \Omega \cdot \text{m})]$
Copper (pure)	1	$2.5 \cdot 10^{-2}$
Iron	6000	$2 \cdot 10^{-1}$

Table 2.1: Approximate values, μ_r see:[19, p. 545f., Tab. 9.2], ρ see:[25, p. 12-39].

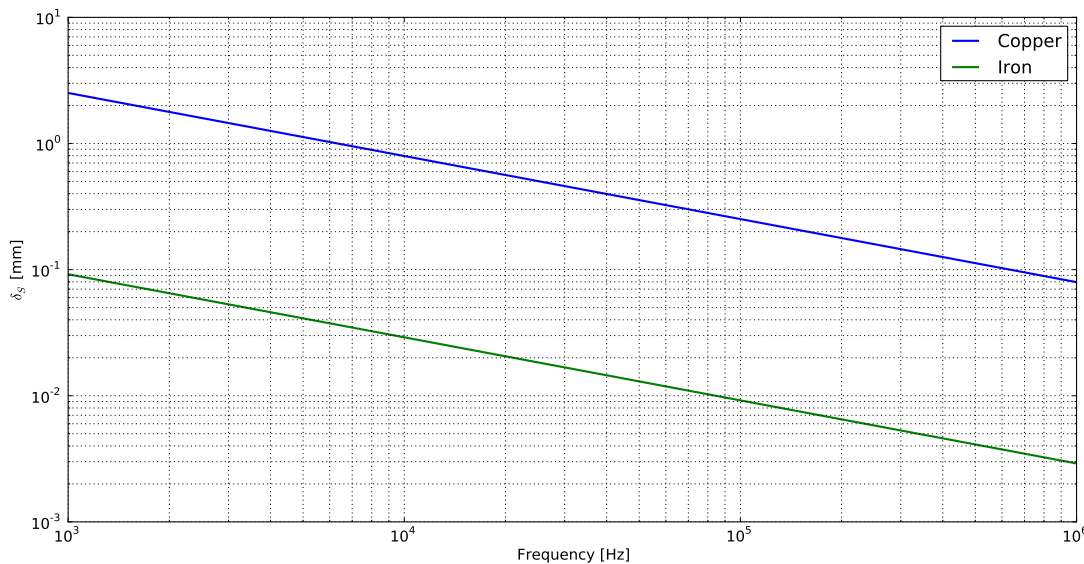


Figure 2.1: Penetration depth of copper and iron at about 100 °C plotted against the frequency.

2.2 Inductive heating

Inductive heating occurs, if an electrically conducting object (most often a metal) is put into an alternating magnetic field, thereby generating eddy currents within the object. This leads to resistive heating caused by the electrical resistance of the object. Depending on the material, heat is also generated by magnetic hysteresis losses.

More precisely, this means: If there is an alternating magnetic field (created e.g. by a wire coil that is switched on and off continuously or by a moving magnet), then this causes an electric field, as stated in Faraday's law. The important thing here is that the magnetic field must change in order to create an electric field. A constant magnetic field does not cause an electric field. If an electrically conducting object is inserted into this electric field, Faraday's law also states that this field causes an electromotive force (EMF) within the object and by that it creates the so-called eddy currents.

Eddy currents are circular currents within an object. In general, this current generates heat owing to the electrical resistance of the object.

In transformers, for instance, this fact will lead to power loss. This is also the reason why

2 Foundations

most transformers have laminated cores that reduce eddy currents and their heating effect. One standard setup for inductive heating is a wire coil wrapped around an electrically conducting material, with an alternating current flowing through that wire. There are some conditions to consider, as discussed in the following sections.

2.2.1 Frequency

The operation frequency is mainly determined by the desired penetration depth of the conductive core. As previously discussed in section “Skin effect” 2.1, the current flow is the more limited to the surface of the object, the higher the frequency rises. This means: If the used frequency is high enough and the penetration depth (δ_S) thereby becomes larger than the object radius/thickness, only the object’s surface will be heated. Vice versa, a low operation frequency will provoke a deep penetration into the object, and by that a more even heat build-up.

If the operation frequency lies in the audible frequency range (which ends at about 20 kHz), the setup will emit audible noise due to small movements of e.g. the core in the coil. Therefore, a frequency above this value should be chosen.

Another factor for the frequency selection would be the losses within the object. Since the permeability of most materials depends at least to some extent on the frequency, the losses within the object are altering as the frequency changes.

2.2.2 Core material

Since a part of the inductive heating occurs due to magnetic hysteresis losses, the permeability highly influences the losses due to the heating of the material and by that the effectiveness of inductive heating. In inductive heating processes, high losses within the object are required to build up heat. Due to this fact, materials with a high relative permeability (μ_r) are preferable, so-called ferromagnetic materials with $\mu_r \gg 1$. The permeability of these materials also depends on the temperature, especially if the temperature exceeds the so-called Curie point. In that case, the permeability drops to almost zero. The Curie point differs for varying materials.

The core material also influences the inductance of the coil, as shown below in section 2.2.3.

2 Foundations

2.2.3 Wire coil

As [27, p. 368, equ. 23.12] states, the inductance of a coil can be estimated using equation 2.3 (if $r \ll l$ is true). This shows that the inductance, apart from mechanical properties such as length and enclosed area, depends very much on the number of loops (N) and also on the permeability of the material surrounding the coil.

If no shield is used around the coil and if the core, an thin metal tube, is the only electroconductive material in the field of the coil with a high permeability, then the field mainly permeates material with a $\mu_r \approx 1$ (air). The relatively small core with a high permeability influences the inductance only to a very little extent. For the estimation of the inductance, this means that μ_r can be approximated to 1.

Since the radius and length of the coil is in most cases given by the mechanical outlines, the only variable parameter affecting the inductance is the number of loops (N). N is also limited to a certain range especially for the purpose of this thesis. The number of loops, for instance, is simply limited by the physical outlines.

Another factor regarding the wire coil is the skin effect (cf. section 2.1) which reduces the conductivity of the wire at higher frequencies. To counteract this, the wire can be divided into multiple thinner ones which are insulated from each other. Since different loops need to be insulated from each other, the coil is made out of enameled copper wire in most cases.

$$L = N^2 \frac{\mu \cdot A}{l} \quad (2.3)$$

$$L = N^2 \frac{\mu_r \cdot \mu_0 \cdot r^2 \cdot \pi}{l}$$

- N: Coil loops []
- A: Enclosed area [m^2]
- l: Length of the coil [m]
- r: Radius of one loop [m]
- μ : Permeability [H/m]
- μ_0 : Magnetic field constant $4 \cdot \pi \cdot 10^{-7}$ (see [25, p. 1-1]) [H/m]
- μ_r : Relative permeability [H/m]

2 Foundations

2.3 Inductive temperature sensing

As described in section 2.2, a change in the magnetic field causes a current in the electrically conducting object which is placed in this field. There are three facts to consider.

First, this current depends on the specific electrical resistance of the electrically conducting object. This resistance depends on the temperature of the object.

Second, Lenz's law states that the magnetic field generated by the induced current opposes the magnetic field that induced that current. In other words: A change in the magnetic field A creates an EMF which then creates a current in electrically conducting objects inside this field. This current causes its own magnetic field B which opposes the original field A.

Third, the behavior of an AC current in a conductor forms a current density distribution that decreases exponentially with an increasing distance from the surface of the object. This is called "skin effect" (cf. section 2.1) and depends on the frequency of the current as well as on the conductivity and the permeability of the material.

Taking advantage of those effects, it should be possible to measure the temperature of an object. For example: If the resistance of the metal is low and the magnetic field is switched off, the flowing current in the metal object becomes high. Vice versa, if the resistance is high, the current becomes small for the same change of the magnetic field. The stored energy in the magnetic field of a current is also known as the inductance L. This means that the temperature can be measured by measuring the inductance. To achieve this, it is possible to set up a resonating circuit and measure the change of the resonance frequency that is caused by the change of the inductance.

2.4 RepRap

The RepRap project was started by Adrian Bowyer in 2005. The objective was to develop an open source / open design 3D-Printer. As the name RepRap (replicating rapid prototyper) implies, these printers were supposed to be able to produce as many parts as possible out of their own components. Currently, there are many different printer variations. One of the most commonly used (September 2012) is called Mendel Prusa. It is shown in figure 2.2(a). Figure 2.2(b) shows the Hugo printer.

These printers work with the so-called "Fused Filament Fabrication" (FFF). In this layout, an extruder (cf. section 2.4.1) pulls in plastic filament (very common is ABS or PLA with a diameter of 3 mm), melts it and extrudes it as much finer filament. Subsequently, these are put side by side to build up a layer. This process is repeated for several layers. As a

2 Foundations

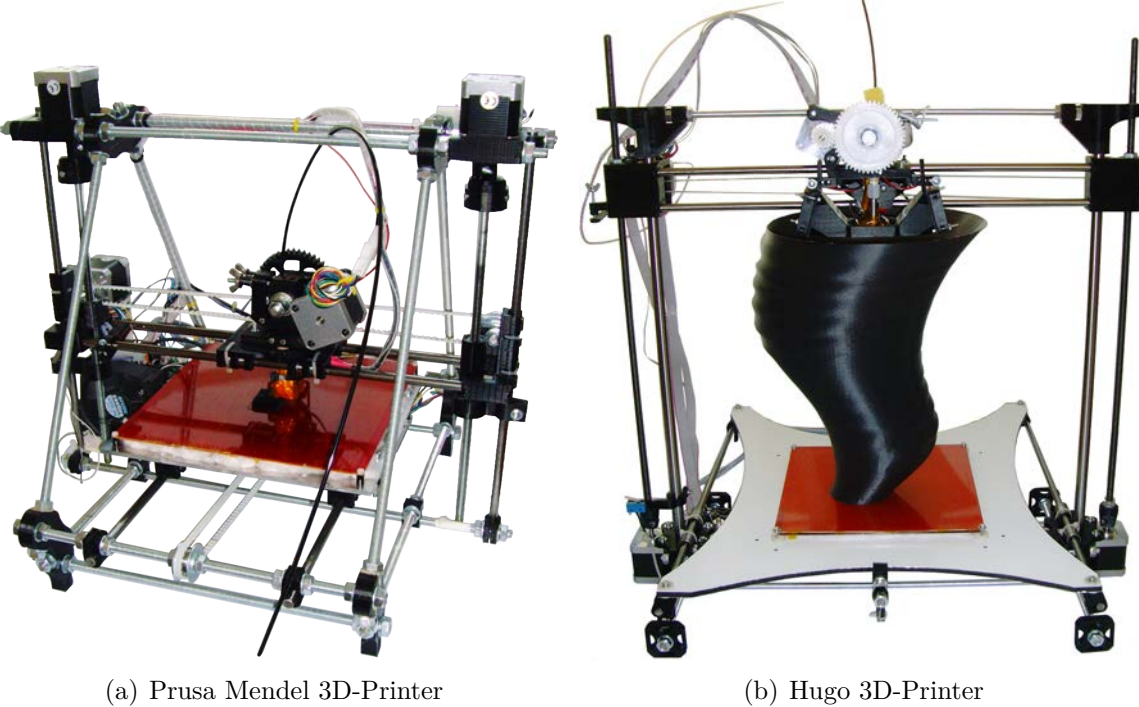


Figure 2.2: RepRap 3D-Printers.

result, a 3D object arises. Some example objects are shown in figures 2.3 and 2.4.
(Compare [15, p. 43] and [28])

2.4.1 Extruder

One of the currently most commonly used extruder types is the Wade's Geared Extruder, which is shown in figure 2.5. It is driven by a stepper motor which turns a screw with knurling attached to a gear transmission (the gears can also be produced with a RepRap printer), as shown in figure 2.5(a). As figure 2.5(b) depicts, the filament is then put through a hole in the center. If the extruder is closed, it is pressed against the knurling of the screw. As soon as this screw starts to rotate, the filament is driven upwards or downwards and by that into or out of the nozzle. An example for a commonly used nozzle (further discussed in section 2.4.1.1) is shown in figure 2.5(c). It also shows a common way to connect the nozzle to the extruder. The connection is a groove in the cylinder which fits into the extruder. The extruder has two holes at the same height as the groove in the cylinder and also orthogonally to the cylinder. By putting screws into the holes, the nozzle is held in place.

In most cases, the assembled extruder is mounted to a movable carriage with two degrees

2 Foundations



Figure 2.3: Printed model of a chair.

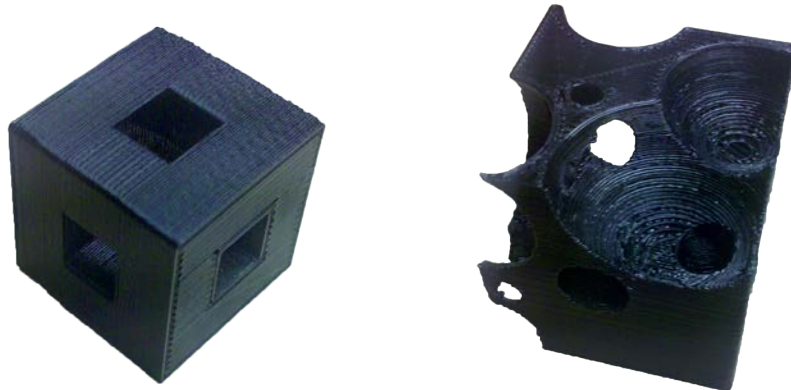


Figure 2.4: Examples of printed objects.

of freedom, which positions the nozzle relative to the print bed which has one degree of freedom.

2.4.1.1 Nozzle

The nozzle shown in figure 2.6 is distributed by Reprap-Fab [32]. It was designed and built by Wolfgang Vogel, the owner of that shop. The most current model consists mainly of five different parts:

1. The nozzle outlet is made out of brass and can be screwed to the middle part (3). In the default setup, the set comes with 0.5 mm and 0.35 mm nozzle outlets. These can be changed without disassembling the extruder (further discussion in section 2.4.1.2).

INDUCTIVE HEATING AND TEMPERATURE MEASURING SYSTEM

2 Foundations

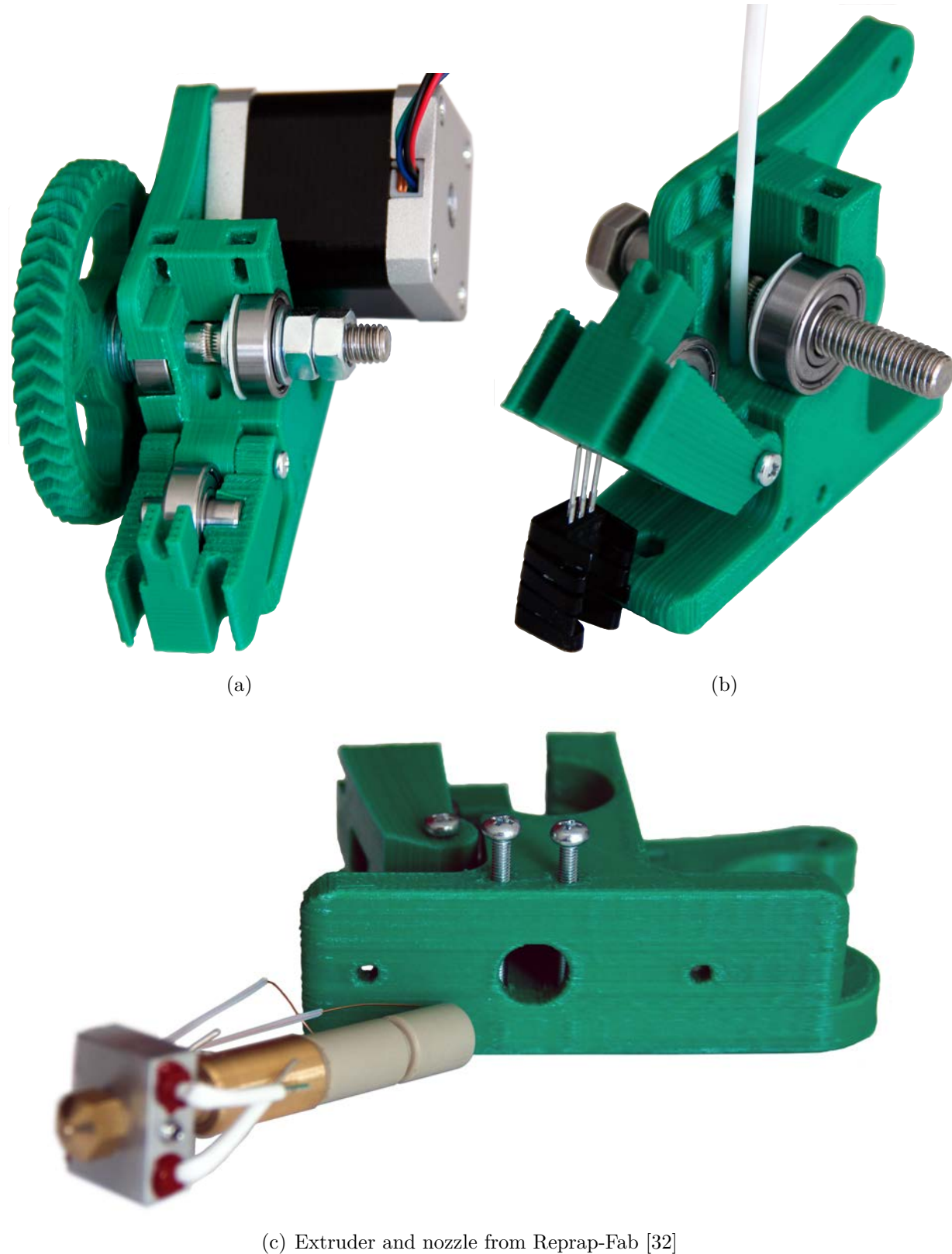


Figure 2.5: Wade's Geared Extruder, partially assembled.

2 Foundations

2. The aluminum heating block contains two heating resistors which are controlled via PWM by the electronics, as well as an thermistor to measure the temperature. Both are inserted into holes within the block and fixed with heat resistant silicone. The block is fixated on the middle part and held by a setscrew.
3. The middle part is also made out of brass. It is a cylinder with a center hole corresponding to the desired filament diameter and the necessary threads to connect it to the other components. It also transfers the heat towards the filament.
4. A Teflon tube which reaches almost through the entire polyetheretherketone (PEEK) (part nr. 5) and is held by the screw connection. It is used to reduce the friction of the filament.
5. PEEK connector part, which provides the connection to the extruder. It is made out of temperature resistant PEEK since the middle part can reach temperatures up to 250 °C. It is necessary to shield this high temperature from the extruder which is made out of plastic, in most cases ABS, to prevent deformation or, in the worst case, destruction.

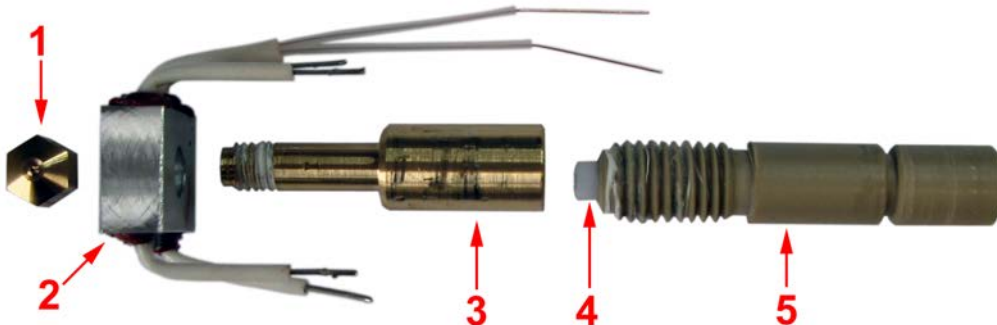


Figure 2.6: Nozzle by Reprap-Fab [32].

2.4.1.2 Outlet

The diameter of the outlet hole has a great influence on the print quality, the stability of the printed object and the print time. A wider nozzle outlet is associated with a lower/rougher print quality due to the wider threads, a faster print time because of the higher volume throughput and, in most cases, also a higher stability, since the wider threads also have a larger contact surface with the ones next to them.

Another design criterion is the length of the outlet hole, particularly because as the printing speed increases, the thread swell at the outlet (see figure 2.7) also increases. According to [24], this effect occurs mainly due to the elastic properties of most melted plastics. The

2 Foundations

main reason for this peculiar effect is the time that the plastic needs to “adjust” to the new diameter of the outlet hole. In order to reduce this effect, either the extrusion speed can be reduced or the length of the small hole can be increased. But the length of the hole is limited since it involves a higher pressure drop.

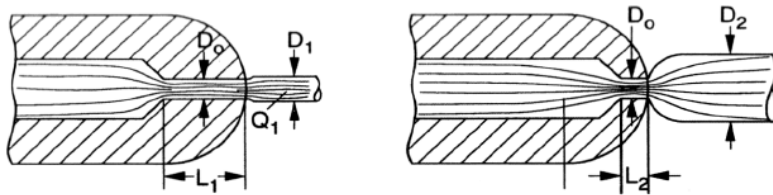


Figure 2.7: Thread swell (source [24, p. 109, fig. 5.23]).

2.4.1.3 Heating zone

The length of the heating zone and the diameter of the filament are the main limitations for the extrusion speed and by that in most cases for the overall printing speed.

The filament enters the nozzle at room temperature and has to be heated to above the corresponding melting point of the material. If the material enters the nozzle with an constant speed, the temperature distribution at the end of the heating zone is almost even across the filament diameter. If the heating zone is too short, the filament does not have enough time to be heated properly and the core of the material is still below the melting point when it hits the reduction point of the outlet nozzle. This would lead to a pressure drop or, in the worst case, the extruder gets stuck because the knurling of the drive screw cuts into the filament.

This means: For high printing speeds a long heating zone and a thin filament such as the also available 1.75 mm filament (which in most cases is more expensive than the 3 mm one) are preferable.

2.5 ADC oversampling

If the accuracy of the available analog digital converter (ADC) is not high enough, it is in some cases possible to increase its accuracy by using a technique called oversampling. Oversampling can only be used properly if certain requirements are met:

- It is necessary that the signal which should be measured is noisy, with a magnitude that at least influences the measured digital value in the least significant bit (LSB).

2 Foundations

The noise also has to be Gauss-distributed and uncorrelated, which applies to most naturally occurring noise.

- If oversampling is used, the sampling rate is reduced. As the Nyquist theorem states, it is necessary to at least sample the signal with twice the frequency than the highest frequency (f_H) occurring in the signal, to avoid e.g. anti-aliasing. According to the application note [29] it is necessary to increase the sampling frequency by the factor 4^x in order to increase the accuracy of the ADC by x bit. As a result, the sampling frequency is $4^x \cdot 2 \cdot f_H$

Figure 2.8 shows an example in which oversampling is used to increase the ADC accuracy by 1 bit. For each measurement four samples are taken and the average is calculated. If the signal is noisy then in most cases this returns a decimal value, but since the ADC values are real, a simple division by four would cut off these digits.

Listing 2.1 shows an example implementation for a C function using fix point numbers. The signal value is measured four times and added up. For a simple average calculation it would be required to simply divide the result by 4 (which would correspond to a right shift of 2 bits). Instead, the sum is only divided by 2 (which corresponds to a right shift of 1 bit) and by that the decimal places are taken into account.

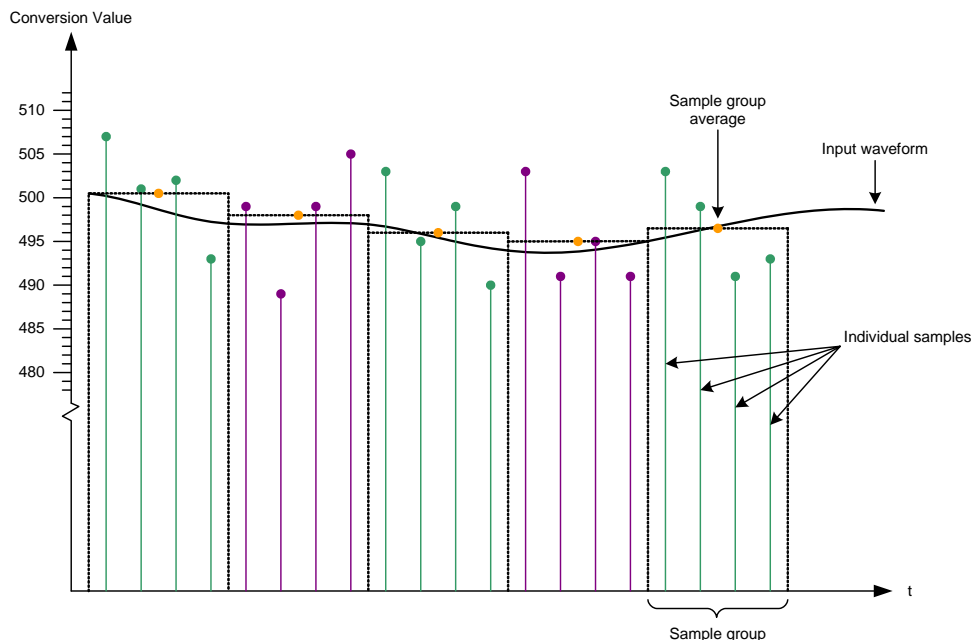


Figure 2.8: Oversampling conversion example to increase accuracy by 1 bit (source [29, p. 5, fig. 1]).

2 Foundations

```

1 for (i = 0; i < 4; i++) {
2     ADCsum += ADC_Read();
3 }
4 return ADCsum >> 1;
    
```

Listing 2.1: Oversampling C example.

2.6 Direct digital synthesis

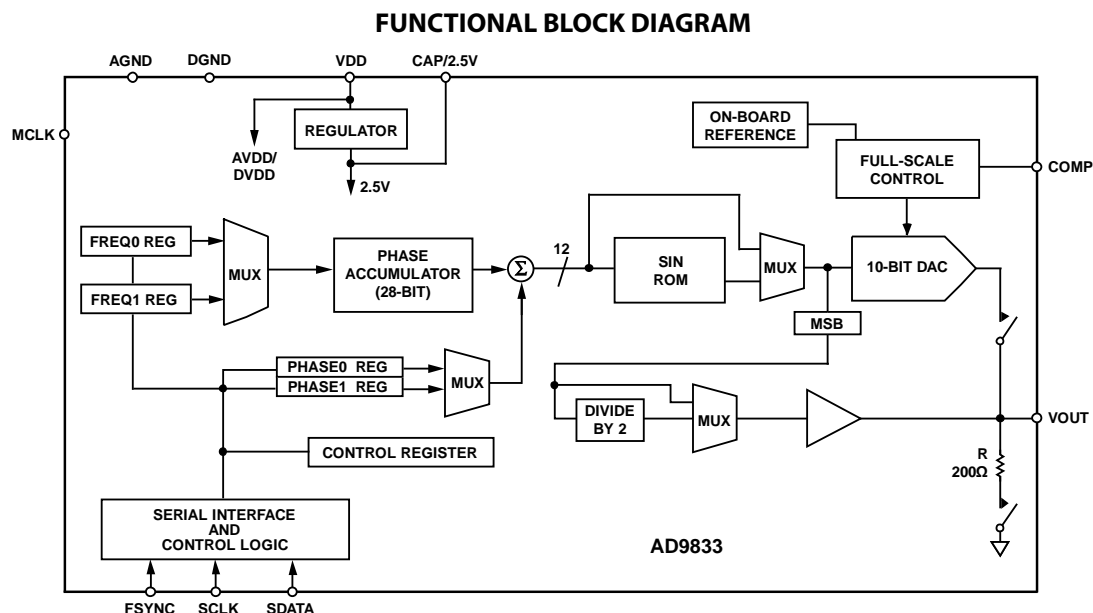


Figure 2.9: Function block diagram AD9833 ([7, p. 1, fig. 1]).

Direct Digital Synthesis (DDS) is a process to create periodic signals with a high frequency resolution. In the following, this process is described, based on the AD9833 IC produced by Analog Devices, which is also used for the test setup.

As the function block diagram 2.9 shows, the device is controlled by a serial interface. Using this, it is possible to set the frequency, phase and shape (e.g. sine, triangle, square) of the output as well as some additional settings. By setting the frequency register and selecting the desired one via the multiplexer, it is possible to change the frequency.

The output is generated by continuously increasing the phase in the phase accumulator, as seen in the lower part of figure 2.10. This is done by adding the value of the frequency register to the actual counter value at every clock cycle. If the counter overflows, this represents $2 \cdot \pi$ and simply restarts the counter at zero. By increasing the value that is added (frequency register), the counter increases faster, causing the output frequency to increase. For the simple square wave output, the most significant bit (MSB) is connected

2 Foundations

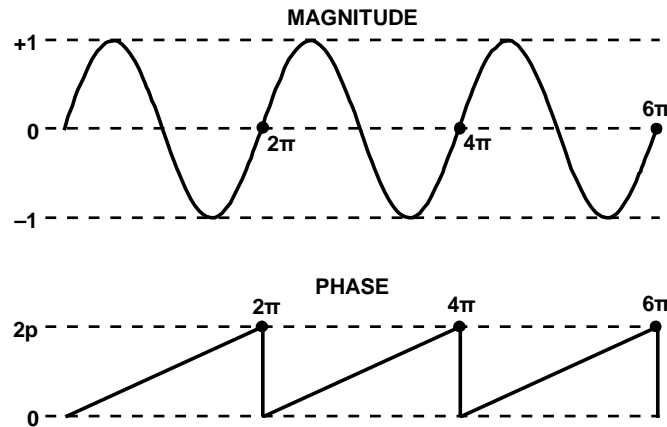


Figure 2.10: Magnitude and phase of a sine wave ([7, p. 11, fig. 23]).

to the output pin. To create a sine wave, the corresponding value of the sine wave for the actual phase is looked up in the SIN ROM (lookup table) and the voltage is then created by the digital-analog converter (DAC) and sent to the output pin.

2.7 Impedance matching

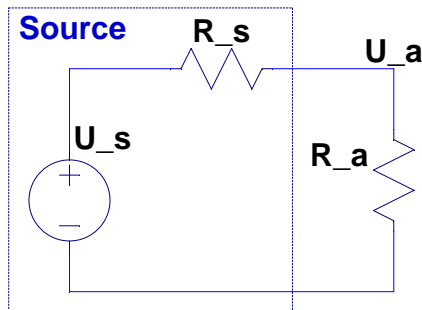


Figure 2.11: Example circuit, source with internal resistance and load resistor.

In this section, the functionality of impedance matching is described only briefly, since only the general idea is important for the later considerations and not the exact mathematical solution.

Figure 2.11 shows a real source, represented with an ideal voltage source and an internal resistance R_s , loaded with the resistor R_a . If R_a became zero, the current would only be limited by R_s , and also the entire power would be consumed there. If the source voltage U_s is set to 1 V and R_s is also set to 1Ω , then figure 2.12 shows voltage, current and consumed power at R_a plotted against R_a . This shows that the maximum power throughput occurs if $R_a = R_s$, but at this point the efficiency is only 50 %, since at R_s is the same voltage as

2 Foundations

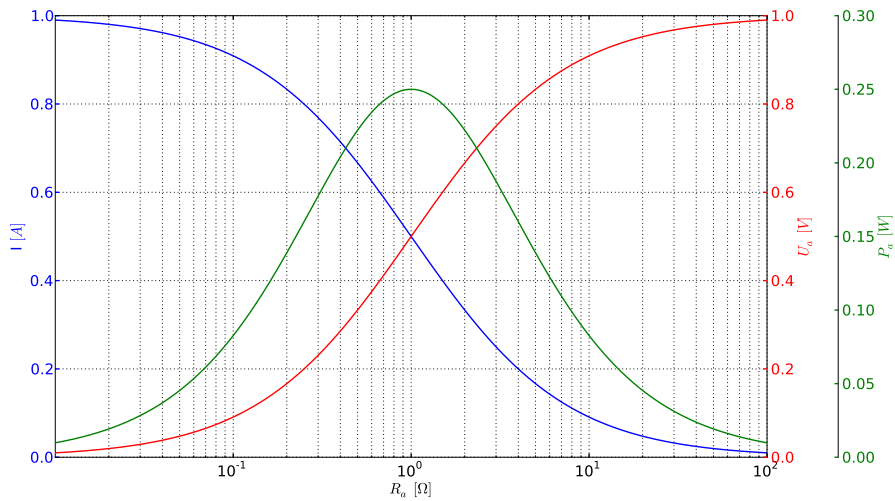


Figure 2.12: Plot of voltage, current and power at R_a against different values of R_a with $U_s = 1$ and $R_s = 1$.

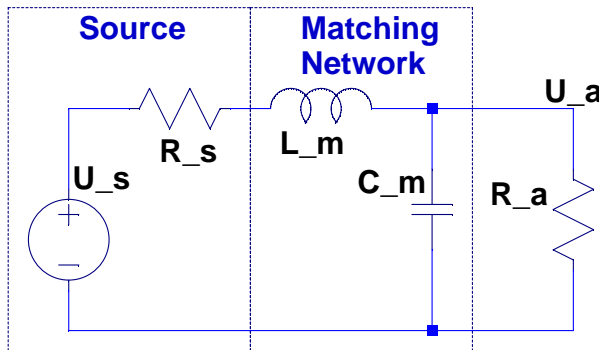


Figure 2.13: Example LC impedance matching circuit, source with internal resistance, load resistor and matching network.

at R_a and the current is also the same.

Since it is not always possible to choose the load Z_a (in this case R_a) and/or the source, the load can be transformed using a real transformer or, as shown below, with an impedance matching network. This allows to change the impedance of the load to better fit the source and to in-/decrease the power throughput.

A possible impedance matching network is shown in figure 2.13. It consists of the inductance L_m and the capacitor C_m , arranged in a L-shape. Equation 2.4 shows the impedance for the entire load including a matching network and in this case the load R_a . By equating this to a desired new impedance (in this case Z_d), it is possible to solve it at a specific frequency f for L_m and C_m by equating the imaginary and the real part of both sides. The result can be seen in equations 2.6 and 2.7, by which the desired impedance can be achieved.

2 Foundations

There are two important remarks necessary. First, the created matching network only works at a specific frequency and the further the working frequency differs from this one, the more the desired impedance disappears. Second, to create the maximum power throughput it is necessary to know the internal resistance of the source (in this case R_s), but it is not always desired to create this state (maximum power throughput). Especially in the application described in this thesis, maximum power throughput would mean that the power source consumes the same amount of energy as the heating process. It is, however, desirable to reduce the impedance of the load to better fit the source. To that end, it is not necessary to know the internal resistance of the source.

$$\begin{aligned} \underline{Z}_l &= \underline{s} \cdot L_m + \frac{1}{\underline{s} \cdot C_m + \frac{1}{R_a}} \\ &= \underline{s} \cdot L_m + \frac{R_a}{\underline{s} \cdot C_m \cdot R_a + 1} \\ &= \frac{R_a}{1 + \omega^2 \cdot C_m^2 \cdot R_a^2} + j \cdot \frac{\omega \cdot L_m + \omega^3 \cdot C_m^2 \cdot R_a^2 \cdot L_m - \omega \cdot C_m \cdot R_a^2}{1 + \omega^2 \cdot C_m^2 \cdot R_a^2} \end{aligned} \quad (2.4)$$

$$\underline{Z}_l = \underline{Z}_d \quad (2.5)$$

$$C_m = \frac{\sqrt{\frac{R_a - \text{Re}(\underline{Z}_d)}{\text{Re}(\underline{Z}_d)}}}{R_a \cdot \omega} \quad (2.6)$$

$$L_m = \frac{\text{Im}(\underline{Z}_d) + \text{Re}(\underline{Z}_d) \cdot \sqrt{\frac{R_a - \text{Re}(\underline{Z}_d)}{\text{Re}(\underline{Z}_d)}}}{\omega} \quad (2.7)$$

3 Mechanics

3 Mechanics

From the mechanical point of view, the design should fit on existing extruder designs. Since the RepRap project is very fragmented and because there are many different printer designs, there is neither a standard for the layout of the connection between nozzle and extruder nor for configuration of the nozzle as a whole. As discussed in the Extruder section 2.4.1, there are some basic requirements but apart from that, there are no limitations to the design.

From an electrical point of view, it is preferable that the metal core (later also called core or secondary coil) is entirely enclosed in the spool to reduce edge conditions which could influence the setup. In order to do so, the spool (later also called primary coil) should at least have the same length as the core. Furthermore, the different loops should be coiled tightly to each other to create an uniform field. From the EMC viewpoint, the supply cables should be located very close to each other, twisted and as short as possible to reduce unwanted emissions, as discussed in the EMC section 4.9.

To counteract the skin effect described in section 2.1, the primary coils should also be made out of several parallel wires to reduce the resistance of the coil and by that the warming due to ohmic losses. Figure 3.2 shows the configuration of the coil that consists of eight parallel wires.

To increase the effectiveness of inductive heating by hysteresis losses, the core should be made out of a ferromagnetic material. Due to the availability of mild steel which is used in different screws, this type is used here. Since this type of steel has a relatively height permeability, the hysteresis losses are also high. Since the skin effect also applies to the core and due to the fact that the volume of the core material limits the temperature gradient, it should be thin. To position the core in the center of the glass tube, some cores were formed with a brim and all with a 3 mm center hole, a width that corresponds with the diameter of most filaments (see figure 3.5).

The material of the tube that encloses the core needs to be temperature resistant up to at least 300 °C. It should not be electrically conductive so that it doesn't influence the inductive heating process. Also, it should have a low thermal conductivity to reduce losses and the stress for the outer components such as the primary coil. Glass would fit these requirements relatively good and glass tubes are easily available. Because the glass tube is

3 Mechanics

exposed to the pressure from inside and in case of an faulty operation the nozzle could hit the build platform, the main criterion for the choice of the glass type should be its ruggedness. One of the most rugged glass types is borosilicate glass which is also used for chemical tools. It also meets the other criteria relatively well. Another possible material would be some kind of ceramic, but since it is harder to process and harder to acquire, this was not further examined.

The primary coil can be coiled around the glass cylinder, but in case the extruder is inactive, there would be no material to transfer the heat out of the core. Over time, the temperature of the primary coil would rise. Even though the glass tube is a bad thermal conductor, most of the energy would migrate though the glass if the core is kept on a steady temperature so that it isn't cooled by the material flow. Due to the fact that most enameled copper wires only withstand temperature up to about 150 °C, this would be destructive. To counteract this fact to some extent, supporting material was added in an additional layer. This supporting material also has to withstand temperatures up to 300 °C and also shouldn't be electrically conductive. Due to proliferation of PEEK material in different types of RepRap extruders, this material was used. The supporting material could also be slotted as shown in figure 3.2 to reduce the heat transfer between core and primary coil and enable some airflow between glass tube and coil. This setup is only an example. For later setups there should be more slots to improve the cooling abilities.

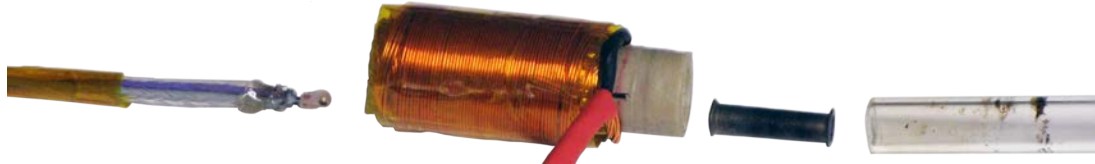
For development and testing purposes, a temperature sensor was needed. The used thermistor (B57560G104F) has a temperature range up to 300 °C. A teflon cable was used as a supply cable for the sensor due to its ability to withstand temperatures as high as that. This test setup can be seen in figure 3.1.

Figure 3.3 shows an example setup of the glass cylinder including the core, as well as a teflon tube to hold the core in place and to reduce friction of the filament. Teflon can withstand temperatures up to 327 °C, but due to the fact that the gases resulting of overheating are very harmful and the teflon can also become soft below this temperature an alternative setup is shown in figure 3.4, with a PEEK distance holder between core and teflon, which serves as an insulating layer.

For purposes of testing, different cores were made, as shown in figure 3.5. They will be examined more closely in chapter 6.

INDUCTIVE HEATING AND TEMPERATURE MEASURING SYSTEM

3 Mechanics



(a) Disassembled setup



(b) Assembled setup

Figure 3.1: Test setup.



Figure 3.2: Assembly of the coil wrapped around the slotted supporting material and consisting of several parallel wires.

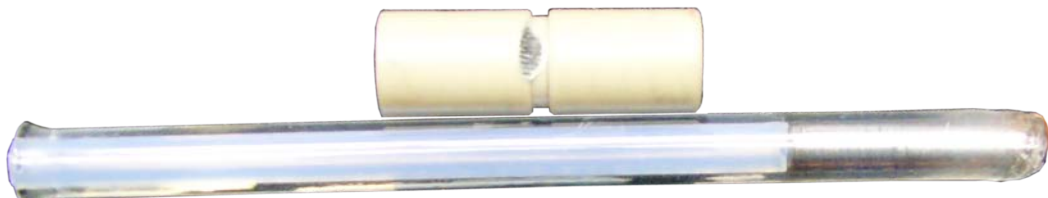


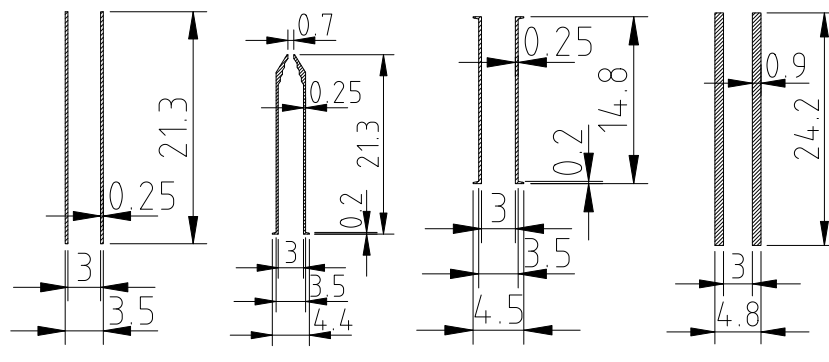
Figure 3.3: Example setup with PEEK extruder connector, glass tube with lip for the extruder connector and closed end with a 0.7 mm outlet hole in the glass, mild steal core and a teflon tube within the glass tube to hold the core in place and to reduce friction of the filament.

INDUCTIVE HEATING AND TEMPERATURE MEASURING SYSTEM

3 Mechanics



Figure 3.4: Setup with PEEK extruder connector, glued to the glass tube for the extruder connection and reduced diameter at the end of the glass tube holding the T2 type (cf. figure 3.5) core in place at the outlet, a teflon tube within the glass tube to hold the core in place and to reduce friction of the filament, as well as an about 2 mm high cylinder of PEEK material as a distance holder between core and teflon.



(a) Technical drawings



(b) Top view



(c) Front view

Figure 3.5: Different cores. Type T1 up to T4 from left to right.

4 Hardware

4 Hardware

The different parts shown in the hardware flow diagram (figure 4.1) below are described in the following sections. First of all, there is a general description of the individual parts including a discussion of different possibilities and models. Subsequently, the actual setup is shown and described. One objective was to allow for an easy replication, which means the use of few and standardized parts, and a simple setup to suit the requirements of the RepRap project.

All circuit simulations in this section were made with LTspice IV. For the other plots or simulations, Python with matplotlib and ParaView have been used.

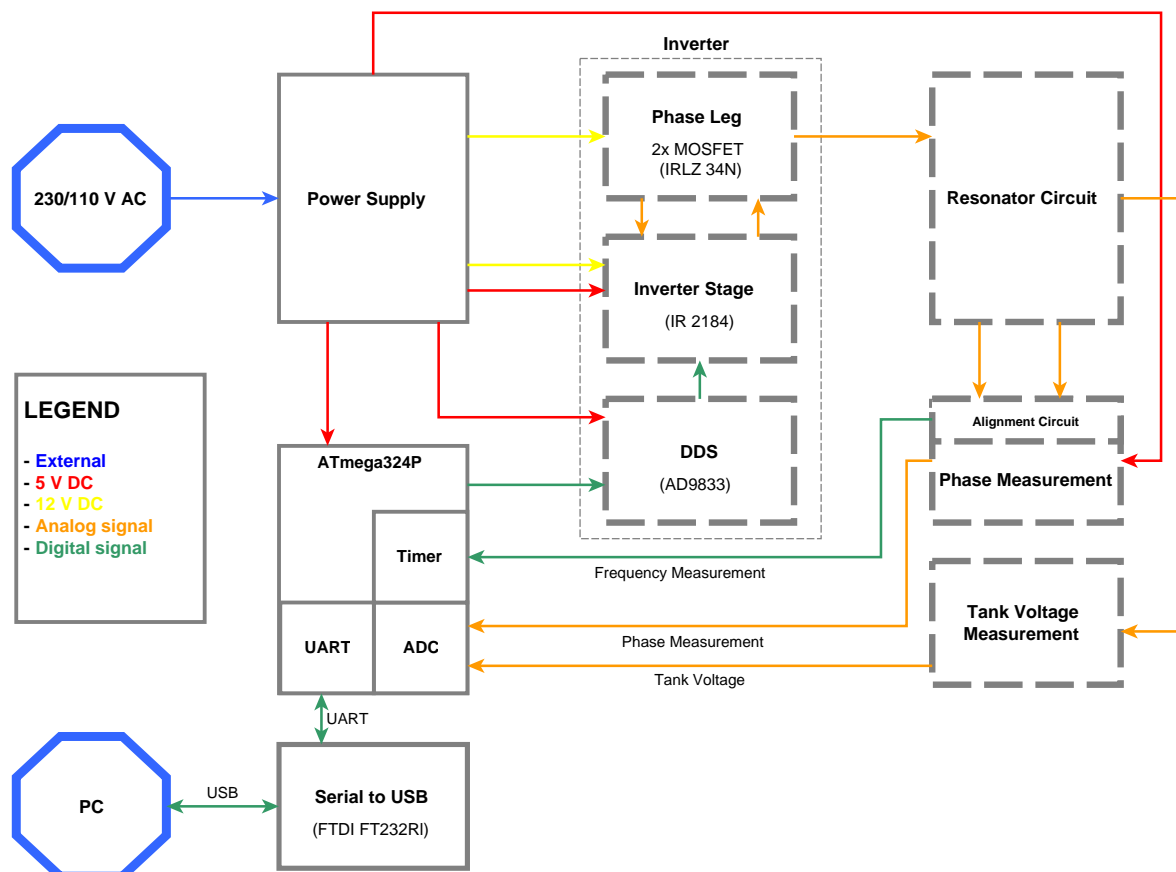


Figure 4.1: Hardware flow diagram.

4 Hardware

4.1 Power Supply

A common power supply for RepRap printers is an ATX power supply unit, usually used in PCs. It is used to supply the entire electronics of the printer including the stepper motor, the heated bed and the nozzle. This provides a variety of voltages, among them 5 and 12 volt, with a tolerance of $\pm 5\%$. Most of the used units allow at least 15 ampere on each of these lines. To allow for a usage in existing setups, the hardware described below is designed for these voltages. As required by the ATX standard, the provided voltages are very stable, (see Intel design guide [20]). They can be used to directly power the microcontroller and, since they provide enough energy, also supply the inductive heating circuit.

4.2 Resonator circuit

As described in the section 2.2, inductive heating occurs because of two main reasons.

- Resistive Heating owing to the high currents in the work piece (core),
- Magnetic hysteresis losses owing to the reorientation of the Weiss domains

To cause these two effects in the metal cylinder and the setups described in the Mechanics chapter 3, it is necessary to create a high alternating current in the primary coil.

To cause such a current, it is possible to directly connect the primary coil to an alternating voltage source, which would cause such a current. The problem here is that the easy to create and control rectangle voltage source would cause a triangular current through the primary coil. This effect occurs because of the definition of inductance (see equation 4.1 from [17, p. 311, equ. 5.150]). As described later in section 4.9: The more the waveform differs from a sinusoidal shape, the higher the voltage and current gradients become, and the worse the EMC properties get. In this case, particularly the high non-sinusoidal current is problematic. Therefore, a direct connection of the primary coil to such a source would work, but owing to the EMC, a more sinusoidal current would be preferable.

To do so, it is possible to drive the primary coil with a sinusoidal voltage which would cause a sinusoidal current. However, in order to create a voltage source capable of providing several amperes, it is a lot easier to use an inverter driver as described in the following sections.

A possible setup for a sinusoidal voltage supply would be a DDS IC with a class A amplifier, but this amplifier type is very inefficient. According to [31, p. 107], it has a maximum theoretical efficiency of 50%. Owing to this fact and also because inductive temperature

4 Hardware

sensing would be more difficult if the primary coil was directly driven, this is not an option either.

Another way to make the current more sinusoidal are LC resonator circuits. This type of setup is common in the inductive heating circuits and the two main types are described in the following sections.

$$i = \frac{1}{L} \int u \, dt \quad (4.1)$$

4.2.1 Load model

The setup with a primary copper spool and a secondary ferromagnetic metal cylinder (see chapter 3) yields a suboptimal inductance. According to [26, p. 91, fig. 2.30], a real inductance can be modeled as shown in figure 4.2, and with the following parts:

- R_{copper} : Represents the ohmic resistance of the copper wire which the coil as well as the connection wires are made of.
- R_{core} : Represents the losses within the core, mainly caused by the heating of the core.
- C_{loops} : Each loop of the coil represents a small capacity with the loops next to it. These capacities add up and are represented by C_{loops} . Its magnitude lies in the range of some pico farad. This capacity creates a resonator circuit with the inductance. If we assume the magnitude of the inductance in this setup to be some micro henrys, the resonance frequency of the parallel inductor and capacitor (according to equation 4.2 from [17, p. 388, equ. 7.22]) lies in the range of several tenth of megahertz. Since the operation frequency is about a hundred kilohertz, this capacity can be neglected. It only influences the circuitry at very high frequencies.

All these model parts depend on the operating frequency. With increasing frequency, the value of R_{Copper} increases since the influence of the skin effect is also increasing (see section 2.1). If direct the current (0 Hz) is connected to the inductance, there are no core losses in this state. Therefore, R_{Core} also has to depend on the frequency.

$$\omega_0 = \frac{1}{\sqrt{L \cdot C}} \quad (4.2)$$

4 Hardware

To simplify the model, the parallel circuit of R_{Core} and L can be transformed into a serial circuit as follows: After equating the impedance of the serial and parallel circuits in equation 4.3, expanding the complex conjugate and then equating the real and the imaginary part, the equations for the component values of the serial circuit are 4.4 and 4.5.

$$R'_{Core} + j \cdot \omega \cdot L' = \frac{1}{\frac{1}{R_{Core}} + \frac{1}{j \cdot \omega \cdot L}} \quad (4.3)$$

$$R'_{Core} + j \cdot \omega \cdot L' = \frac{R_{Core} \cdot \omega^2 \cdot L^2 + j \cdot R_{Core}^2 \cdot \omega \cdot L}{R_{Core}^2 + \omega^2 \cdot L^2}$$

$$R'_{Core} = \frac{R_{Core} \cdot \omega^2 \cdot L^2}{R_{Core}^2 + \omega^2 \cdot L^2} \quad (4.4)$$

$$\omega \cdot L' = \frac{R_{Core}^2 \cdot \omega \cdot L}{R_{Core}^2 + \omega^2 \cdot L^2} \quad (4.5)$$

After this simplification, R_{Copper} and R'_{Core} can be combined to one R_{load} representing all losses and L' is L_{load} . Figure 4.2 (2) shows the final load model.

R_{Core} and R_{Copper} depend on the frequency. The parallel serial transformation also introduces a frequency dependency as seen in equation 4.4. The new R_{load} also depends on the frequency in a very nested way. Due to the fact that the circuitry will only operate in a small range around the resonance frequency, the change in this value should also be small. Since the frequency range of operation also depends on several factors, e.g. core material, it might be necessary to further investigate these.

For further considerations and simulations it is necessary to at least know the decimal power of R_{load} . Since the value depends on the actual setup in various ways, it is easier to measure the value than to calculate it. To do so, an LC serial resonator circuit (as described in section 4.2.3) is used. As also shown in this section, the impedance of this circuit at resonance frequency is only determined by R_{load} . For example: If the primary coil with a T3 core (cf. chapter 3) is serially connected to a known capacitor and driven at resonance frequency with a known voltage, the value of R_{load} can be calculated by dividing the RMS values of the voltage and the current.

If this setup is driven with a square wave voltage with an RMS value of 6 V at resonance frequency (as shown chapter 6, especially figure 6.4(c)), the RMS value of the current is about 4 A. The value of R_{load} can therefore be calculated to $1.5 \Omega (= \frac{6}{4})$. As described, this value is not constant. Since only the approximate value is necessary for further simulations, it can be rounded to 2Ω . This value will be used in the following considerations.

If the value of the used capacitor is known, the value of L_{load} can also be determined with

4 Hardware

this test (see equation 4.12). So if the serial resonator circuit is set to resonance, the value can be calculated. The value of L_{load} also depends on different factors. Due to this fact, the measurement is only an approximation of the inductance of the used coil at this specific frequency.

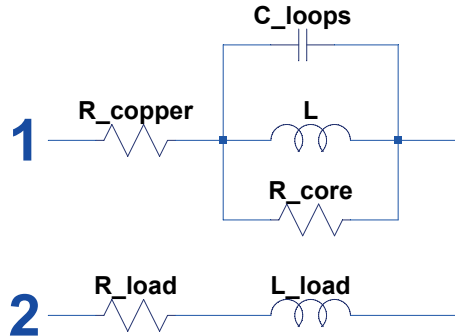


Figure 4.2: 1: Model of a non-ideal inductance; 2: Used model.

4.2.2 Parallel resonator circuit

An ideal parallel resonator circuit is a capacitor with a parallel inductor. As seen in section 4.2.1, the inductor can be modeled as an inductance in series with a resistor. This resistor represents the corresponding losses. Because the losses of the capacitor are small (for capacitor used in such an application, the ESR is several ten $m\Omega$) compared to the ones in the inductance ($R_{load} \approx 2 \Omega$), these can be neglected.

As described in section 4.1, the available power supply has a voltage level of 12 V. To increase the power throughput, an impedance matching network as described in section 2.7 is used, represented by L_{match} und C_{match} .

The capacitor C_{filter} decouples the network from the inverter. This capacitor filters out any DC part of the supply voltage and current. Without this element, the currents and voltages in the circuit would be overlaid by a DC part due to the only positive driver voltage. This may become problematic since the capacitor can only tolerate a certain voltage and the DC part would add up to the AC part. If the value of C_{filter} is chosen high enough, it hardly influences the rest of the circuit.

The complete setup can be seen in figure 4.3. The parallel capacitors C_{match} and C_{tank} can be summarized into one capacitor C_{tank} seen in figure 4.4 which displays the final circuit for all further considerations.

For further calculations, the impedance of this network Z (c. equation 4.6) is necessary. By setting up the voltage transfer function (equation 4.7), a representative Bode diagram can be plotted as seen in figure 4.5(a). This shows the magnitude and phase of the voltage

4 Hardware

across the tank versus the source voltage. Using the equation for \underline{Z} , it is also possible to plot the absolute value as well as the imaginary and real part of the impedance against the frequency (figure 4.5(b)).

$$\begin{aligned}\underline{Z} &= \frac{1}{\underline{s} \cdot C_{filter}} + \underline{s} \cdot L_{match} + \frac{1}{\underline{s} \cdot C_{tank} + \frac{1}{\underline{s} \cdot L_{load} + R_{load}}} \\ &= \frac{1}{\underline{s} \cdot C_{filter}} + \underline{s} \cdot L_{match} + \frac{\underline{s} \cdot L_{load} + R_{load}}{\underline{s}^2 \cdot C_{tank} \cdot L_{load} + \underline{s} \cdot C_{tank} \cdot R_{load} + 1}\end{aligned}\quad (4.6)$$

$$\frac{U_{tank}}{U_{source}} = \frac{\frac{\underline{s} \cdot L_{load} + R_{load}}{\underline{s}^2 \cdot C_{tank} \cdot L_{load} + \underline{s} \cdot C_{tank} \cdot R_{load} + 1}}{\underline{Z}} \quad (4.7)$$

$$0 = Im(\underline{Z}) \quad (4.8)$$

$$Im\left(\frac{1}{\underline{s} \cdot C_{filter}}\right) = Im\left(-\frac{j}{\omega \cdot C_{filter}}\right) = -\frac{1}{\omega \cdot C_{filter}} = Q$$

$$Im(j \cdot \omega \cdot L_{match}) = \omega \cdot L_{match} = W$$

$$\begin{aligned}Im\left(\frac{\underline{s} \cdot L_{load} + R_{load}}{\underline{s}^2 \cdot C_{tank} \cdot L_{load} + \underline{s} \cdot C_{tank} \cdot R_{load} + 1}\right) &= \\ &= \frac{\omega \cdot L_{load} - \omega^3 \cdot C_{tank} \cdot L_{load}^2 - \omega \cdot C_{tank} \cdot R_{load}^2}{\omega^4 \cdot C_{tank}^2 \cdot L_{load}^2 + \omega^2 \cdot C_{tank}^2 \cdot R_{load}^2 - 2 \cdot \omega^2 \cdot C_{tank} \cdot L_{load} + 1} = E\end{aligned}$$

$$0 = Q + W + E \quad (4.9)$$

For the following considerations, the exact values of the components are not important since the general shape of the curves is the same if the component values are in the necessary boundaries to ensure a sound operation.

By definition, a point of resonance is where a circuit only consumes real power. This means that the imaginary part of the impedance is zero (eqation 4.8 and 4.9). As seen in figure 4.5(b), lower plot, there are three frequencies where this is the case. They are marked with red vertical lines, to which the numbers one to three have been assigned. These different cases are discussed below.

4 Hardware

Marker 1.: As can be seen in the magnitude plot of the Bode diagram (figure 4.5(a), voltage as well as current), there is a local maximum, in this case at about 1.5 kHz. At this point the filter capacitor C_{filter} resonates with the rest of the circuit. The amplification at this frequency mainly depends on the real load of the circuit R_{load} : The lower the real load, the higher the peak. The frequency at which this occurs depends on the value of C_{filter} , since this capacitor creates a high pass. By increasing this value, the peak moves further left and by that the influence of this filter capacitor on the network is reduced. Depending on the approach of control and the magnitude of the real load it is important to not drive the circuit for too long in this frequency range, since in most cases the circuit (especially C_{filter}) is not designed for such high loads.

Marker 2.: As seen in figure 4.5(b), the impedance and the magnitude of the current transfer function in 4.5(a) have a maximum at this marker. At this point the parallel resonator circuit would operate at its resonance frequency and the parallel resonator only has a real impedance, represented by its losses (R_{load}). However, due to the impedance matching this resistance is transformed up since it is not at the operating frequency of the matching circuit. Since the current amplification has reached its maximum at this point, this would be a good operating point, but as the impedance at this point is very high, it would be necessary to drive this circuit with a high voltage to create the necessary power throughput. Due to the available power supply this is not an option.

The two main components determining at which frequency this point occurs are C_{tank} and L_{load} . The magnitude of this peak in the current transfer function mainly depends on the load resistance R_{load} (low R_{load} corresponds with high amplification and vice versa).

Marker 3.: At this point the matching circuit runs at its operation point. The voltage and the current/voltage transfer function has a maximum at this point. The frequency difference between the second marker and this one mainly depends on the L_{match} inductor. By increasing its value, the third marker can be moved closer to the second marker and by that the current throughput can be increased. If C_{tank} has a fixed value, e.g. due to a desired resonance frequency and a fix value for L_{load} , L_{match} can only be increased up to a certain point, since, as described in section 2.7, it is necessary to also set the capacitor to a certain value for an proper operation of the matching network. Another aspect is the size of the matching inductor which is also limited by the size of the coil, since in most cases a higher inductance is associated with a bigger physical size.

If the value of L_{match} exceeds a certain value, the zeros ($Im(\underline{Z}) = 0$) at markers two and three disappear. If that happens, the resonator does not work properly. The waveform,

4 Hardware

especially of the current, deforms and the resonator also consumes reactive power when driven at resonance frequency.

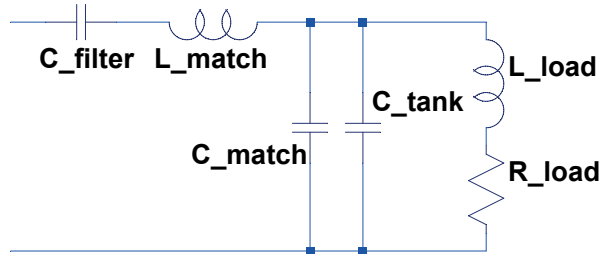


Figure 4.3: Real parallel resonator circuit, with impedance matching network and DC blocking capacitor.

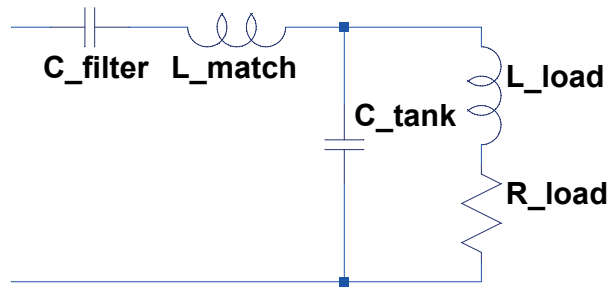


Figure 4.4: Simplified final circuit.

Figures 4.6 show corresponding values for different values of L_{load} and L_{match} . They all have in common that the function value jumps at a boundary. This occurs due to the fact that the equation $Im(\underline{Z}) = 0$ returns no further solutions for the corresponding component values (refers to marker 2 and 3 in figure 4.5), and in this case the displayed value is the one at marker 1 in figure 4.5. The position of this skip is mainly affected by R_{load} and also C_{tank} . If R_{load} is reduced, the function values rise/fall more and continue further before the skip occurs.

Figure 4.6(a) shows the value of the current transfer function at the resonance frequency (referring to marker 3 in figure 4.5). It also shows that the current amplification increases for bigger values of L_{match} and L_{load} while the current voltage amplification (figure 4.6(b)) decreases. This means: If a steady supply voltage is stated, the load current decreases. Figure 4.6(c) shows the resonance frequency (marker 3 in figure 4.5) and demonstrates that L_{match} also influences the resonance frequency, though to a lesser extent than L_{load} (note the different ranges of L_{match} and L_{load} in the plots).

The plots in figure 4.7 show the same function values as in figure 4.6, represented by the colors of the blocks and with an third axis for C_{tank} .

This shows that a smaller C_{tank} reduces the current amplification, increases the current

INDUCTIVE HEATING AND TEMPERATURE MEASURING SYSTEM

4 Hardware

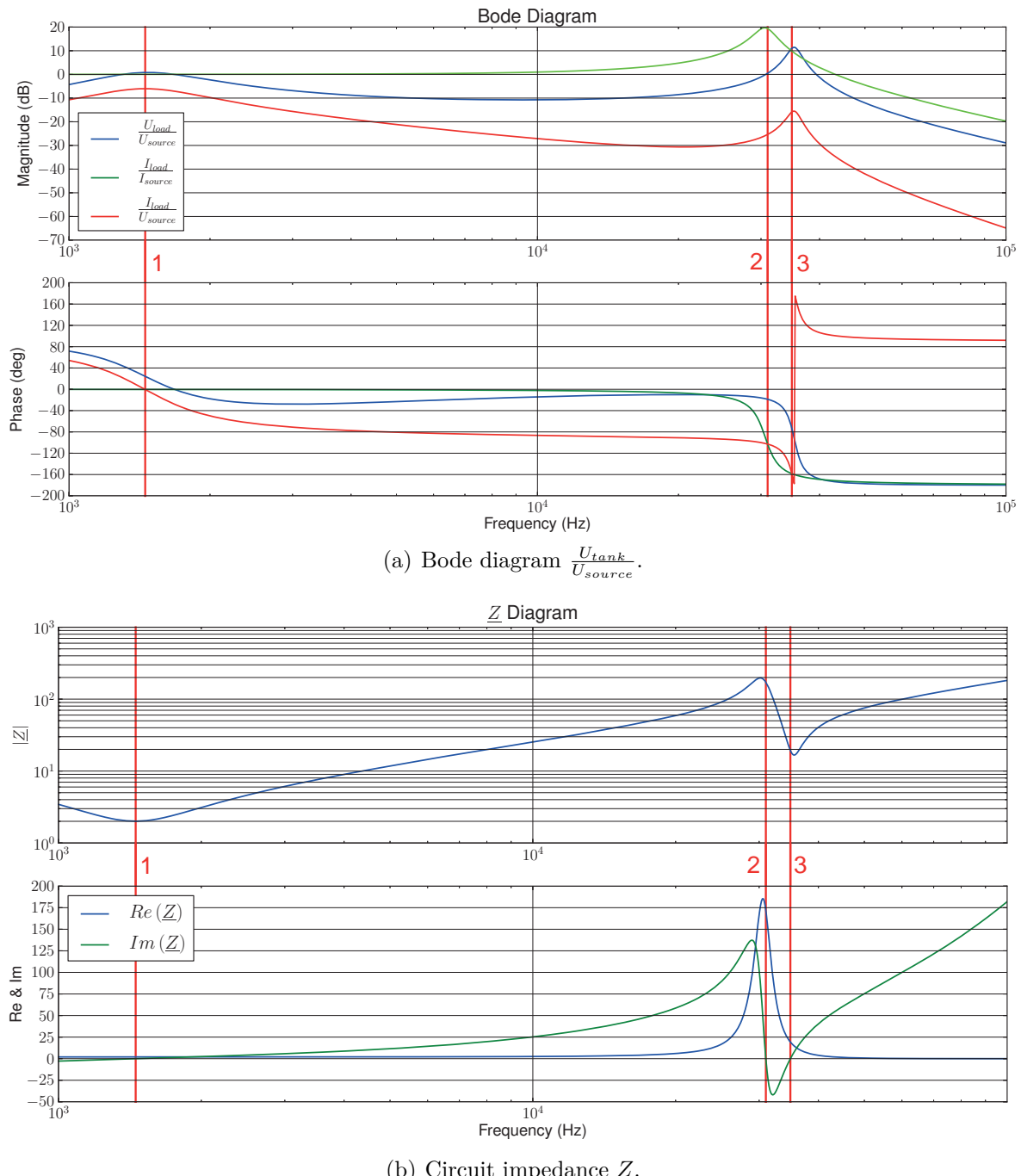


Figure 4.5: Plots with $L_{load} = 100 \mu\text{H}$, $R_{load} = 2 \Omega$, $C_{tank} = 270 \text{ nF}$, $L_{match} = 300 \mu\text{H}$, $C_{filter} = 30 \mu\text{F}$.

4 Hardware

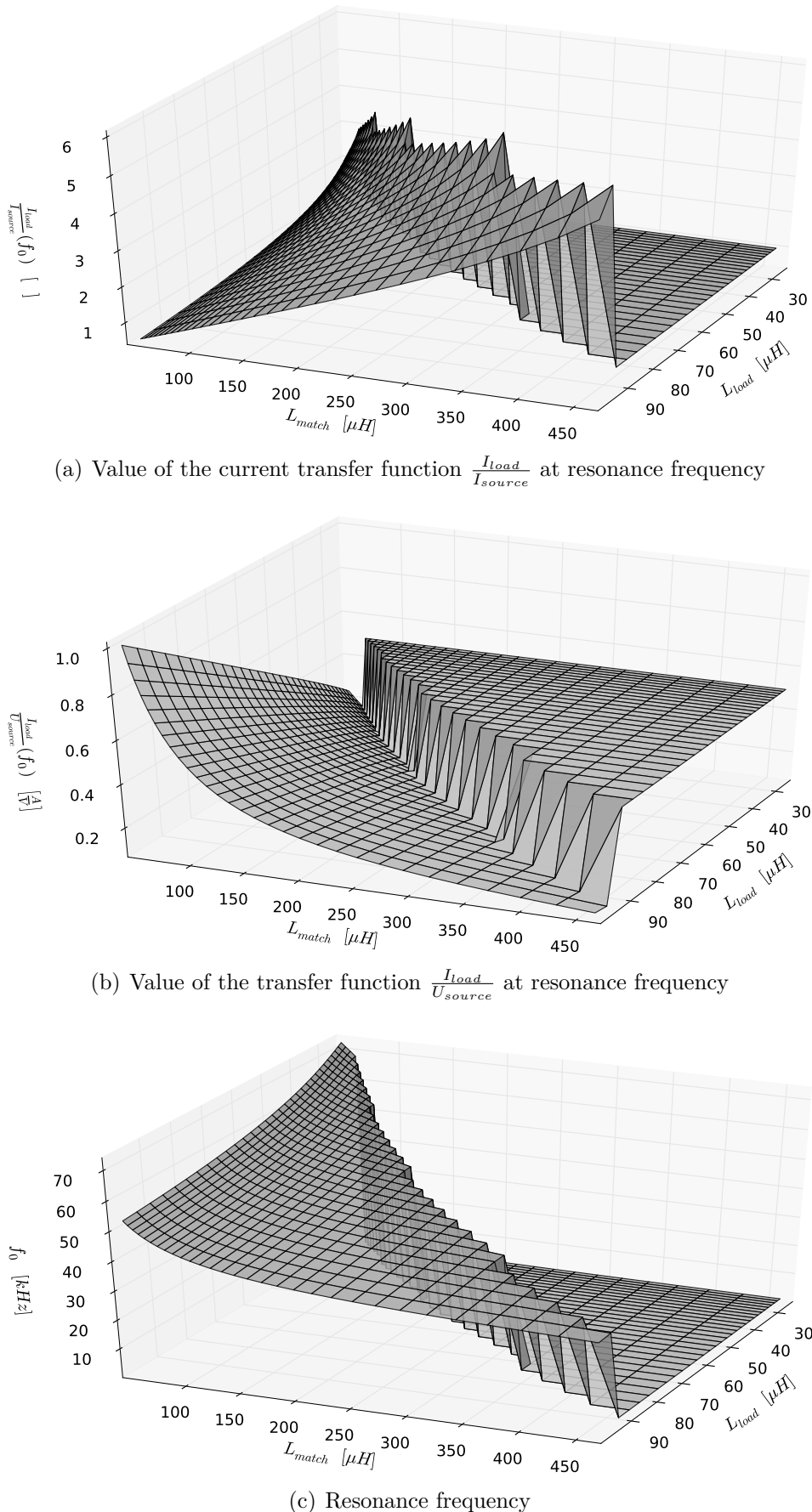


Figure 4.6: 3D Plots with $R_{load} = 2 \Omega$, $C_{tank} = 270 \text{ nF}$, $C_{filter} = 30 \mu\text{F}$.

4 Hardware

voltage amplification while the resonance frequency increases. Moreover, it implies that there is a skip if C_{tank} exceeds a certain value, similar to the skips in the plots shown in figure 4.6. The function values for increasing values of C_{tank} in figure 4.7(a) increase to a certain point and above that the filter cuts off the corresponding low values. Vice versa, the resonance frequency decreases as seen in figure 4.7(c) and the filter cuts off the much lower values of the resonance point of C_{filter} .

4.2.2.1 Conclusion

As the simulation shows by variation the component values, an increase in the current amplification (also called Q-factor) comes along with a decrease of the current/voltage amplification which means less current through L_{load} at a steady supply voltage U_{source} . A Q-factor higher than 1 would reduce the load and the losses on the supply path via C_{filter} and L_{match} . This would also allow for a smaller dimensioning of the supply path as well as longer cables since only a relatively small current would flow through this path and the high current would flow only between C_{tank} and L_{load} .

However, as previously shown, a high Q-factor would also involve a lower load current at a constant supply voltage. This means that either the minimum Q-factor or the minimum load current have to be predefined. After doing so, it is necessary to check whether the desired other value and the resonance frequency can be achieved with reasonable values for the components.

An important thing to note here is that the values of the simulation for the Q-factor and the current/voltage amplification highly depend on the value of R_{load} . This means: If R_{load} is reduced, the edge occurs later (at higher L_{match} and lower L_{load}) and also comes along with higher values in the relevant range of the component values. As a result, this type of circuit suits setups with small loads and/or high supply voltages a lot better.

4.2.3 Series resonator circuit

Figure 4.8 shows a diagram of a real serial resonator circuit in which the load model of section 4.2.1 is already implemented. It is a serial circuit of an inductor and capacitor with the losses represented by a resistor. The circuit impedance is shown in equation 4.10 and the voltage transfer function of U_{tank} and U_{source} is shown in equation 4.11.

INDUCTIVE HEATING AND TEMPERATURE MEASURING SYSTEM

4 Hardware

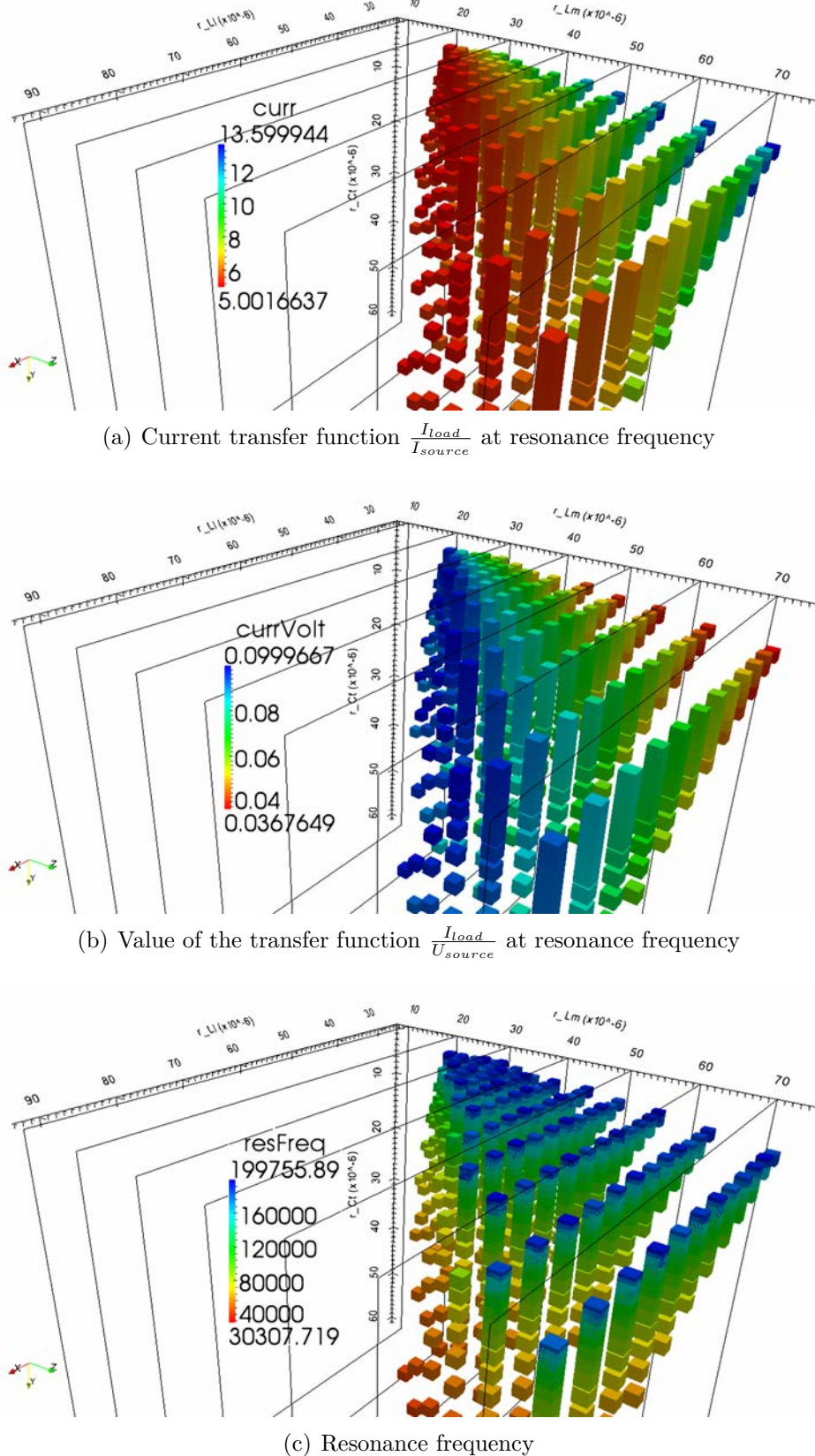


Figure 4.7: Plots with $R_{load} = 2 \Omega$, $C_{filter} = 30 \mu\text{F}$ (axis factors: $L_{load} = r_{Ll} \cdot 1$, $L_{match} = r_{Lm} \cdot 0.15$, $C_{tank} = r_{Ct}/150$ and filters: $10 \text{ kHz} < f_0 < 200 \text{ kHz}$ and $5 < \frac{I_{load}}{I_{source}}$).

4 Hardware

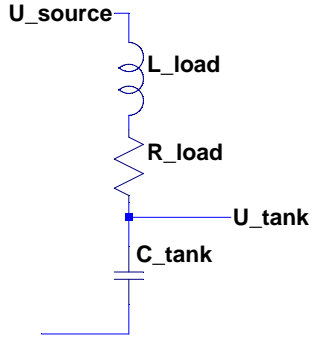


Figure 4.8: Serial resonator circuit.

$$\begin{aligned} \underline{Z} &= \frac{1}{\underline{s} \cdot C_{\text{tank}}} + \underline{s} \cdot L_{\text{load}} + R_{\text{load}} \\ &= R_{\text{load}} + j \cdot \frac{\omega^2 \cdot C_{\text{tank}} \cdot L_{\text{load}}}{\omega \cdot C_{\text{tank}}} \end{aligned} \quad (4.10)$$

$$\begin{aligned} \frac{U_{\text{tank}}}{U_{\text{source}}} &= \frac{\frac{1}{\underline{s} \cdot C_{\text{tank}}}}{\underline{Z}} \\ &= \frac{1}{1 + \underline{s} \cdot C_{\text{tank}} \cdot R_{\text{load}} + \underline{s}^2 \cdot L_{\text{load}} \cdot C_{\text{tank}}} \end{aligned} \quad (4.11)$$

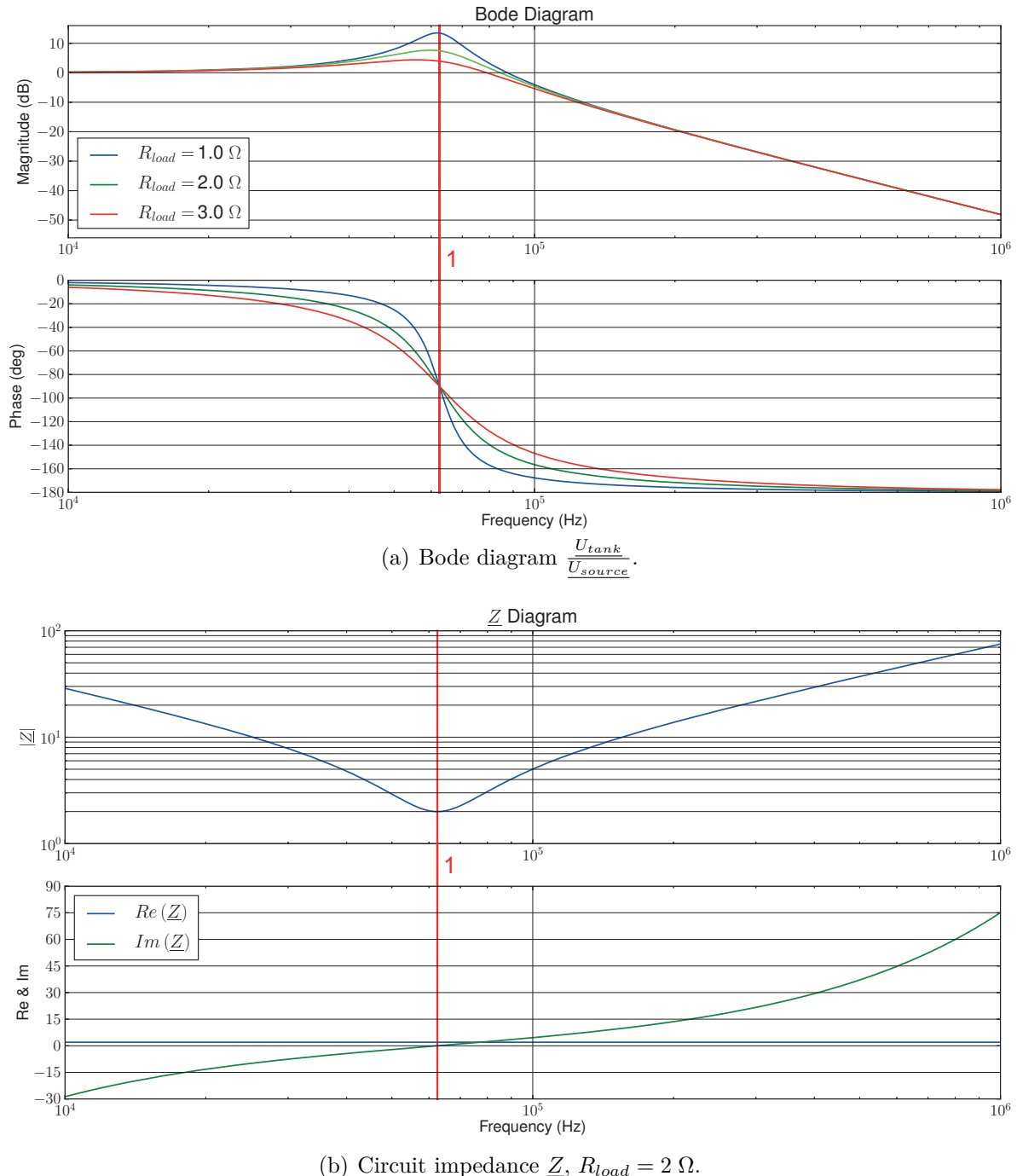
With these equations it is possible to create a Bode diagram as well as a plot of the impedance (cf. figures 4.9). The Bode diagram (figure 4.9(a)) shows that at resonance frequency (marker 1) the voltage amplification is increased and the phase shift between source and tank voltage is 90° . As the impedance plot (figure 4.9(b)) shows, $\text{Im}(\underline{Z})$ becomes zero at resonance frequency and the circuit impedance is purely real. According to equation 4.10, the impedance is R_{load} if the imaginary part is zero.

Given the general assumption that $\text{Im}(\underline{Z}) = 0$ at resonance frequency, the equation for this frequency can be set up as seen in equation 4.12.

$$\begin{aligned} \text{Im}(\underline{Z}) &= 0 \\ \Rightarrow \omega_0 &= \frac{1}{\sqrt{L_{\text{load}} \cdot C_{\text{tank}}}} \end{aligned} \quad (4.12)$$

As seen in the magnitude plot of the Bode diagram in figure 4.9(a), at resonance frequency the voltage can become higher than the source voltage. This amplification value is also called Q-factor and is shown in equation 4.13. Since the current flowing through the circuit

4 Hardware


 Figure 4.9: Plots with $L_{load} = 12 \mu H$, $C_{tank} = 540 nF$.

4 Hardware

is the same for different combinations of L_{load} and C_{tank} at the same resonance frequency (since at this frequency the impedance is R_{load}), this voltage should be kept at a low level. If the setup is not protected against physical contact, safety issues may result (further discussed in section 6.1).

$$\left| \frac{U_{tank}}{U_{source}} (\omega_0) \right| = \frac{1}{R_{load}} \cdot \sqrt{\frac{L_{load}}{C_{tank}}} (= Q) \quad (4.13)$$

As the phase plot of the Bode diagram in figure 4.9(a) shows, the phase transition at resonance frequency is mainly determined by the value of R_{load} . With a rising value, the transient gets wider and flattened.

The plots in figure 4.10 show the load current and the tank voltage at a resonance frequency of 60 kHz (equation 4.14) for different ratios of L_{load} and C_{tank} (equation 4.15, with the component values according to equations 4.16 and 4.17 for $x = 0.001, 0.01, \dots, 100$). It can be seen that the current shown in figure 4.10(a) is almost a square wave if $L_{load} \ll C_{tank}$ and that it gets sinusoidal if x increases. Due to the facts that square waves are unfavorable according to EMC (see section 4.9) and that high currents are switched hard (high $\frac{di}{dt}$), the switching losses and the stress on the switches are higher. As expected, due to equation 4.13, figure 4.10(b) shows that the voltage at resonance frequency becomes bigger as the ratio $\frac{L_{load}}{C_{tank}} (= x)$ rises.

$$f_0 = \frac{1}{2 \cdot \pi \cdot \sqrt{L_{load} \cdot C_{tank}}} \quad (4.14)$$

$$x = \frac{L_{load}}{C_{tank}} \quad (4.15)$$

$$L_{load} = \frac{\sqrt{x}}{2 \cdot \pi \cdot f} \quad (4.16)$$

$$C_{tank} = \frac{1}{2 \cdot \pi \cdot f \cdot \sqrt{x}} \quad (4.17)$$

4.2.3.1 Conclusion

It can be stated that the resonance frequency is only determined by C_{tank} and L_{load} . Due to the equations 4.10 and 4.12, the impedance at this frequency only consists of a real part (R_{load}). This means that the current flow through all components at resonance frequency is only determined by R_{load} (at resonance frequency: $I = U_{source}/R_{load}$).

For EMC reasons it is also preferable that L_{load} is at least twice C_{tank} , so that the current gets almost sinusoidal as shown before.

INDUCTIVE HEATING AND TEMPERATURE MEASURING SYSTEM

4 Hardware

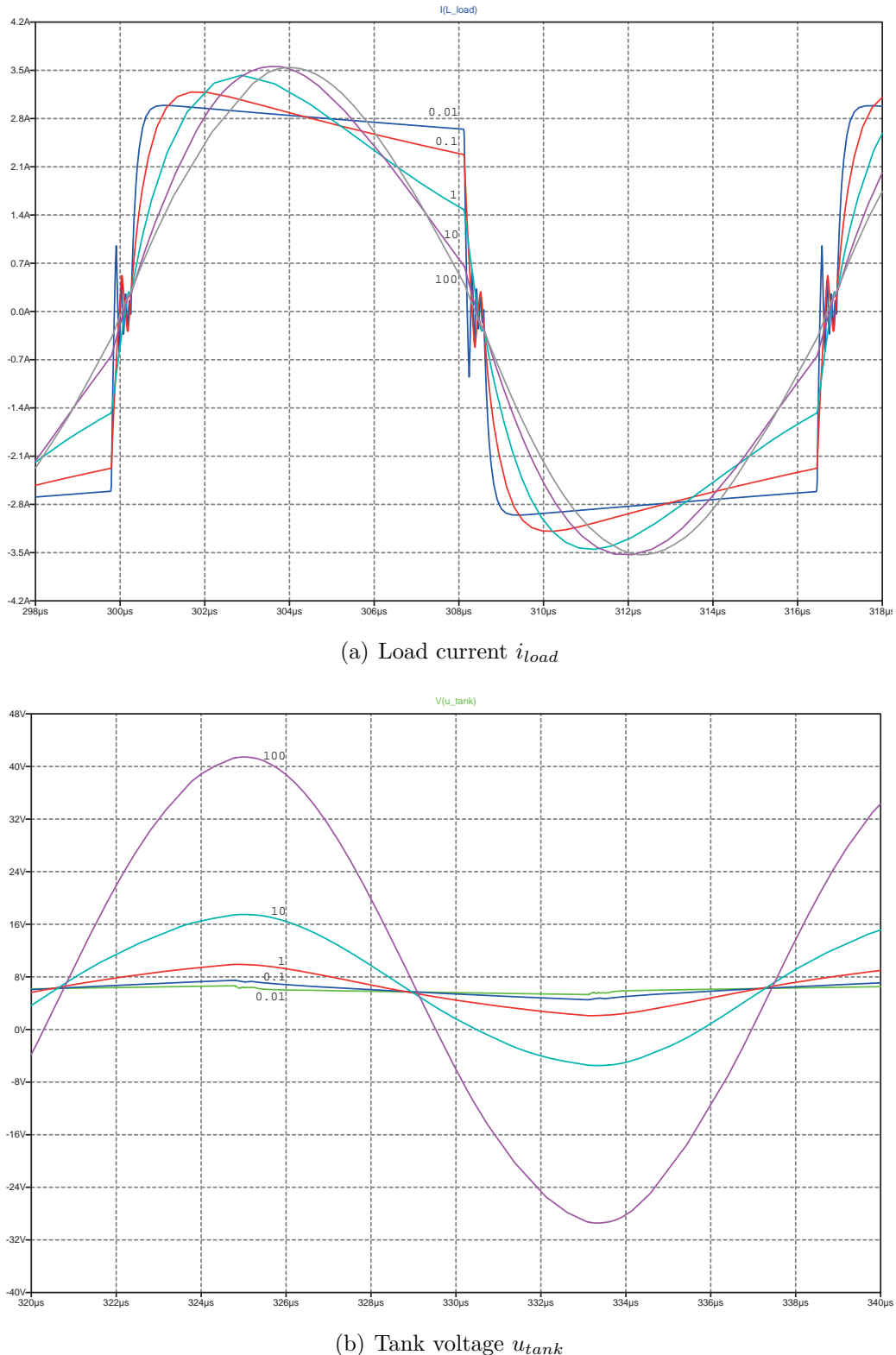


Figure 4.10: Sweep of component values of L_{load} and C_{tank} for the same resonance frequency according to equation 4.16 and 4.17, for $R_{load} = 2 \Omega$, $x = 0.001, 0.01, \dots, 100$ (see labels) and $f_0 = 60 \text{ kHz}$.

4 Hardware

4.2.4 Comparison

If the hardware design is seen in the context of the RepRap project a simple design is preferable. So in the following are comparisons in different points:

Part count: For the serial resonator, only the capacitor for C_{tank} is necessary. This capacitor also filters out all DC components as the C_{filter} dose for the parallel resonator. Three components are necessary for the parallel resonator: C_{tank} , L_{match} and C_{filter} .

Value adjustment and dimensioning: For a sound operation of the parallel resonator, it is necessary to at least adjust the value of L_{match} properly for different combinations of C_{tank} and L_{load} . For the serial resonator circuit this isn't required, but it is necessary to set the value for C_{tank} corresponding to the desired resonance frequency. This is also necessary for the parallel resonator.

The minimum requirement to be met by both is to know at least the approximate value of L_{load} , which in most cases can be calculated accurately enough by the number of wire loops, the diameter and the length of the coil (see equation 2.3).

A properly set parallel resonator circuit could allow for a higher power throughput but it is also limited by the possible values for L_{load} . Since the diameter and length of L_{load} is in most cases only variable in a relative small range, it is necessary to increase the number of loops in order to increase the inductance. It is harder and more time-consuming to build a coil with more loops and also the weight is increased because the length of the coil wire increases with the number of loops. To keep the losses low, the wire diameter must be increased. The additional loops add do not only add weight but also increase the diameter. In the case of a serial resonator the inductance value of L_{load} doesn't influence the current flowing through the coil at resonance frequency. The necessary amount of loops is mainly defined by the desired resonance frequency and as the simulation in figure 4.10 shows, it is necessary that $L_{load} \gg C_{tank}$ stays true. Otherwise, the current isn't sinusoidal but more rectangular, which will lead to EMC problems due to the emission in a wider frequency range. Besides that, the coil should be coiled tightly and at least be as long as the core to generate a uniform field that entirely penetrates the core.

If the power throughput of the serial resonator is high enough, this one is preferable since it is easier to build and there are no extra components to dimension.

Activation: The inverter of a serial resonator needs to carry the same current as the resonator since it is directly connected. In comparison, the inverter of the parallel resonator

4 Hardware

only needs to carry the current that is lost as an effect of the losses in the L_{load} , C_{tank} parallel circuit by the losses of R_{load} .

Because the loads at this setup are relatively low, the dimensioning of the inverter is not a problem. For high power applications this could however be important.

In conclusion it can be stated that a serial resonator circuit is more suitable for the RepRap project due to the fact that it is easier to build and no circuit parts have to be accurately dimensioned. Since the inverter has a relatively wide operating frequency range, the dimensioning of C_{tank} to set the resonance frequency is less critical.

4.3 Capacitor

The used capacitor type for C_{tank} in the serial and the parallel resonator has to involve low dissipation factors (\approx low ESR) to reduce losses in the capacitor and by that also the temperature rise of the component. It also needs to withstand the applied voltages, which can exceed 100 V AC (RMS) in the discussed test setup. For an accurate and consistent indirect temperature measurement it is necessary that the capacity values depend only to a low extent on e.g. the component temperature or the applied voltage. Besides that, the capacity must be available with the desired value, which in this case lies approximately between 100 nF and 1000 nF. It is possible and preferable to use several parallel capacitors to achieve the necessary value. As an effect, also the overall ESR is reduced.

Film capacitors meet these criteria best. Another good choice would be ceramic capacitors which were used in the setup described below.

The used ceramic capacitor is a 2220CC274KAT1A built by AVX (datasheet see [9]). This capacitor is an X7R type that is also available as C0G. This would feature even better properties for this application (e.g. the dissipation factor ($\tan(\delta)$) of the C0G type would be at the maximum 0.001). The used X7R type is rated up to 630 V (DC) and has a dissipation factor at the maximum 0.025 (see datasheet [9] for further information).

A possible film capacitor would be an SMD-PPS produced by the company WIMA. As the name implies, this capacitor is available as an SMD component and in the necessary capacitance, but only for voltages up to 250 V (DC) (160 V (AC)). Under comparable conditions, these capacitors have a dissipation factor ($\tan(\delta)$) of at maximum 0.0025, which is ten times less than the value of the ceramic one used here.

As the plots published by WIMA in figures 4.11 (not objective, since an C0G ceramic capacitor should have quite similar properties as the shown PPS) shows, the PPS type film

4 Hardware

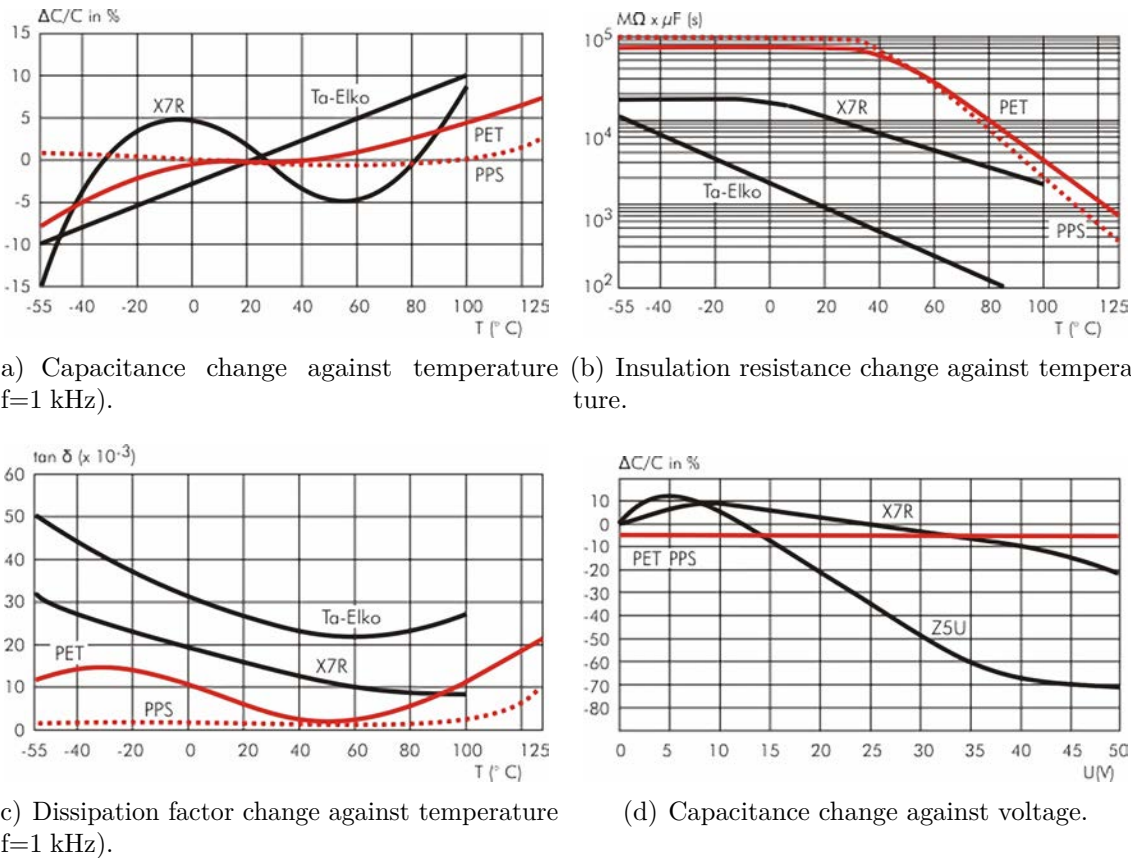


Figure 4.11: Different capacitor type properties plotted against temperature and voltage (source [33], created by WIMA).

capacitor has quite stable capacitance values (figure 4.11(a)), insulation resistance (figure 4.11(b)) and dissipation factor (figure 4.11(c)) over a wide frequency range. The change in capacitance for different voltages is not as dominant either, as figure 4.11(d) shows.

Equation 4.18 shows the correlation of the dissipation factor and the ESR. X represents the impedance of the component, since the dissipation factor could also be used e.g. for an inductor. Equation 4.19 shows the impedance of an capacitor.

$$\tan(\delta) = \frac{ESR}{|X|} \quad (4.18)$$

$$X_C = \frac{1}{j \cdot \omega \cdot C} \quad (4.19)$$

4 Hardware

4.4 Inverter

To create the necessary AC supply for the tank circuit from a DC source, a standard way is to use a half or full bridge inverter as described in the following sections. This is also a common way to supply and control e.g. DC motors or to convert the DC power from solar panels to AC. There are many variations of this type of circuit, especially for solar panels there are costlier setups to improve the efficiency and also setups to reduce the EMC troubles. Since this application is relatively low power and efficiency is no big issue. The circuits described in the following sections show the standard type.

4.4.1 Half bridge

Figure 4.12(a) shows a simple setup for a half bridge inverter. This setup of two switches in a row between Vcc and GND is also called “phase leg”. The serial resonator circuit discussed in section 4.2.3 is used as a load. The switches M1 (low side switch) and M2 (high side switch) are N-channel MOSFETs and the driver logic in this simulation are simple pulsed voltage supplies. The design of the driver logic is discussed below (see section 4.4.4). One important thing to note is that if M1 and M2 are switched on, at the same time this would correspond to a short circuit, which needs to be prevented. To do so, in most cases a dead time is implemented within which neither M1 nor M2 are switched on.

Since MOSFETs are voltage-driven switches, the connection between source and drain is cut off at an N-channel type, in case the voltage level between gain and source is zero. If the level of the gain input is increased relative to the source input, the resistance between source and drain will be reduced until it reaches its minimum at the so-called R_{DSon} , a component-specific value. For most standard MOSFETs the value R_{DSon} is reached if the voltage between gain and source reaches 12 V or more. Despite the fact that MOSFETs are called voltage-driven switches: If the MOSFET is switched it can require high currents at the gain input to reverse the polarity at the gain pin. If the available current at the switching point is too low, the switching time will be increased. Depending on the circuit setup, this can become a problem. The reason is: If the MOSFET is switched, the resistance between source and drain will be decreased continuously so that the flowing current creates ohmic losses. Within the MOSFET, these are transformed into heat, by which the efficiency is reduced. As a result, the MOSFET is stressed or can even be destroyed if the type or the cooling is poorly designed.

4 Hardware

Figure 4.12(b) shows a simulation of the setup from figure 4.12(a). It shows the current and the voltage (U_{l1} to GND) at the load. It is important to note here that the voltage U_{l1} to GND can only be positive.

The sequence is as follows:

- **State 1: M2: ON, M1: OFF:**

The supply voltage is connected to the load. During this time, the load current is positive until the capacity has completely reversed the polarity.

- **State 2: M2: OFF, M1: OFF:**

Both switches are off, the current commutes from M2 to the diode (depending on the MOSFET type, the body diode) of M1.

- **State 3: M2: OFF, M1: ON :**

M1 is switched on and the current commutes from the diode of M1 to the drain source path of M1. The current is negative until the capacity has completely reversed the polarity. At this cycle, no power is added. Only the stored energy in the inductor and the capacitor lets the current freewheel through M1.

- **State 4: M2: OFF, M1: OFF:**

Same as state 2. The current commutes from M1 to the diode of M2.

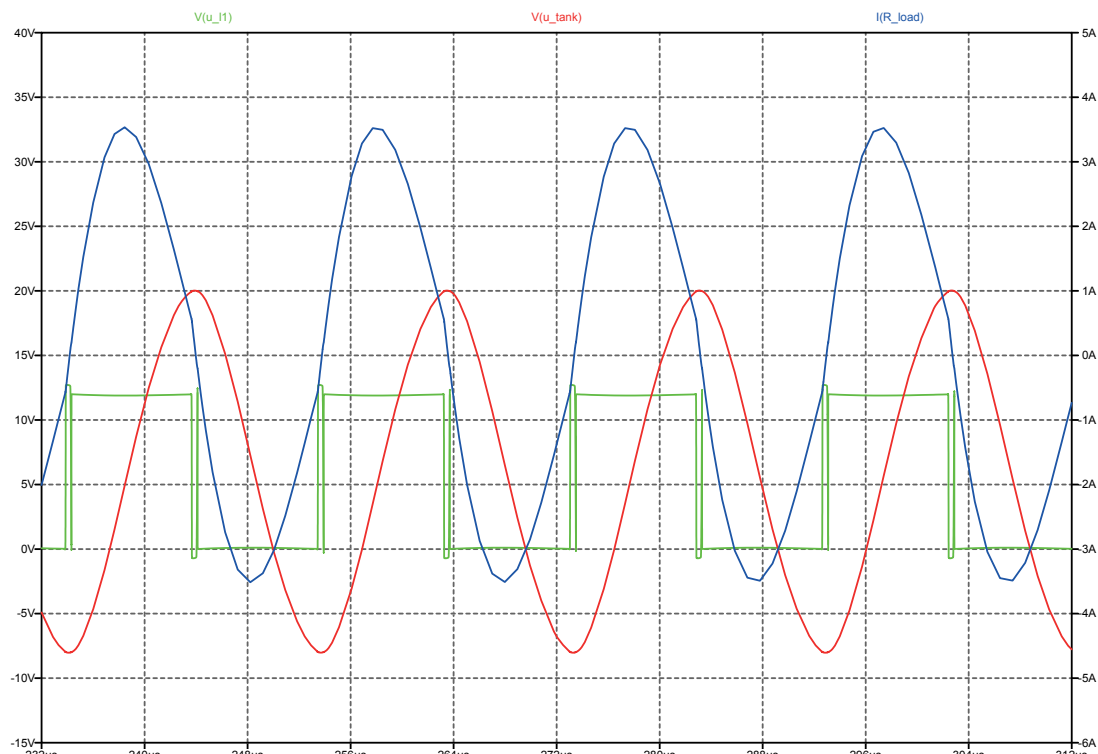
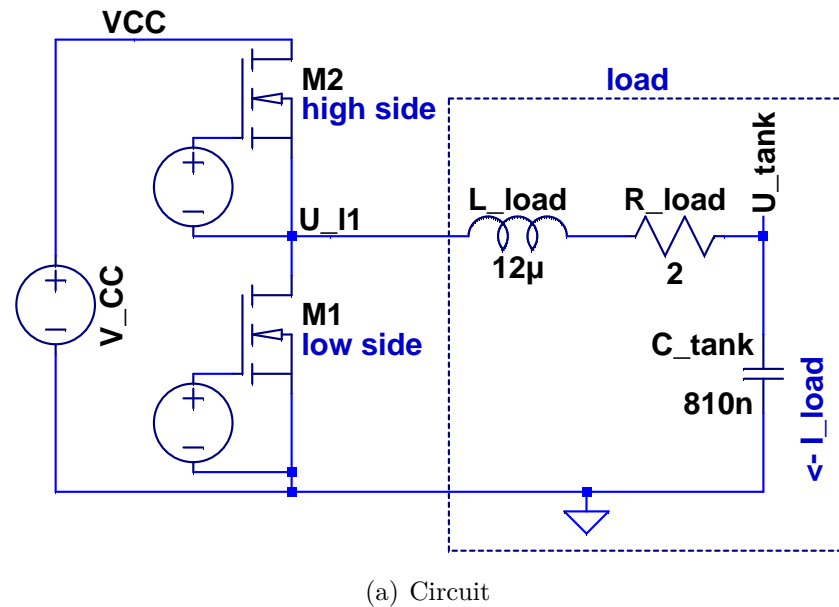
4.4.2 Full bridge

Figure 4.13(a) shows the circuit of a full bridge setup, also called H-Bridge. The setup consists of two phase lags as from the half bridge section 4.4.1. The switches M1 to M4 are controlled in a similar way as in the case of the half bridge. The only difference is that M1 and M4 as well as M2 and M3 are simultaneously switched to the same state (On/Off). If two switches of one phase lag are turned on at the same time, this causes a short circuit. Therefore, the dead time is also necessary for this type.

Figure 4.13(b) shows a simulation of the setup from figure 4.13(a). It's important to note here that during one period the voltage U_{l1} to U_{l2} becomes positive as well as negative. The sequence is the same as for the half bridge, except for the fact that in state 3 the current isn't freewheeling but is instead driven by the negative voltage over U_{l1} to U_{l2} . For this reason, the current flow through the load is twice as big as the one of the half bridge.

INDUCTIVE HEATING AND TEMPERATURE MEASURING SYSTEM

4 Hardware



(b) Simulation for load current (label U_{I1} to GND, I_{load}) (blue), the voltage over the load (label U_{I1} to GND) (green), and the voltage over C_{tank} (label U_{tank} to GND) (red)

Figure 4.12: Half Bridge circuit and simulation.

4 Hardware

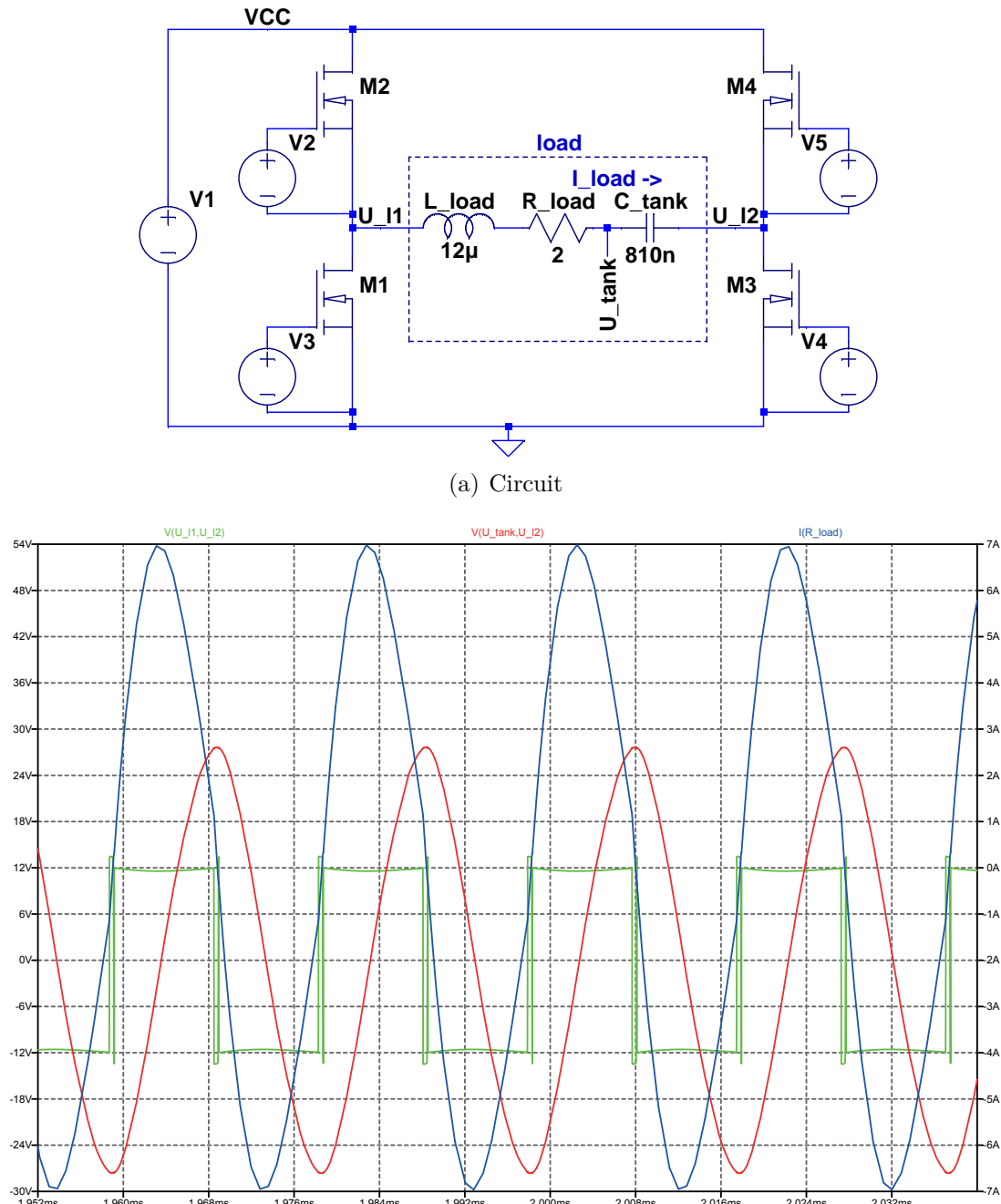


Figure 4.13: Full Bridge circuit and simulation.

4 Hardware

4.4.3 Comparison

As seen in the last two sections, the current flow of the full bridge is twice as big as the one of the half bridge, which also increases the power throughput. The downside of the full bridge is that it requires two more MOSFETs and a costlier control logic. Both phase lags have to be controlled separately because the switches are always switched on or off diagonally. It is for example possible to use exactly the same setup for both phase lags and simply add an inverter at one of the control signals.

A full bridge setup needs about twice as much hardware as a half bridge, increasing not only the cost of the components but also the necessarily bigger PCB. That's why the half bridge is the more preferable option.

4.4.4 Control circuit

To control a bridge circuit it is possible to setup a discrete circuit or to use proper IC's. The second solution reduces the circuit complexity and is in most cases more ruggedized than a discrete setup. The solution involving an IC is in most cases more expensive than an discrete setup but the necessary development work for a prototype would exceed the costs of an setup with an IC by far.

In the following, a half bridge driver based on the IR2184 from International Rectifier is described. According to the datasheet [21], the IC can be used to drive half bridges with N-channel MOSFETs or IGBTs. It also implements the necessary dead time with a fixed value of 500 ns. It can be controlled via CMOS or TTL digital signals with levels as low as 3.3 V. It has two inputs: one to enable or disable the output and one to control the high and low side switches. If an on-signal is applied to this input, the high side MOSFET is switched on whereas the low side is switched off, and vice versa.

A general circuit setup of the IC is shown in figure 4.14. According to test circuit in the application note [22], the so-called bootstrap capacitor between the V_B and V_S pin of the IC should be $0.47 \mu F$ or higher. This minimum value could also be determined via the equation in the application note [22, p. 6]. The application note also shows that the resistor between the gate input of the MOSFET and the corresponding IC output are not essential. They are necessary to move the power losses that occur while charging and discharging the gate capacitance out of the IC (internal resistance of the path) and towards the resistor. However, they can become necessary, e.g. at high frequencies.

The diode between V_{CC} and the pin V_B is called bootstrap diode. According to the application note, it needs to carry about 12 mA and must be able to block approximately the

4 Hardware

magnitude of voltage of the bridge supply, in this case about 12 V. The blocking/stabilization capacitors, one between V_{CC} and the GND(/COM) pin of the IC and one between the drain of the high side MOSFET and the GND are important, as are described in the EMC section 4.9.

Due to the fact that the fix dead time per period is $1 \mu s$ for the used IC, the upper limit of the drive frequency is given by that. Since each switching cycle produces losses in the MOSFETs and in the drive circuitry, this would also limit the frequency. However, in this setup the dead time is the limiting factor. This is at about 1 MHz at which the on-time of both switches would be zero due to the dead time.

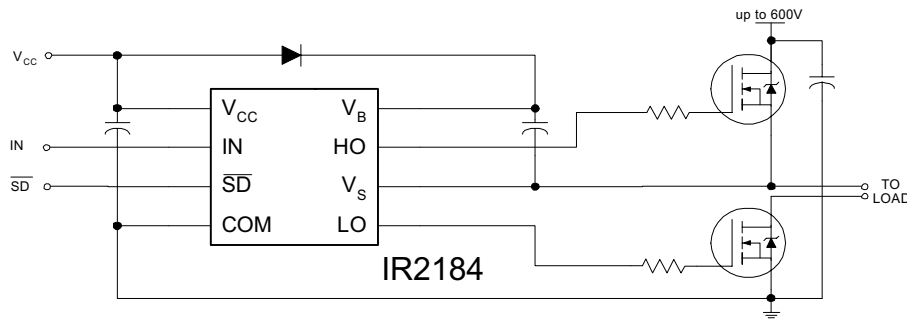


Figure 4.14: Circuit diagram for the IR2184 ([21, p. 1]).

4.5 Phase measurement

As shown in the section 4.2.3 about the series resonator circuit, the phase shift between the voltage C_{tank} to GND and U_{source} to GND at resonance frequency is 90° . Due to the relatively high value of R_{load} , the phase transition between 0° and 90° is relatively wide and slow. If this phase shift could be measured, this would allow for a good way to control the resonance frequency.

To measure the phase it is necessary to know the frequency of the signal and the time difference between the zero crossings of two rising or falling edges of U_{source} and U_{tank} (compare figure 4.8). The frequency is known since it is given by the microcontroller.

Since the voltage level of U_{source} and U_{tank} are both far too high to directly connect them to the microcontroller, it is necessary do break them down without influencing the source signal too much. A very simple and cheap way to do that is to use a high-ohmic resistor with an Z-diode (Zener diode) against GND, as shown in figure 4.15(a) on the left side of the phase measurement circuit. If the Zener voltage is chosen properly to suit the logic level between 4 and 5 V, the Zener diode limits the maximal positive voltage to the value

4 Hardware

of the Zener voltage. Owing to the fact that a Zener diode operates like a normal diode if the anode voltage is higher than the cathode voltage, the Zener diode also limits the negative voltage to at least about -0.7 V, depending on the type of Zener diode. Most digital circuits can withstand such a small negative voltage.

If this Zener diode is connected directly to the desired signal, this would produce a high current flow through the diode and a voltage drop at the signal, resulting in a malfunction of the entire circuit. If a high-ohmic resistor is connected to the signal (see figure 4.15(a)), the current is limited by the resistor and by that the influence on the source signal is minimal.

In the simulation seen in figure 4.15(b), the blue and green signals show the output of each serial circuit, consisting of a resistor and a Zener diode. As the figure shows, both signals are limited to the necessary voltage boundaries. Also, it shows that the signal created by U_{source} (blue) has sharp edges compared to the one created by U_{tank} (green). This occurs due to the fact that U_{tank} is purely sinusoidal, which means that the signal doesn't cross zero very steeply. Because the Zener diode only cuts off the signal above a certain voltage level, the output signal within these boundaries are almost the same as the input signal. Since most logic inputs detect a 1 or 0 always at the same voltage level and because the gradient of a sinus wave is relatively high at the zero crossing, the resulting error is relatively small and constant.

To measure the time difference, it is possible to directly use the timer of the microcontroller. Most microcontrollers only allow to drive the timer clock with the same frequency as the system frequency, which is in most cases around 20 MHz. Since it is necessary to measure the phase between 0 and 180°, it would correspond to half the period time of the signal (see equation 4.20). As the time can only be divided in steps of the size of the system clock, the resolution for one degree could be calculated as shown in equation 4.21. If a system clock of 20 MHz and a signal frequency of 100 kHz is given, this would correspond to a resolution of 1.8°. Since in most cases the system clock is far lower than the described 20 MHz and because the error also depends on the signal frequency, another solution without these dependencies would be preferable.

$$180^\circ \hat{=} \frac{1}{f_{signal} \cdot 2} \quad (4.20)$$

$$\begin{aligned} x^\circ &\hat{=} \frac{1}{f_{system}} \\ \Rightarrow x^\circ &= \frac{180 \cdot 2 \cdot f_{signal}}{f_{system}} \end{aligned} \quad (4.21)$$

4 Hardware

To achieve this, both signals are fed into an XOR gate (the gate output is 1 if only one of the two inputs is 1). The output signal of the XOR gate is plotted as a red signal in figure 4.15(a). If the setup is considered ideal, then at 0° phase shift the average on-time of the XOR output would be 0%. At $\pm 180^\circ$ it would be 100% and between these two, the on-time would rise linearly with the phase.

By adding a low-pass filter to the XOR output, this signal can be converted into a steady analog signal. The voltage range of this signal depends on the used XOR gate. In the case of the simulation in figure 4.15 it is 0 to 1 V. For the XOR gate used in the test setup, the 74HC86, it is 0 to 5 V. As most microcontrollers feature at least a 10 bit ADC with a selectable reference voltage (which determined the voltage input range of the ADC), it is possible to measure the phase shift with a resolution of about 0.18° (see equation 4.22), which is independent of the single and system frequency.

Depending on the configuration of the values of R and C, the RC filter is either fast or has a low ripple on the output voltage. Since both are desirable for the setup, it could be necessary to use other filter types for the next generation setup. For the prototype, the values for RC are determined in a few simulation steps so that it has a rise time off less than 1 ms. To counteract the ripple on the signal, it is sampled several times, as described below in section 5.3.

$$180^\circ \hat{=} 2^{10} \quad (4.22)$$

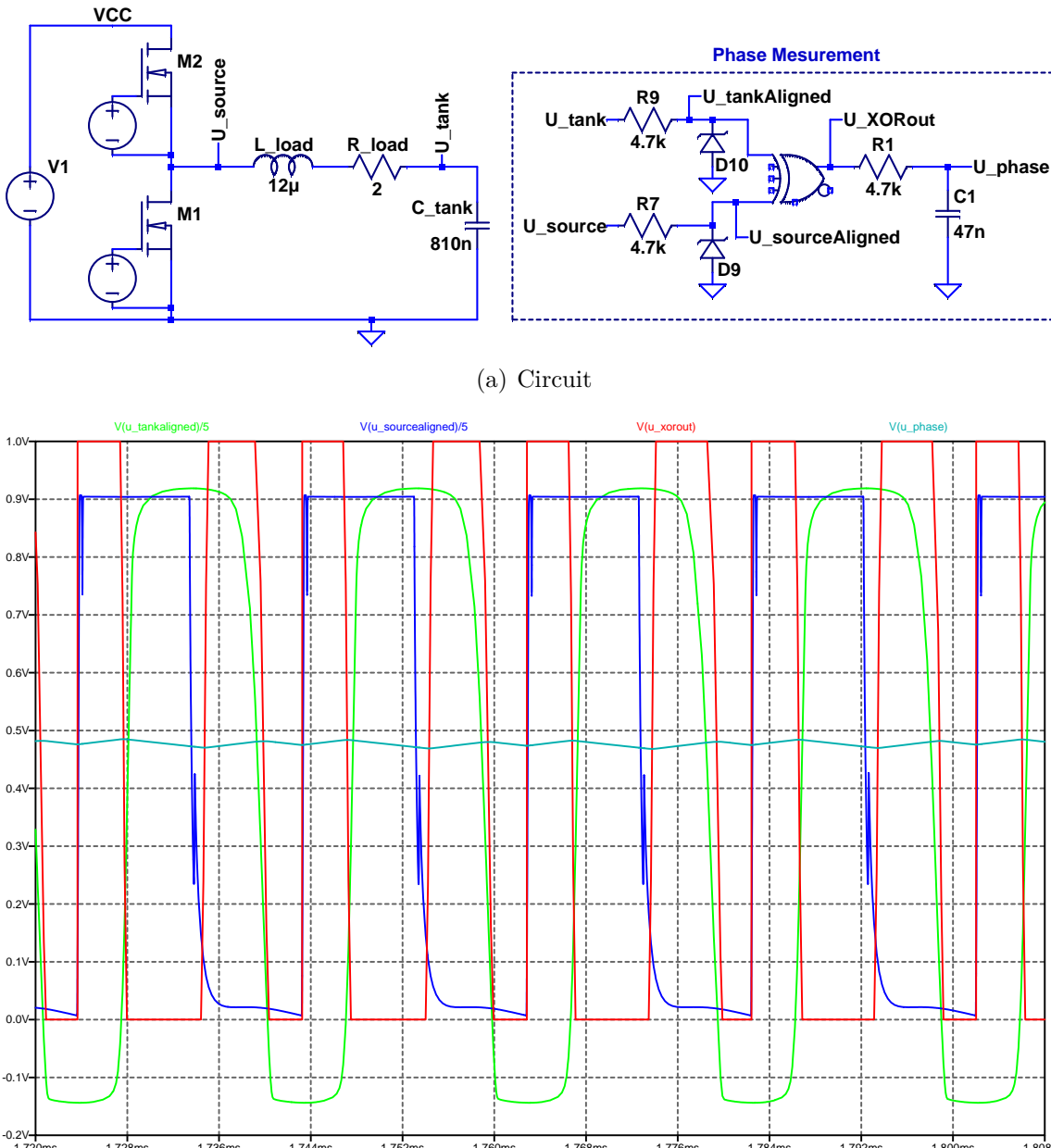
$$0.1758^\circ \hat{=} 1$$

4.6 Tank voltage measurement

As described in section 4.2.3, the voltage amplification has a peak at resonance frequency. To measure this tank voltage for development purposes, it is necessary to convert the AC tank voltage (being too high to be directly connected to the microcontroller ADC) to a measurable DC voltage.

To do so, the circuit shown in figure 4.16(a) is used. The resistors R4 and R5 are a simple voltage deviate reducing the voltage amplitude. It is also used as current limitation for the further part. The diode D6 is used to align the voltage by cutting off everything below 0 V, which leaves only the positive half of the sin wave. C2 then smoothes the aligned voltage to a DC voltage. R6 is necessary to discharge the capacitor if the voltage level drops, since the diode would block any current in direction of R5. Furthermore, the impedance of the microcontrollers ADC I/O is too high for this purpose. The Zener diode D7 is used to

4 Hardware



(b) Simulation of the aligned tank voltage (green) and source voltage (blue). Both are scaled along the vertical axis by the factor 0.2. Output of the XOR gate (red) and the output of the RC low pass filter (cyan).

Figure 4.15: Phase measurement circuit and simulation.

4 Hardware

protect the microcontroller I/O from over- or under voltage. Since the voltage could gain high levels if e.g. the metal cylinder is removed, which would reduce R_{load} . By that the voltage amplification rises, as seen in figure 4.9(a).

For detection of resonance, the absolute value of the tank voltage (U_{tank}) is not required since it is only necessary to detect the maximum. Due to this fact, all component values were determined in several simulation steps to suit the range of the ADC input. As seen in the simulation in figure 4.16(b), the output voltage has a relative high ripple. This can be reduced by increasing the value of C2 at the expense of the reaction time to changes. As the absolute value is not necessary and it is only interesting for purposes of development, the signal can be measured several times and then averaged.

4.7 Setup

Figure 4.17 shows the complete final setup and all components that are also seen in the flow diagram in figure 4.1. Images of the different enlarged parts are shown in the appendix A.1 as well as on the data storage.

The setup shows a serial resonance circuit (section 4.2.3) with a half bridge driver (section 4.4.1). In this case, a lab power supply instead of an ATX PC power supply is used because the first one allows the limitation of the current. This is very practical during prototyping because a possible short circuit can't destroy the power supply. The current is also limited to a set value which can protect the circuitry. Below, the different markers of figure 4.17 are described:

1. AVR Dragon by Atmel [3] is a debugging and programming device for different Atmel controllers. It allows debugging and programming of the Atmega 324p via JTAG.
2. A small PCB populated with an FTDI FT232RL and all the necessary periphery parts for this IC. This enables communication via serial interface between microcontroller and PC via USB. In this setup it is connected to the USART of the microcontroller and to the PC at which it is recognized as a virtual COM port.
3. BM02 module, a small PCB containing the microcontroller Atmega 324p including all the necessary peripheral components, as well as the connection for JTAG, ISP and some I/Os available on pinheads. In this setup, the microcontroller is connected to an external 12 MHz oscillator. For a more thorough description see section 4.7.1.

4 Hardware

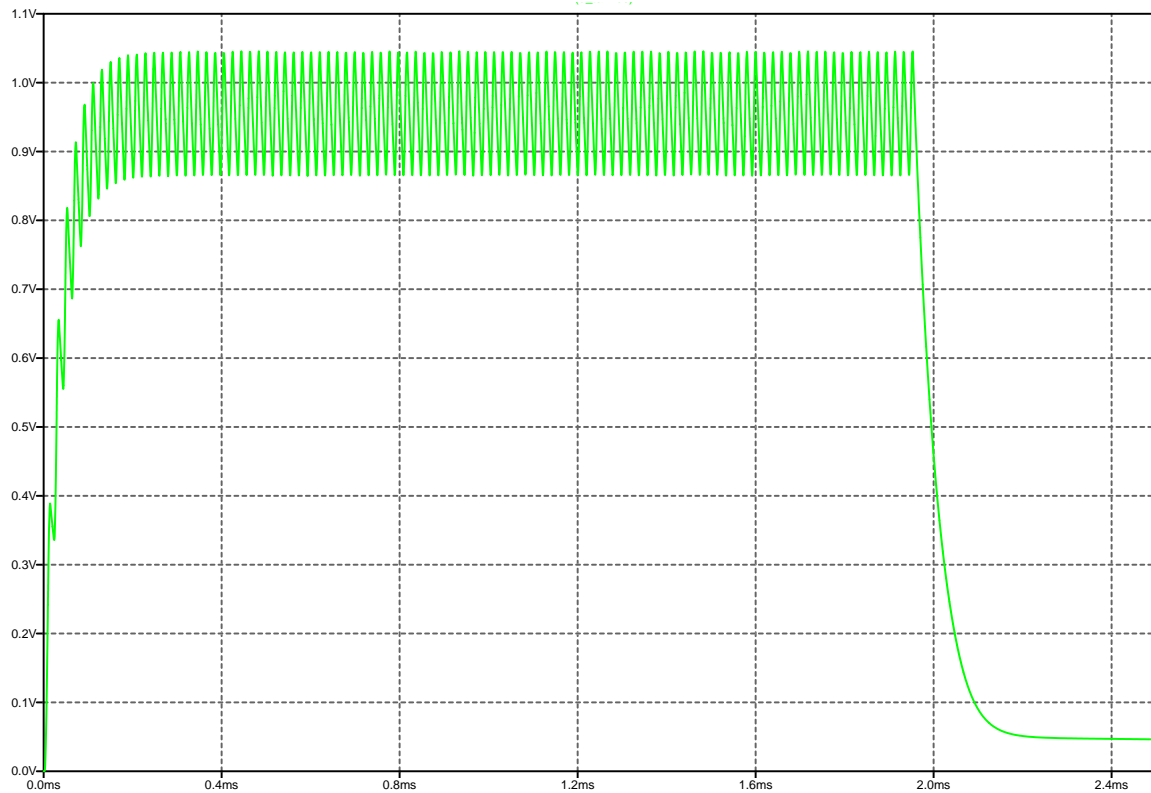
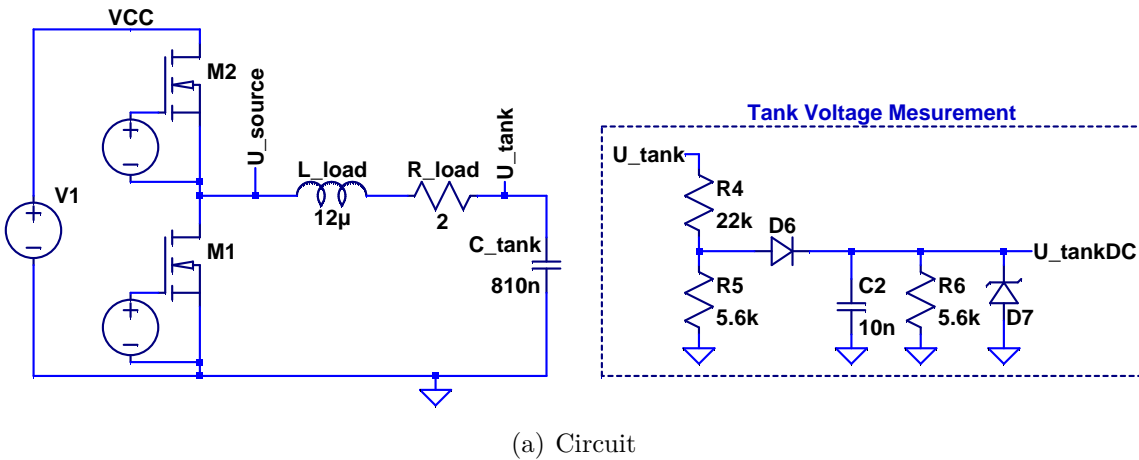


Figure 4.16: Tank voltage measurement circuits and simulation.

4 Hardware

4. DDS based on the AD9833 IC by Analog Devices [1] an fanned out on a small perfboard, connected to a 20 MHz oscillator and all necessary periphery.
5. Darlington transistor array ULN2803A, an eight channel transistor array which can be connected directly to logic level signals. It switches the corresponding output to GND if the input is 1. In combination with an pull-up resistor this is used as a safety measure to protect the costly DDS.
6. Half bridge driver IR2184 by International Rectifier [5]. This IC allows to drive the phase lag as described in section 4.4.4.
7. The Quad 2-Input XOR gate 74HC86, used for the phase measurement as described in section 4.5.
8. NTC-thermistor sealed in a glass body B57560G104F, which allows temperature measurement in a range between -55 and 300 °C. It is used to measure and observe the temperature while development and testing but not to control the temperature. It is pocketed in a metal cylinder and held in place by a piece of Kapton tape. The sensor doesn't plug the entire hole. This is necessary for the cooling as described in section 4.8.
9. Glass tube with a steel cylinder (core) inside, which is heated and the temperature is measured.
10. The primary coil made of enameled copper wire and it is the inductance for the resonator circuit. The setup is described in chapter 3.

4.7.1 BM02-Modul

The BM02 module (see figure 4.18) is a hardware component developed by Arcus-EDS [2] and used in several of their products. It contains the controller (Atmega 324p, datasheet see [8]) as well as another IC which is not used and not necessary for this work. It also contains the necessary peripheral components for the microcontroller, such as capacitors and supply voltage preparation.

In addition to separate connectors for JTAG (10-pole) and for ISP (6-pole), it also features two 10-pole pinheads for several I/Os as well as for GND and VCC of the microcontroller. Figure 4.19 shows the available pins of the BM02 module. For this setup several I/Os that would have been necessary were not available on the pinheads. These were simply connected to the bread board via enameled copper wire.

4 Hardware

The available JTAG pinhead can be directly connected to the AVR dragon via flat cable for in-system debugging.

4.8 Cooling

If the inductive heating system is operating without any heat dissipation (which in the future should be done by the plastic filament), the entire setup consisting of primary coil, glass cylinder and metal cylinder would simply heat up until the entire nozzle almost has the temperature of the heated metal cylinder. Because of this, the created heat isn't actively transported away. If both ends of the glass tube are open, there is a very weak stack effect, but that is by far not enough to cause the primary coil to heat up to a very high level.

If the setup is operated in an uncooled state for too long, the enameled copper wire gets damaged permanently because most standard wires only tolerate a maximum temperature of about 150 °C, as seen in figure 4.20.

If this happens, the copper wire creates short circuits between some of the loops. By that the inductance of the coil changes and the resonance frequency of the serial resonator increases as described in section 4.2.3. This would be acceptable to a certain point, as the resonance frequency controller would simply resettle to this new frequency and the temperature measurement system could simply be recalibrated. But since the connection between two short circuit loops has in most cases a much smaller conductive diameter, this would increase the resistivity of the coil, so that the heat generation of the coil due to ohmic heating would increase. Owing to the named reasons and the obvious effect that this would be an irreversible effect, it should be avoided.

For the test setup this is done by two fans as seen in figure 4.17. One cools down the outer primary coil and the other simulates the load. In the future, the load would be the filament. If no material is extruded, the heat transportation would be very limited. It might therefore be necessary to switch off or reduce the inductive heating, which shouldn't be a problem in most cases, because the time to heat up the nozzle with inductive heating should be far less than one minute. Another favorable design feature could be a slotted support material for the coil as described in chapter 3, e.g. in combination with an fan. This would limit the heat transportation from the metal cylinder to the coil.

4 Hardware

4.9 EMC

In this section the load circuitry is discussed from an EMC viewpoint and some suggestions for later setups are made. It is important to note that there is no electrical connection as ideal as the ones used in the simulations. Each electrical connection has at least an ohmic resistance. As long as it is no superconductor, due to the physical properties of the conducting material, and depending on the setup, it also has parasitic capacitance and inductance, which is important for the following considerations.

Among other factors, the intensity of the magnetic field caused by a circular current-carrying conductor depends on the enclosed area and the change in current against time. Therefore, it is important to keep the area of loops with high current gradients as small as possible in order to reduce the emission.

In this setup the corresponding loops in figure 4.21 are marked red. The left loop is confined by C_{stab} , the stabilization capacitor of the setup. If this component was neglected, the loop would go through the power supply, which in most cases is located further away. With non-ideal connections and a non-ideal power source, a high current gradient at the switch M2 could create a voltage drop at the drain of M2 (VCC). This voltage drop at the VCC could affect the driver IC of the phase lag. For instance, the IC could reset and switch off both switches, which would at first cut off the actual flowing current (high $\frac{di}{dt}$). If the VCC is then stabilized, the IC would activate the corresponding switch again and after that, the VCC would drop again. If C_{stab} is added with short connections to drain (M2) and source (M1) of the two switches, the influence of these short connections is in most cases small and can be neglected. The capacitor provides the energy necessary for fast current changes. In most cases this stabilization capacitor consist of several different parallel capacitors to reduce the influence of the ESR. It is also used at the supply input of different other ICs such as microcontrollers, and also at the driver IC to prevent supply voltage from dropping. Most ICs do not steadily draw the same power, but in most cases it is some kind of clocked process with a fluctuating power draw.

The primary coil is not directly located upon the PCB and has to be connected through wires. These wires should be tightly together to reduce their enclosed area. It is also recommend to twist them. This creates counteracting magnetic fields which also reduce the emission. The reason for this is: If a twisted cable is viewed from one side, two twists would appear as an eight (∞). At one twist, the current at the top would flow e.g. to the right and at the bottom to the left, in the next loop it would be the other way round. Owing to this fact, the magnetic field would be orientated out of the plain in one twist and point into the plain in the other, so the field would be bound tightly to the wires. The path marked green in figure 4.21 (as implied by the routing) should be short and the

4 Hardware

trace should be connected directly to the corresponding source pin of the switch. If there is a common used electrical connection (e.g. M1 source to GND of driver IC, shared with the power path of the phase lag), it could occur that the voltage drops over this common path. Due to a high load, the current causes the reference voltage of the driver IC to be lower than the actual level at the source PIN of the MOSFET switch. By that it can happen that the control signal at the gain input doesn't reach the necessary level to switch it on completely. This can mean that either the switch is not turned on at all. Alternatively, this can end up in a stage were the losses within the switch are higher. In case of the M2 switch the V_s pin of the driver IC should be directly connected to the source pin. If a common ground is used for the M1 switch and the driver IC, the source and the GND pins should be close to each other and the connection should feature a low impedance, at least a wide trace. This effect mainly depends on the magnitude of the load current. Since in the actual setup this current is relatively small, this effect is not very dominant.

In order to reduce the voltage gradients over the switches M1 and M2, so-called “snubbed circuits” can be used as shown in figure 4.21 by R1 C1 and R2 C2. They limit the voltage gradient ($\frac{dV}{dt}$) and increase efficiency. As the operation voltage is only 12 V and this small increase in efficiency isn't crucial to the prototype, these were neglected.

If the emissions are too high, it might be necessary to shield the primary coil. To screen a magnetic field, it is necessary to use ferromagnetic material, e.g. ferrite, to bundle the magnetic field in this shield, since magnetic fields can only be diverted and not shielded. This would also increase the efficiency of the setup, but the necessary shield would be relative heavy.

Figure 4.22 shows the spectrum of the current i_{load} seen in figure 4.10(a). The purple line represents the spectrum of an almost sinusoidal current ($x=0.01$) and the green one belongs to the nearly square wave current ($x=100$). Both are derived from the signal with the frequency of 60 kHz. It can be seen that the sinusoidal current produces a relatively clean spectrum with a spike only at the signal frequency 60 kHz. There are very small spikes at higher frequencies due to a not perfectly sinusoidal shape, but they are not worth mentioning. By contrast, the square wave current also has a main spike at the signal frequency as well as several other spikes at 180, 300, 420, 540, ... kHz (every second harmonic). This way, the sine wave produces interferences at only one frequency, compared to the wide range of the square wave.

INDUCTIVE HEATING AND TEMPERATURE MEASURING SYSTEM

4 Hardware

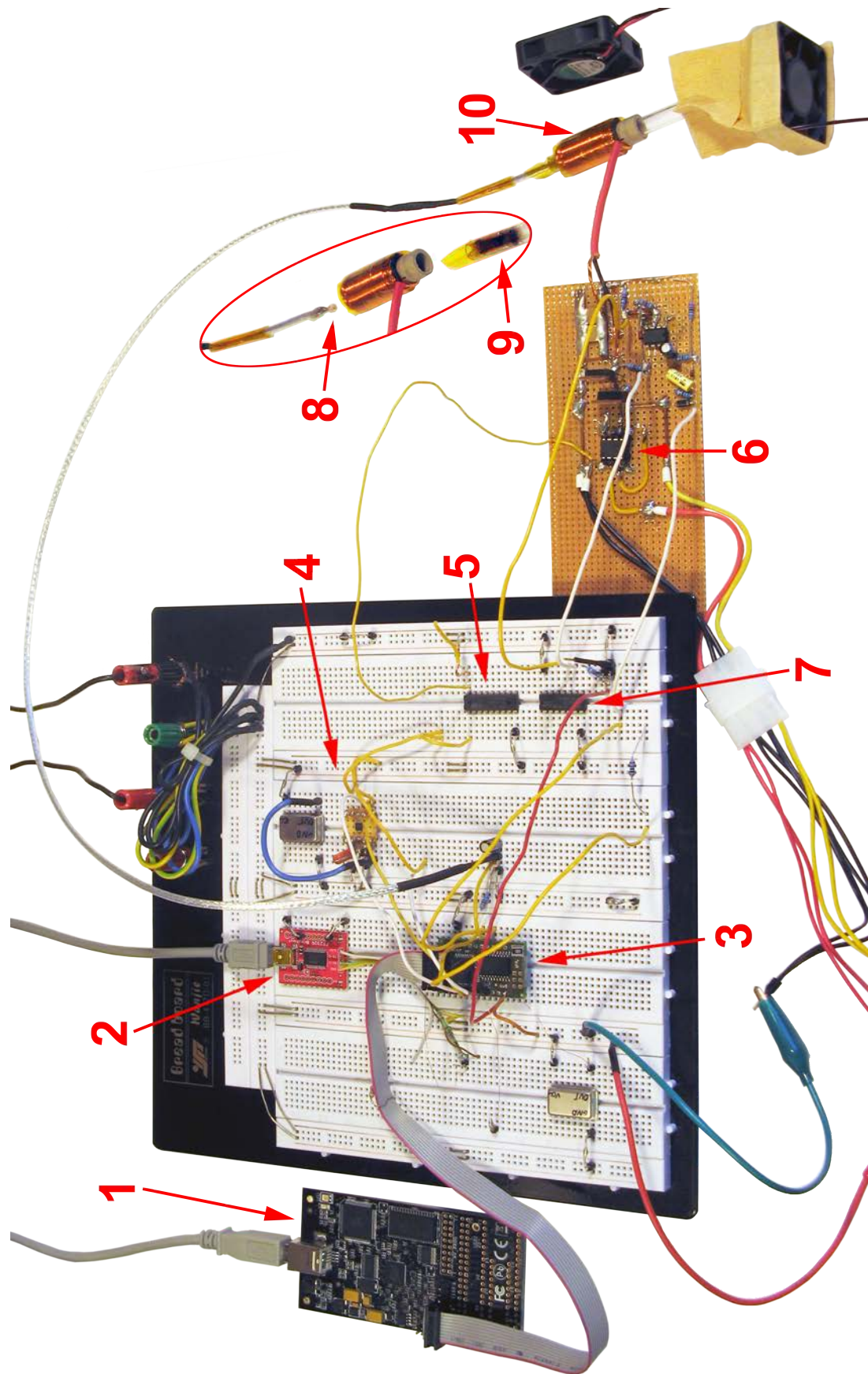


Figure 4.17: Complete hardware setup (see section 4.7 for label description).

INDUCTIVE HEATING AND TEMPERATURE MEASURING SYSTEM

4 Hardware

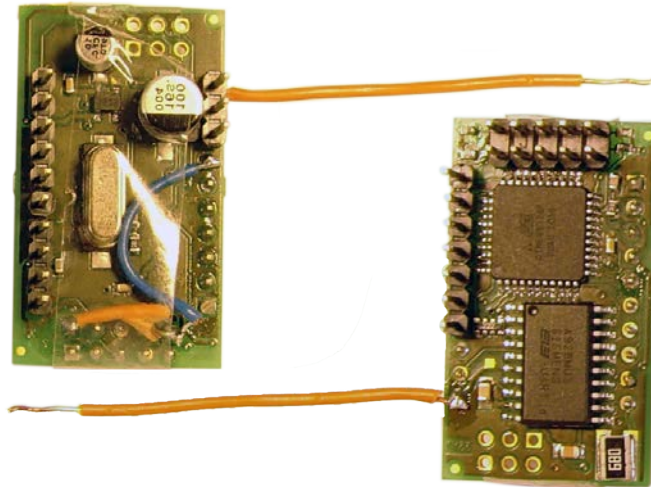


Figure 4.18: BM02 module with available 5 V VCC at the orange wire and some cable bridges due to errors in the layout of the JTAG connector (left: bottom; right: top).

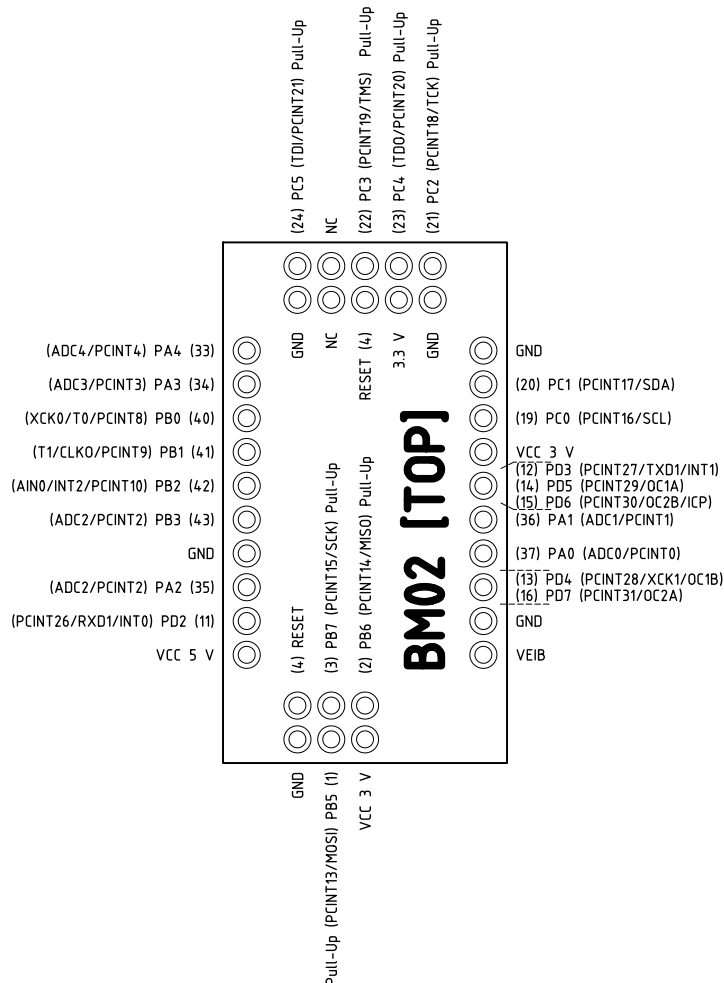


Figure 4.19: BM02 pin configuration (TOP view) (identifier see [8, p. 2]).

4 Hardware



Figure 4.20: Magnified view on an overheated enameled copper wire.

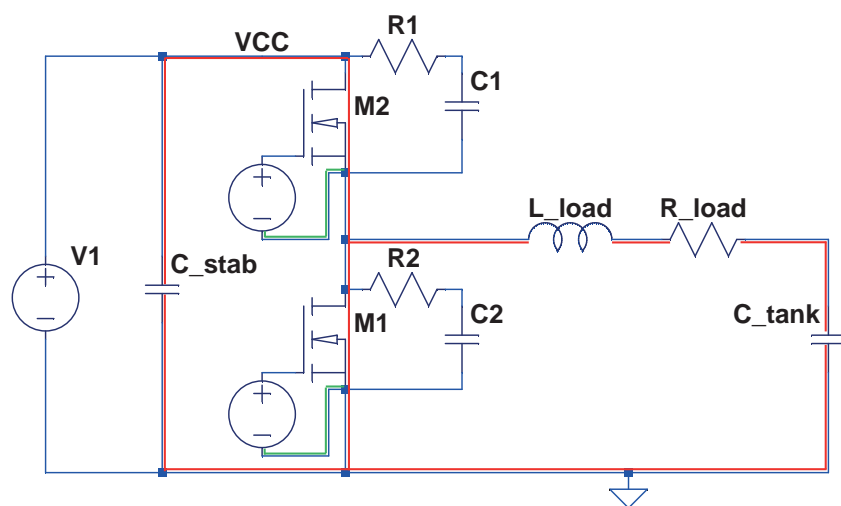


Figure 4.21: Load circuit with snubbed and stabilizing capacitor.

4 Hardware

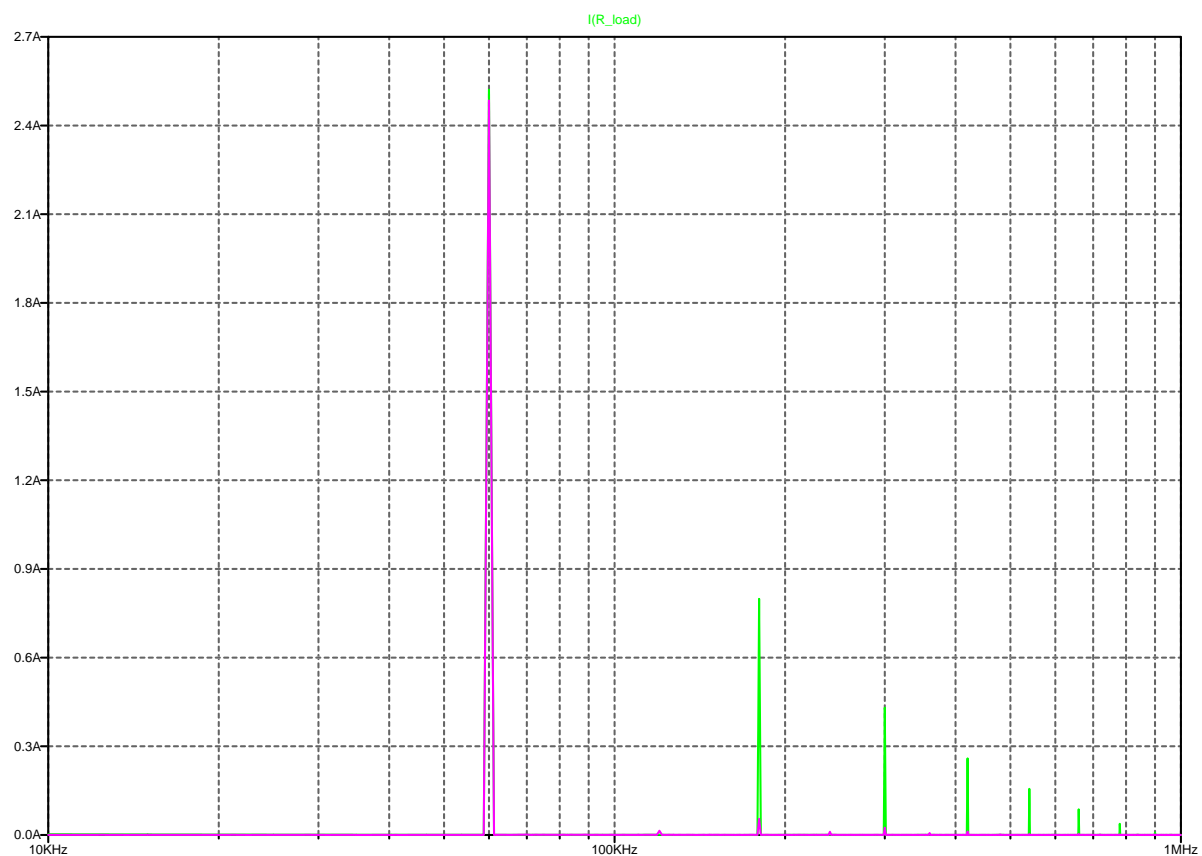


Figure 4.22: Spectrum of the current i_{load} as seen in figure 4.10(a), for $x=100$ in green and for $x=0.01$ in purple.

5 Software

5 Software

The software was created for development and testing which means that it is neither completely tested nor ready to be used in production. It is a collection of software necessary to test the setup and prove its functionality.

The software was written for the Atmega 324p in C. If necessary, porting it to other Atmega microcontrollers should be possible as long as the controller supports the necessary hardware (e.g. the timer).

As the software hierarchy is flat and most of the modules (*.c and *.h files) are relatively simple and straight forward, each of the modules is described separately in one of the following sections. They are labeled with the respective filename in the section title, which is the same for the *.h and the *.c file. These files can be found on the data storage.

5.1 global

Contains global definitions such as clock frequency F_{CPU} and others, which are used in all modules. This should be included in each module.

5.2 AD9833

This module is used to control the DDS AD9833 IC. For the general functionality of the DDS, see section 2.6. This module is based on the library of Martin Wende (cf. www.fritzler-avr.de/HP/Librarys/AD9833_his.php, last check: August 28, 2012) and only small changes were made.

This module is necessary to control the DDS IC and by that to control the frequency signal for the inverter stage. The DDS allows for the production of a very accurate and steady frequency output which can be set with a very fine resolution of less than 1 Hz, depending on the clock supply of the AD9833.

The square wave signal necessary to control the inverter stage could as well be directly

5 Software

created by means of the microcontroller, e.g. with the internal 16-bit timer as described in section 5.5. However, this section also shows that the resolution would be far lower than with a DDS. For the development process, this solution is more suitable due to its simplicity and its higher accuracy. For later work it is necessary to check whether the frequency generation can be solved in a different way or if the direct frequency generation via the controller would work, since the DDS ICs are relatively expensive.

The usage of this library is relatively simple. It allows to be used either with a hardware or a software SPI. Because the hardware SPI interface of the BM02 module is not directly available at the pinheads, the software SPI was used and the necessary settings were carried out in the AD9833.h file defining the software SPI pins as well as the frequency of the AD9833's clock supply. This is necessary because according to the datasheet of the device [7, p. 15], the value of the frequency register (FREQREG) is calculated as seen in equation 5.1. This also shows that the clock supply frequency of the IC is necessary to calculate the value of the DDS IC's frequency register. These calculations are made using the library. In this, there are functions available to directly set the desired frequency.

Listing 5.1 shows an example usage of the library. First, it is necessary to initialize the library (line 4). After that, the desired signal shape can be chosen (line 5). As seen in figure 2.9, there are two frequency registers available that can be selected via `DDS_reg`. The value of these registers can be set using `DDS_freq`, wherein the first parameter is the desired output frequency and the second one is the corresponding register. In case the frequency needs to be changed it is possible to directly call `DDS_freq` and write the value to the actual active frequency register. To minimize interference while writing the register, it is possible to write into the inactive register and then switch it via `DDS_reg`.

The settings for the output phase is similar to the one of the frequency but since it is not necessary for this setup, this will not be described here.

$$f_{out} = \frac{f_{MCLK}}{2^{28}} \cdot FREQREG \quad (5.1)$$

$$FREQREG = \frac{f_{out} \cdot 2^{28}}{f_{MCLK}}$$

- f_{out} : Output frequency of the AD9833
- f_{MCLK} : Frequency at the MCLK pin (pin No. 5) of the AD9833
- 2^{28} : Phase accumulator maximum of the AD9833
- FREQREG: Register value of the AD9833 to control the output frequency.

5 Software

```

1 #include "AD9833.h"
2
3 int main(void){
4     DDS_init();
5     DDS_signal(RECHTECK);
6     DDS_reg(FREQ0);
7     DDS_freq( 31415, FREQ0);
8     while(1){}
9 }
```

Listing 5.1: Usage of the AD9833 module.

5.3 adc

This module handles the initialization and the measurement process of the ADC. It also implements some additional features such as the possibilities to measure several values and to calculate the average, as well as the oversampling method described in section 2.5. Listing 5.2 shows the function `ADC_Read`. As apparent in line six to nine, there is a delay of several microseconds. This is necessary to allow the capacitors (ADC equivalent circuit diagram [8, p. 249]) to settle down at the value of the newly selected channel. Without this delay, the measured value would include a large error. If the connected circuit has a low impedance, this delay can be reduced or removed entirely as the level change of the capacitor voltage is a lot faster.

Through the seen implementation, the function waits until the conversion is complete (so-called busy waiting). For further work it could be carried out using an interrupt routine. In this case, the function would simply start the conversion and the interrupt routine would be called as soon as the conversion is complete, so that the value could be read. Due to the fact that the conversion time for one reading lies in the range of only several $10 \mu s$ and that it is much easier to handle without interrupt, only this implementation was made.

The implemented oversampling method takes 512 samples and calculates the 12 bit value. According to 2.5, it would only be necessary to make 4^2 samples for each measurement in order to increase the accuracy by 2 bit. However, to counteract the high ripple of the signal, the number of samples was increased since this routine is only used for measurements in which the measurement time is not relevant (for example the measurements in figure 6.5).

5 Software

```

1  uint16_t ADC_Read(uint8_t channel)
2  {
3      uint16_t result = 0;
4      uint16_t cycles = 0;
5
6      ADMUX = (ADMUX & ~(0x1F)) | (channel & 0x1F); // Select the channel
7      _delay_us(5); // wait to let the capacitors settle on the new selected channel
8
9      ADCSRA |= (1<<ADSC); // start a conversion
10     _delay_us(10);
11     while ( ((ADCSRA & (1<<ADSC))) && (MaxADCcycles > cycles) ) // wait while
12         conversion is running
13     {
14         cycles++;
15     }
16
17     if (MaxADCcycles > cycles) {
18         result = ADCW;
19     }
20     else
21     {
22         ADCSRA &= ~(1<<ADSC);
23         result = ADC_FAIL;
24     }
25     return result;
}

```

Listing 5.2: Function to measure the voltage level at an ADC channel.

5.4 FrequencyMeasurement_raw

Module to measure the frequency at a particular pin of the microcontroller via a 16 bit timer over several periods of the signal and to average it. This module is not used and due to this, it is not further described here.

5.5 FrequencyOutput_raw

Module to generate a frequency at an particular pin of the microcontroller via a 16 bit timer. Due to its inaccuracy it wasn't used and has been replaced by the DDS.

The 16 bit timer of the used microcontroller (in this case timer 1) provides a configuration at which it toggles a special I/O pin between VCC and GND and it resets the counter to 0 if the counter value reaches the set value in the OCR1A register (domain 0 to 2^{16}). The timer clock at which it counts can either be provided by the used CPU clock (F_{CPU}). It is possible to set a prescaler at which the clock signal is divided (1, 2, 4, 8, ...), which in

5 Software

this case is 1 so that the CPU clock is used as timer clock. Alternatively, the clock can be provided by an external source, but with the limitation that the frequency has to be lower than half of F_CPU.

Since the timer can only count with the speed of F_CPU, the output has a quantization error. The toggle frequency of the output pin can be calculated using equation 5.2. The step size is given by equation 5.3. Figure 5.1 shows the toggle frequency of the output pin, plotted against the step size up to the next lower value of OCR1A for three different values of F_CPU: 8 MHz (the maximal frequency of the controller's internal oscillator), 12 MHz (the used frequency of the external oscillator used in this setup), and 16 MHz (the maximal possible frequency of the used microcontroller). Example: For a desired output frequency (= toggle frequency divided by two) of 100 kHz, the step size for the necessary toggle frequency of 200 kHz of the maximum F_CPU is at about 2.5 kHz. Even for the minimal recommend frequency of 20 kHz, the step size is still at about 100 Hz. The necessary accuracy (see table 6.1) for a resolution of 1 °C is at about 16 Hz. Therefore, this is not accurate enough.

$$f_{toggle} = \frac{F_CPU}{OCR1A} \quad (5.2)$$

$$\begin{aligned} f_{step} &= f_{toggle}(OCR1A) - f_{toggle}(OCR1A + 1) \\ &= F_CPU \cdot \left(\frac{1}{OCR1A} - \frac{1}{OCR1A + 1} \right) \end{aligned} \quad (5.3)$$

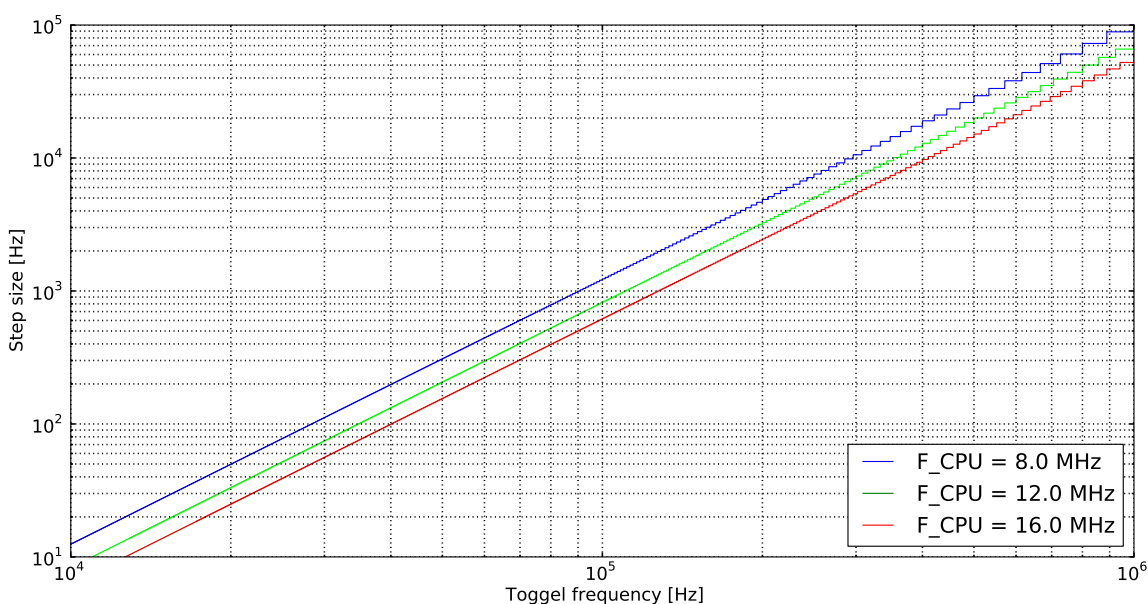


Figure 5.1: Next step size, plottet against the toggle frequency of the output pin.

5 Software

5.6 thermistor

This module simply uses the ADC module (section 5.3) to measure the voltage at the selected channel and to calculate the corresponding temperature for the B57560G104F thermistor (see data sheet [16]). The thermistor is connected to the microcontroller via a voltage deviator. The ADC then measures the voltage over the thermistor. According to the look-up table in the data sheet of the thermistor [16], an look-up table with a temperature corresponding to the ADC value was created. If the temperature is calculated, the corresponding value in the table is looked up. If the exact value is not available, the temperature is interpolated linearly between the given values next to the measured ones.

5.7 usart

For the information and the debugging output, the USART interface of the controller is used in combination with the FTDI FT232RL IC which makes the communication available at the PC via USB as a virtual COM port. On the PC, the communication is evaluated with the tool Hterm which simply outputs the communication of a selected serial port. The available functions can be seen in listing 5.3. To use this module, it needs to be initialized via `USART_Init`. The desired baud rate has to be set by calling `USART_setBAUD`. There are two functions to send data to the PC, `USART_write` and `USART_string`. The first one sends single one-byte values whereas the second one can send complete strings. Almost all other functions are necessary for communication from the PC to the controller. Since this is not necessary for this setup, it is not further described here.

```

1 void USART_Init(void);
2 void USART_setBAUD(uint32_t BAUD);
3 void USART_enableEmptyInterrupt(uint8_t onOff);
4 void USART_enableRxInterrupt(uint8_t onOff);
5 uint8_t USART_read(uint8_t *data);
6 uint8_t USART_write(uint8_t data);
7 void USART_string(char *data);
8 uint8_t USART_isBusy(void);

```

Listing 5.3: Available functions of the USART module.

5 Software

5.8 controller

In this module, the entire controller structure as shown in figure 5.2 is implemented. As the flow diagram shows, there are two controllers which are referred to as inner (phase/resonance frequency controller) and outer controller (frequency/temperature controller). The inner controller aligns the phase so that the setup runs at resonance frequency by regulating the actual frequency output of the DDS. The outer controller controls the resonance frequency and through that, it indirectly controls the temperature of the core by setting the off time of the PWM. This PWM switches the entire inductive heating setup off or on.

The procedure for the outer controller is as described below:

- State 1.: Measurement of the resonance frequency:
 1. Letting the inner controller adjust over several control cycles
 2. Measuring the controller output of the inner controller, the resonance frequency, over several cycles and averaging it.
- State 2.: Letting the inner controller run for the PWM on-cycles determined by the outer controller.
- State 3.: Pausing the inner controller for the PWM off-cycles determined by the outer controller by setting the DDS frequency to 0.

The entire controller setup is processed in an interrupt routine of a 8 bit timer. This routing is called every 1 ms which also represents one PWM cycle (not PWM period). The controller constants of both controllers are set up for testing empirically and with some trial and error. Due to that fact, these are not calibrated properly so that they do not generate perfect results. This is also due to the relatively big PWM period time (depending on the settings, in the cases shown later up to 400 PWM cycles are one PWM period) and the not steady PWM properties in general.

For further setups it could be necessary to check for alternatives for the outer controller since the PWM is not steady. For example, the outer controller could also control the phase not at resonance frequency but at a slightly higher or lower value at which the power throughput is less. It would be preferable to control at a point above the resonance frequency since the continuous decline of the amplification shown in the Bode diagram seen in figure 4.5(a) (top).

Below, all variables of the used PID controller for the inner and the outer controller (see listing 5.4) are described. All examples refer to the inner controller:

INDUCTIVE HEATING AND TEMPERATURE MEASURING SYSTEM

5 Software

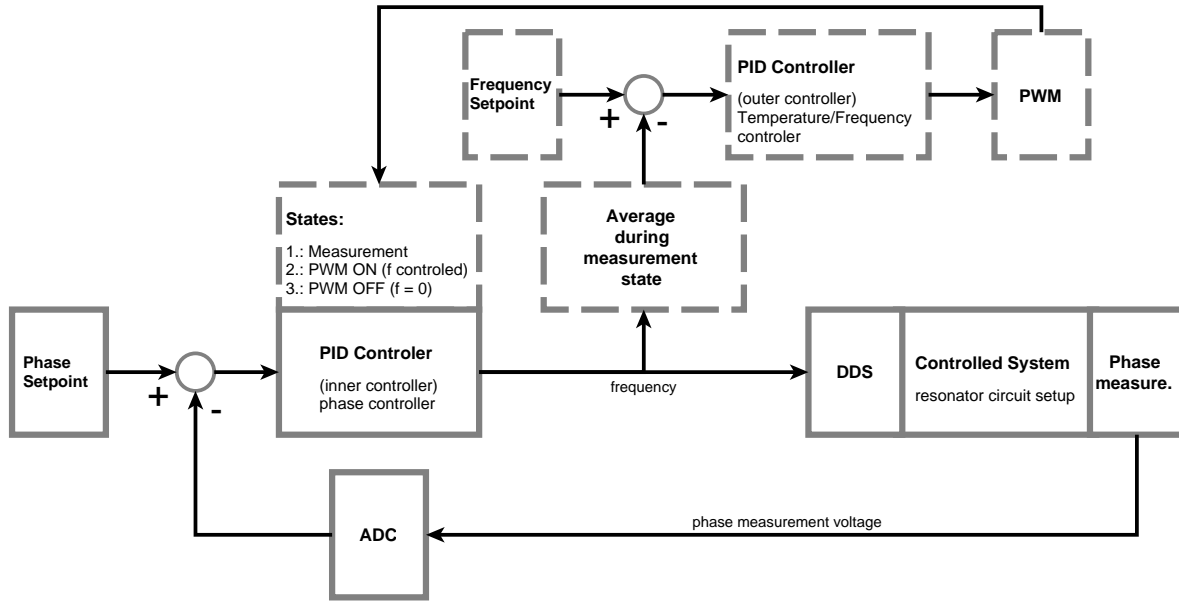


Figure 5.2: Controller setup. Solid line boxes: inner control loop; phase/resonance frequency controller. Dashed line boxes: outer control loop; frequency/temperature controller.

```

1 error = setpoint - currentValue
2 errorSum = errorSum + error
3 controllerOutput = Cp * error + Ci * Ts * errorSum + Cd * (error - errorOld)/Ts
4 errorOld = error

```

Listing 5.4: Standard PID controller.

- setpoint: Represents the desired value of the control variable (e.g. the desired phase of 50%).
- currentValue: The actual measured value (e.g. the actual phase voltage of the phase measurement circuit, measured via ADC).
- error: The actual deviation of the actual value from the desired value.
- errorSum: An integration of the error over time, necessary for the integral term.
- errorOld: The value of the error produced at the last run, necessary for the derivative term.
- Ts: Sample time at which the controller repeats.
- Cp: Controller constant for the proportional term. Must be set when calibrating the controller.

5 Software

- Ci: Controller constant for the integral term. Must be set when calibrating the controller.
- Cd: Controller constant for the derivative term. Must be set when calibrating the controller.
- controllerOutput: Actual output of the controller (e.g. the frequency set via the DDS).

5.9 main

The standard main.c file which in this case is mainly used for initializing and setting up all necessary modules. It also handles the output via USART.

6 Test and measurement

6 Test and measurement

In this chapter, the different measurements carried out on the circuit are discussed. Also, it contains a comparison with the simulations and a description of the results of several test runs. Figure 6.1 shows the complete schematic of the circuitry's power unit including all necessary labels for the different voltages and currents used in this chapter. The different measurements were carried out upon the hardware setup shown in figure 4.17, for different component values, and for different mechanical setups.

6.1 General circuitry measurements

The general measurements were carried out while using a T3 core (see figure 3.5), with $12 \mu\text{H}$ inductance (L_{load}) and a 540 nF capacitor (C_{tank}).

Figure 6.2 shows the voltage measurement at the gain pins of both MOSFET switches of the phase lag. It is important to note that the measurements were made with AC coupling. This means that the DC component of the measured signal is filtered out. As the measurement shows, both MOSFETs are controlled properly with at least the necessary minimum voltage of 12 V between gain and source. Since the drain voltage of the high side MOSFET has a voltage level of 12 V (if it is switched on, the source voltage is almost the same) and as seen in the measurement, the high side gain voltage (pink) rises to about 22 V . It also shows that the dead time of the driver IC is at about 500 ns which corresponds to the datasheet (see [21]).

Figure 6.3 shows the source voltage (U_{source}), the tank voltage (U_{tank}) and the voltage at the output of the phase measurement circuit (U_{phase}), measured with DC coupling. It shows that the tank voltage has a DC portion due to the fact that the resonator circuit is only driven for half the period time and freewheels for the rest of it. How large this offset is depends mainly on the magnitude of R_{load} . If it was reduced, the offset would be less distinct. The cyan signal is the voltage at the output of the phase measurement circuit discussed in section 4.5. Due to the fact that the used XOR gate (74HC86) works with 5 V levels (as opposed to the one used in the simulation working with 1 V), the average

6 Test and measurement

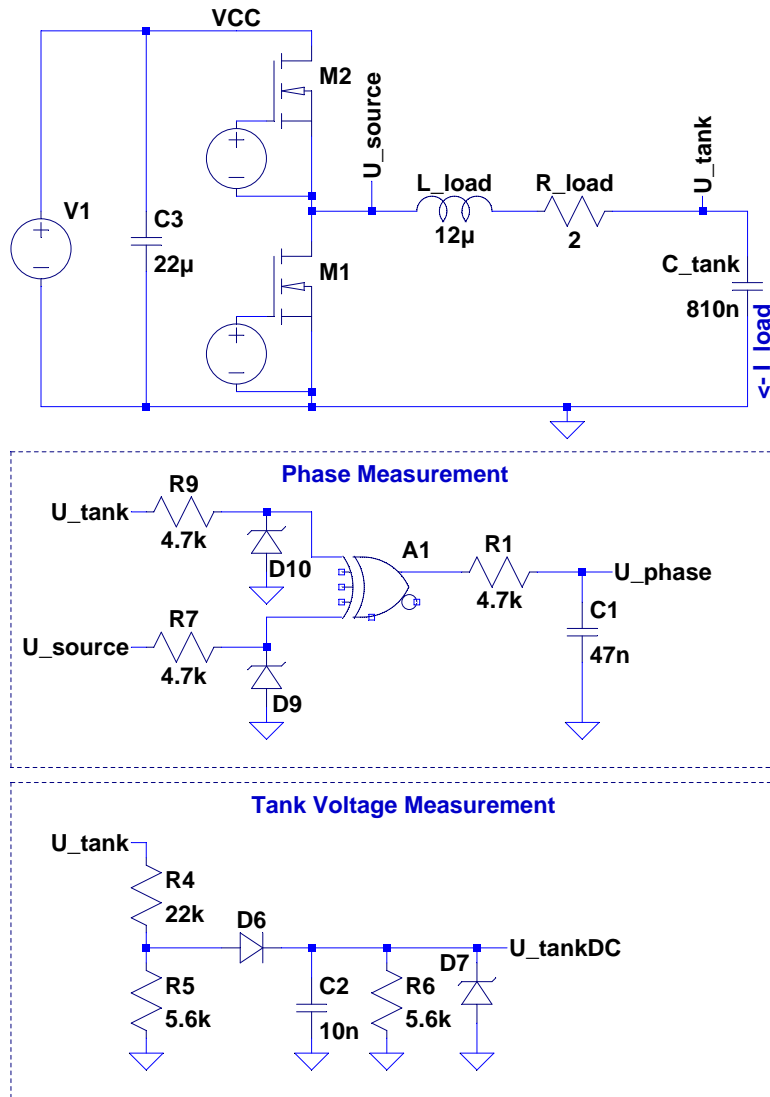


Figure 6.1: Complete schematic of the power unit.

of this signal lies at about 2.5 V and has a ripple of about 0.2 V. The increased ripple can be explained with the increased operation voltage level, but this is not a problem. As discussed in section 5.3, the signal is sampled several times and averaged. U_{source} is represented by the pink signal and there is a small voltage drop towards the center of the on-state of the high side MOSFET. As the simulation in figure 4.12(b) shows, the current through the high side MOSFET has a maximum at the same point. With this increased current, the voltage drop over the MOSFET's R_{DSon} also increases. This is also the reason for the drop at the U_{source} signal.

In figure 6.4, the currents on the left and the voltages on the right side are shown for different drive frequencies. At the top (figure 6.4(a) and 6.4(d)), it shows the signals if the circuit is driven above the resonance frequency. In the center (figure 6.4(e) and 6.4(f)),

6 Test and measurement

it shows the signals at resonance frequency. At the bottom, the signals below resonance frequency are shown.

On the right side, the phase difference between the tank and source voltage is less than -90° if above resonance frequency, about -90° at resonance frequency and above this value if below resonance frequency. The current on the left side shows that at resonance frequency, the signal is almost perfectly sinusoidal. With increasing frequency, the signal gets triangular and the magnitude decreases. At frequencies lower than the resonance frequency, the magnitude also decreases and the signal shape deforms. This is in both cases problematic from the EMC viewpoint.

As stated in section 4.2.3, the impedance of the serial resonator circuit at resonance frequency is only defined by R_{load} , so this can be used to measure the value of R_{load} as shown in section 4.2.1.

As figure 6.4(d) shows, the peak to peak value of the tank voltage is about 52 V for sinusoidal signals and the RMS value can be calculated to about 37 V ($= \frac{52}{\sqrt{2}}$). According to IEC 60449 standard, the acceptable contact voltage for an adult human is an RMS value of ≤ 50 V AC, for children and animals it is ≤ 25 V AC. Due to this fact it is necessary to either isolate the setup and protect it against contact, or to reduce the magnitude of the voltage, e.g. by reducing the value of L_{load} and/or increasing C_{tank} (see equation 4.13). As the voltage level also depends on R_{load} , it should be designed with a high enough margin in case of a failure, e.g. if the nozzle breaks and the core drops out.

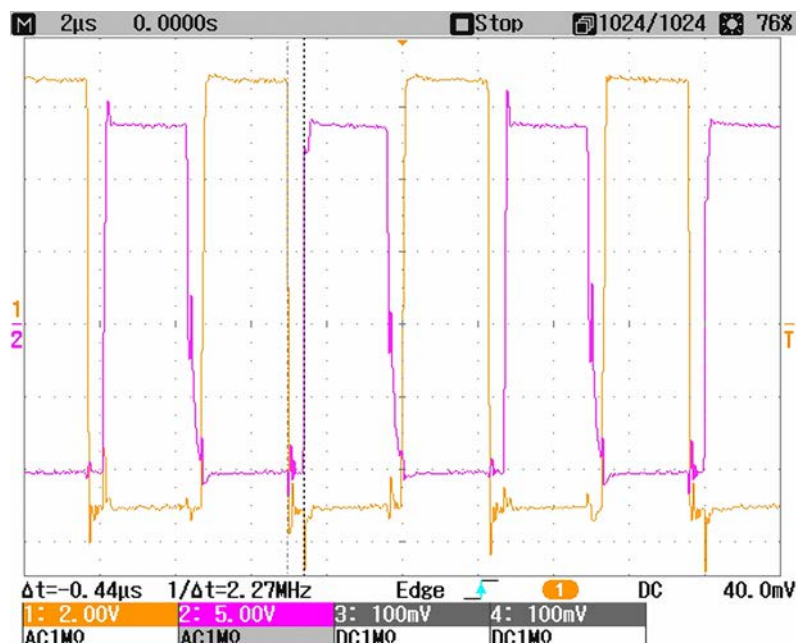


Figure 6.2: Phase lag driver output. Both the low side (orange) and the high side (pink) are measured against GND with AC coupling.

INDUCTIVE HEATING AND TEMPERATURE MEASURING SYSTEM

6 Test and measurement

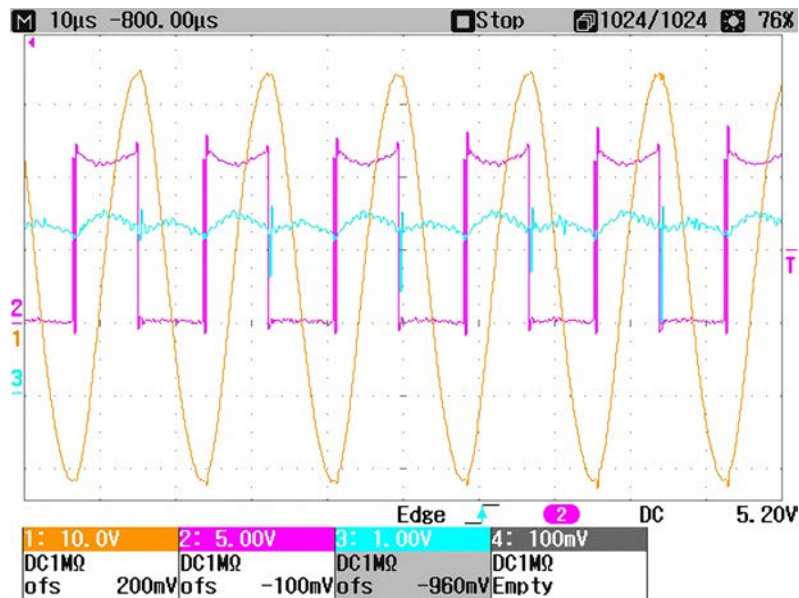


Figure 6.3: Tank voltage (U_{tank} , orange), source voltage (U_{source} , pink) and phase measurement circuit output voltage (U_{phase} , cyan) at resonance frequency.

Figure 6.5 shows the ADC values measured with the microcontroller at several frequencies. It was created with the C-code shown in listing 6.1. The values of the phase and the tank voltage were measured with the 10 bit ADC of the microcontroller. The signals were oversampled (see section 2.5) with 12 bit resolution and the ADC were connected to 3.3 V reference voltage in order to increase the ADC resolution in the relevant signal range. As described in section 4.5, the output range of the phase measurement circuit reaches from 0 to 5 V. Due to the smaller reference voltage, the ADC can't measure the entire signal range, as can be seen in figure 6.5 where the ADC maxes out over about 67 kHz for the phase voltage (green).

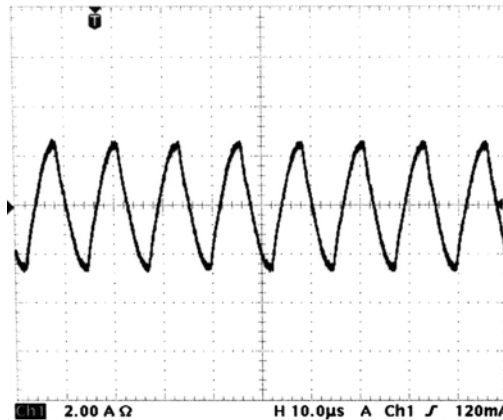
Since the spikes in the blue and the green signal occur at the same time, it doesn't seem like a transmission error but more like an error in measurement. For the test run this was not a problem. For further work it is necessary to further investigate this if it occurs in later setups too.

Compared to the simulated Bode diagram in figure 4.9(a), the tank voltage has its maximum at about the same frequency as in the simulation. At resonance frequency the phase shift should be -90° which would correspond to an output of the phase measurement circuit of 2.5 V (50%) (see section 4.5). According to equation 6.1, the ADC value should be 3103 at resonance frequency, but it is at about 2500. This is due to the not ideal phase measurement circuit as described in section 4.5.

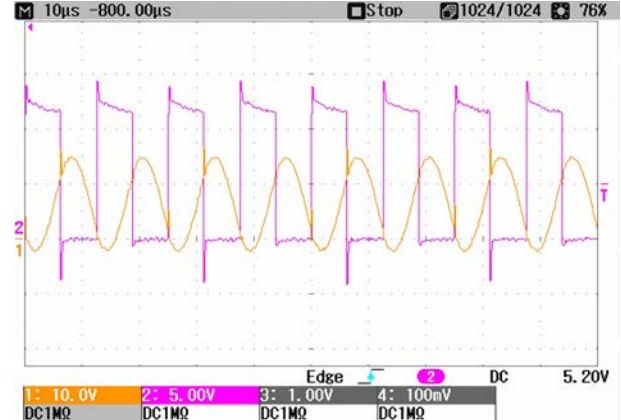
As the measurement shows, the maximum of the tank voltage (and by that also of the load current) is relatively wide. If the set point had been chosen to 3103 instead of 2500,

INDUCTIVE HEATING AND TEMPERATURE MEASURING SYSTEM

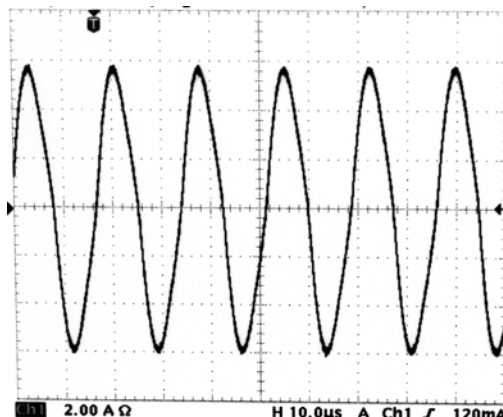
6 Test and measurement



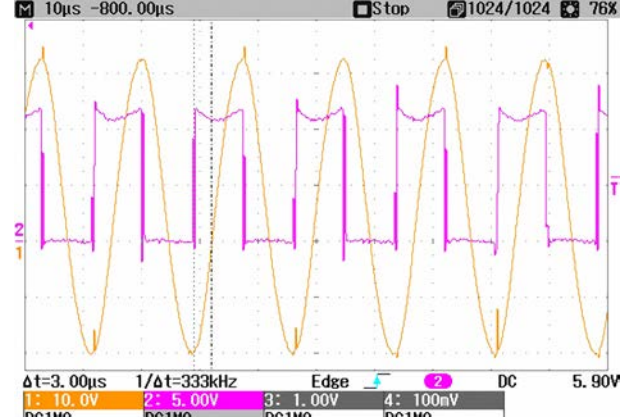
(a) Current above resonance frequency.



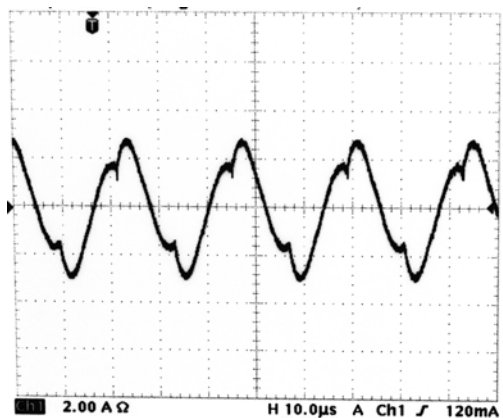
(b) Voltages above resonance frequency.



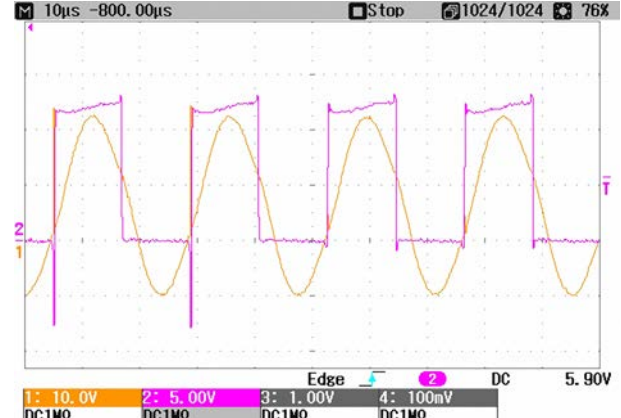
(c) Current at resonance frequency.



(d) Voltages at resonance frequency.



(e) Current below resonance frequency.



(f) Voltages below resonance frequency.

Figure 6.4: Current (i_{load}) and voltages above, at and below resonance frequency. black: current, pink: source voltage (u_{source}), orange: tank voltage (u_{tank}).

6 Test and measurement

the error in the power throughput would be only slightly smaller compared to the one at the maximum.

$$3.3 \text{ V} \hat{=} 2^{12} = 4096 \quad (6.1)$$

$$2.5 \text{ V} \hat{=} 3103$$

Listing 6.1 shows that the time per frequency step is far lower than 1 s (USART baud rate is 9600. At 8 bits per character, a maximum of about 4×10 characters result in approximately 30 ms necessary to send one message). This means that the system doesn't have enough time to reach its thermal equilibrium at each frequency so that the measured temperature is not the temperature at which the system would settle at that frequency. It is merely supposed to show that the temperature also drops if the frequency is higher than the resonance frequency, due to the fact that the magnitude of the current also drops and by that the power throughput is reduced. This fact could be used to control the setup, but since the signal shape deforms as seen in figure 6.4, this could become problematic due to EMC. Also, the development of the controller would be more complex than the one described in the section 5.8.

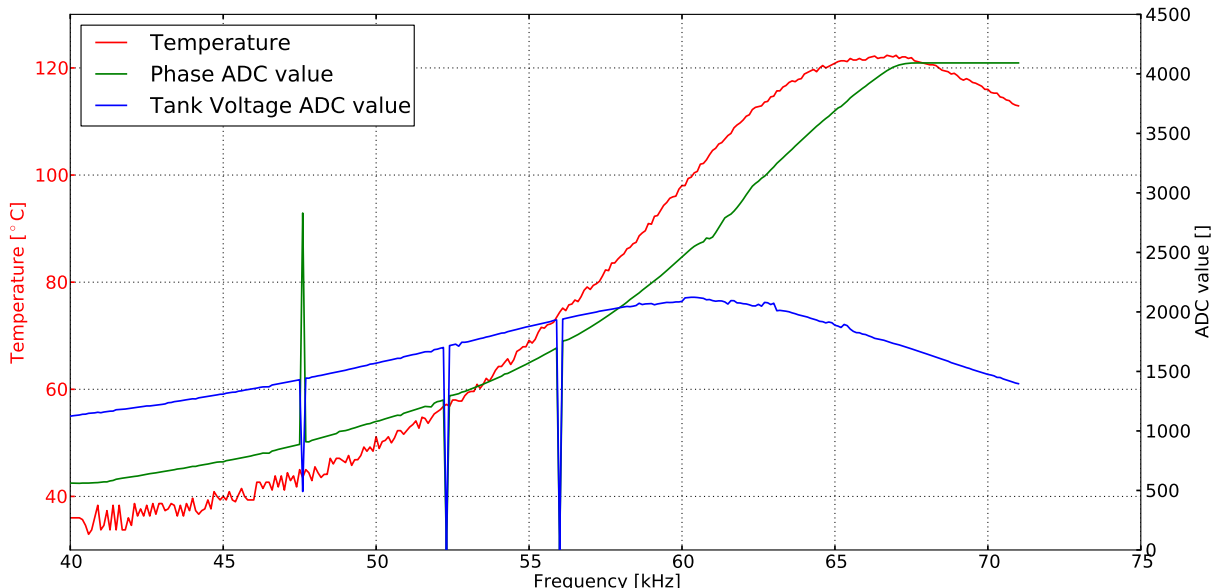


Figure 6.5: Plot of tank voltage (U_{tankDC} , blue), phase measurement voltage (U_{phase} , green) and temperature (red), plotted against frequency. Since the measurement time for each frequency is relatively short, the setup doesn't reach its thermal equilibrium.

6 Test and measurement

```

1 while(1){
2     DDS_freq( actFreq, FREQ0);
3     _delay_ms(10);
4     USART_string(ultoa( actFreq, s, 10 ));
5     USART_string(ultoa( (uint32_t)(T_readTermistor(0)), s, 10 )); // actual temp
6     USART_string(ultoa( (uint32_t)(avrADCval12bit(1,4)), s, 10 )); // actual tank
7         voltage
8     USART_string(ultoa( (uint32_t)(avrADCval12bit(2,4)), s, 10 )); // actual phase
9         voltage
8     actFreq += 100;
9 }
```

Listing 6.1: Code snippet to measure the values of the plot in figure 6.5.

6.2 Test runs

In this section, three test runs are described with different values for L_{load} and C_{tank} .

6.2.1 First test run

This test run was carried out with the same setup as the general measurements.

If the system is driven with the controller described in section 5.8 and with two different frequencies as set points for the frequency controller, the plots in figure 6.6 show the results of the raw measurement data. It shows the actual frequency being the control variable of the phase controller (the inner controller which adjusts the resonator to resonance frequency) in blue. The green signal shows the control variable of the temperature controller (the outer controller which controls the temperature indirectly via the actual resonance frequency), the PWM off-cycles of the actual control cycle. In comparison to the needed accuracy, both signals have high ripples. This is mainly the result of a poorly calibrated controller that was set up empirically and by means of trial and error, and also due to the ripple on the measured signals caused by the simple measurement circuits. The red signal shows the actual temperature which also has a high ripple.

The enlarged plot in figure 6.7 shows the temperature (red) as well as a separate measurement of the output of the phase measurement circuit. It can be seen that the temperature declines significantly if the induction heating is on (during the PWM on-cycles). This happens since the thermistor is placed inside the core and by that within the field of the primary coil, so that the sensor is influenced. Since the temperature measurement is only needed for testing, this problem wasn't further investigated. It could be prevented if the temperature measurement was carried out only if the induction heating is in off state.

The temperature in figure 6.6(a) shows that the system reaches its thermal equilibrium

6 Test and measurement

somewhere between measurement 4000 and 4500, whereas in figure 6.6(b) it is somewhere between 2000 and 2500. For a set point of 56 kHz, the temperature adjusts to about 215 °C and for 56.2 kHz to about 170 °C.

This inverse correlation corresponds with the simulation of Bayless seen in figure 6.8 showing the inductance (L_{load}) plotted against the frequency and the temperature. With rising temperature, the inductance increases and as equation 4.12 shows, the resonance frequency decreases if the inductance increases. This means that a higher frequency comes along with a lower temperature. This is consistent with the result in figure 6.6.

Figures 6.9 show thermal images during a test run at resonance frequency for several minutes. It has to be noted that glass acts as a mirror for infrared rays. This is important since the tube is made out of glass. Also note that the temperature scales differ for all three pictures.

Figure 6.9(a) shows the nozzle from outside. As is evident, the coil temperature on the surface is higher at the bottom where the core is placed inside the glass tube. The maximum coil temperature at the surface is about 100 °C and the temperature at the inner coil loops lies above that value, but as copper is a good heat conductor, the temperature gradient shouldn't be too high. The used enameled copper wire is heat resistant up to about 150 °C, which should leave enough margin for continuous operation. To reduce the heat gradient of the different coil loop layers it would be preferable to have less layers. This would also be in line with the already described maximum AC voltage which can also be achieved by using less loops.

Figure 6.9(b) shows the load circuit. It also shows that the general circuitry remains almost at room temperature and only the used capacitors heat up to about 70 °C. This lies still in the range of the component specifications. The heating values are mainly due to the ESR of the capacitors. To reduce them, more capacitors could be put in parallel as described in section 4.3. Alternatively, a different type with lower ESR can be used.

Figure 6.9(c) shows the T3 type core (see figure 3.5) of the setup, seen from the top. The image shows the inside of the glass tube, which adulterates the reading. However, it can be estimated that the core temperature is at least 300 °C which is also in line with the temperature readings of the thermistor maxing out at this temperature.

These thermal images show a worst-case scenario. The setup should, however, withstand this permanent load but by means of several improvements, some characteristics can still be optimized.

6 Test and measurement

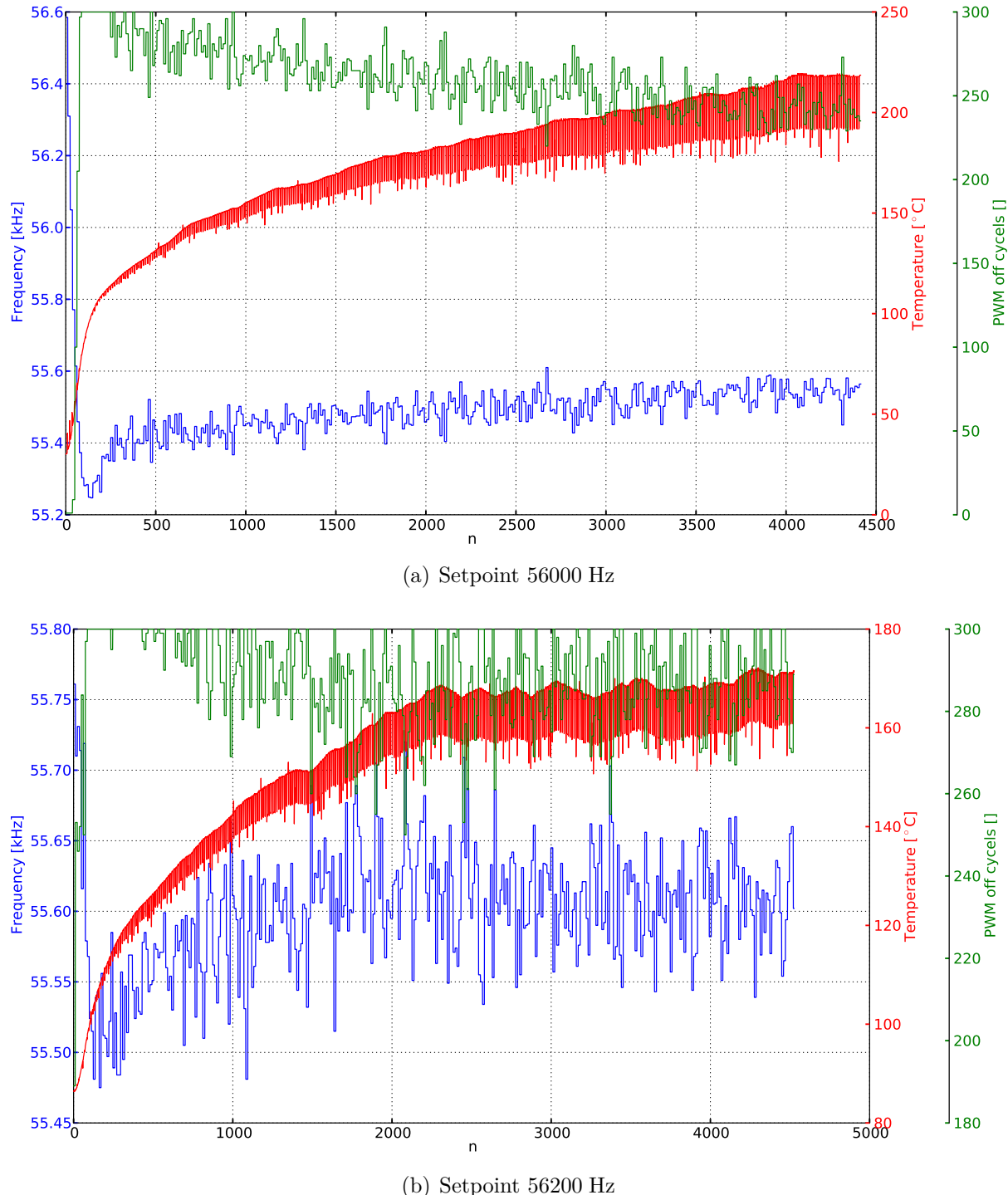


Figure 6.6: Plots of the resonance frequency (blue), the core temperature (red) and the PWM off-cycles (green), with a PWM period consisting of 300 PWM cycles.

6 Test and measurement

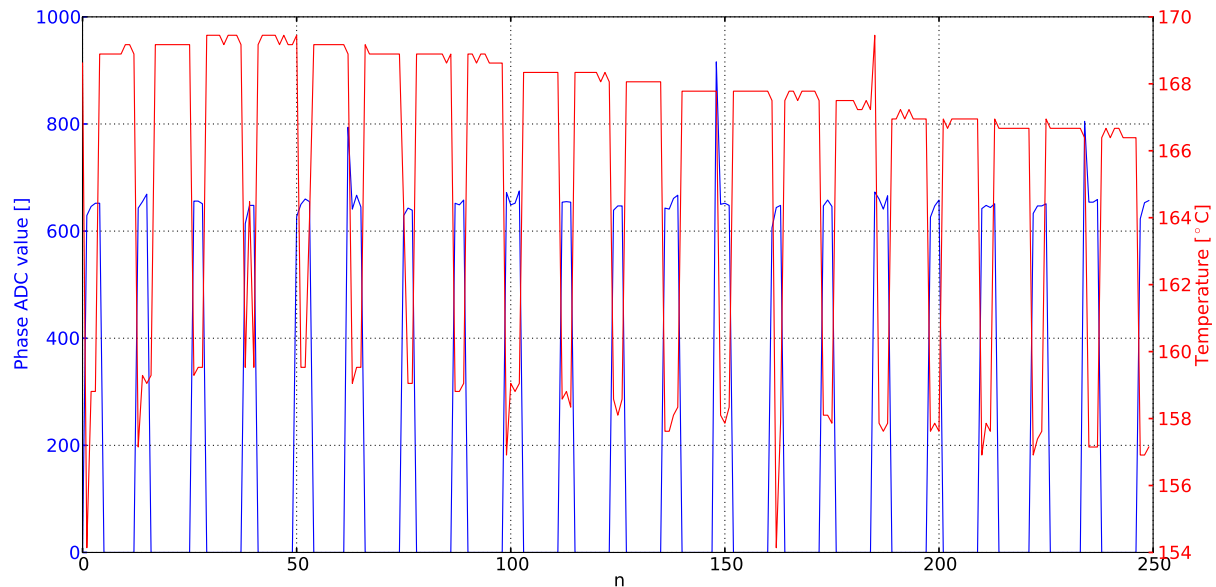


Figure 6.7: Error temperature reading. Blue: ADC measurement of the phase measurement circuit, red: core temperature.

6.2.1.1 Extrusion test

An extrusion test was carried out with this setup consisting of a T3 core, the setup shown in figure 3.3 and with white ABS filament. This setup is similar to the one described by Bayless ([12], see figure 1.1). As a result, the nozzle clogged after extruding approximately 5 mm of fine filament. Also, the glass tube slivered at the head, around the extrusion hole. A possible explanation for the clogging could lie in the relatively low heat conductivity of the glass and also in the low heat capacity of the molten plastic. Due to these factors, that filament solidified in the outlet hole and clogged it. To prevent this, the plastic could be heated to a higher temperature. However, this is only possible to a certain extent since the ABS releases harmful vapors when heated above a certain temperature.

Another reason could be the thermal expansion of the core. Due to the not perfect controller, the temperature drops as soon as load is applied (filament is pushed in) and by that the core shrinks and is pushed slightly deeper into the glass tube. If the controller then adjusts to the load, the temperature rises again and the core expands. This happens at every load change.

6.2.2 Second test run

For this test run, the primary coil was made up of a smaller number of loops and by that with a smaller inductance of about $7.5 \mu\text{H}$ (L_{load}). To counteract the increase of

6 Test and measurement

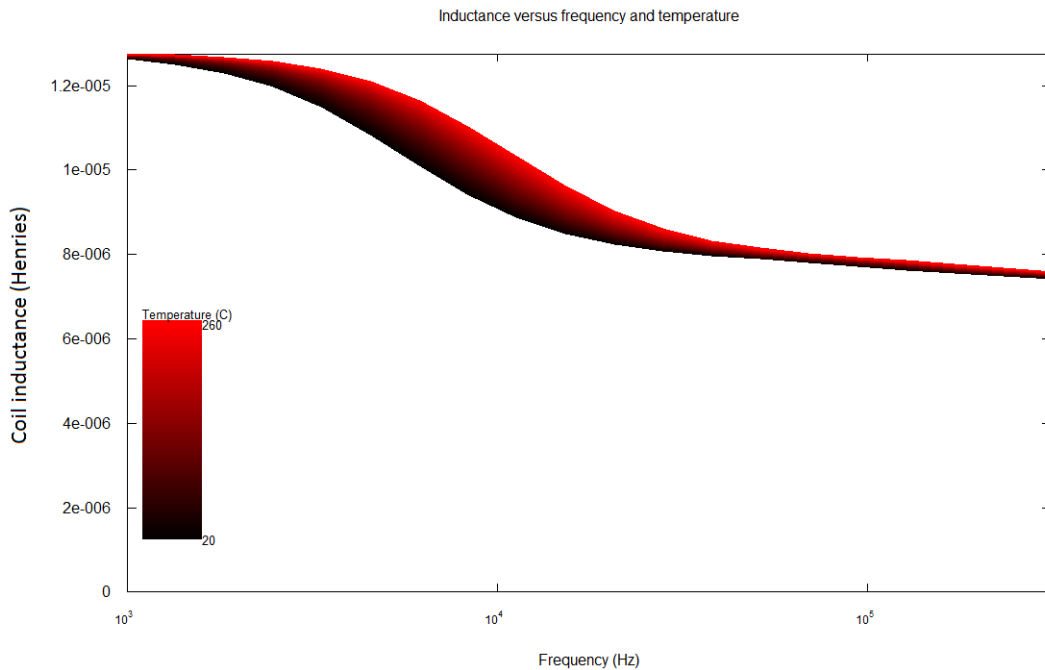


Figure 6.8: Inductance plotted against frequency and temperature (by Bayless).

the resonance frequency according to equation 4.12, the capacitor C_{tank} was increased to 810 nF by means of an additional parallel capacitor.

Table 6.1 shows a comparison of different types of cores including plots of the resonance frequency against the temperature. These were measured slowly so that the system could reach a thermal equilibrium at each frequency. This plot shows that the correlation for all cores is almost linear. It also shows that the T3 core differs from the other core types, mainly in regard to its shorter length. By that, the effective material within the field of the primary coil is a lot smaller. It can be seen that the narrowing and the brim of the T2 core have almost no influence compared to the T1 type. It also shows that, the resolution for the thinner cores (T1 and T2) is higher than for the thicker T4 core. This corresponds with the observation of Bayless (compare [12] by Bayless) who states that thinner cores have a higher $\frac{\Delta f_0}{\Delta Temp}$. Due to the facts that cores with a wall thickness of 0.25 mm are quite hard to build by hand and that they are not very stable, this way to increase the resolution is limited.

The step response measurements shown in figures 6.10 illustrate that the thermal response time mainly depends on the mass of the core in the field of the primary coil. If the mass is too small (as in T1), the energy transfer is limited and the heating time is slow. If the mass is too big (as in case of the T4), the heating time is simply limited by the mass that has to be heated up. T2 and T3 are very similar, with the only exception that T3 is faster due to its small mass and its relatively large brims.

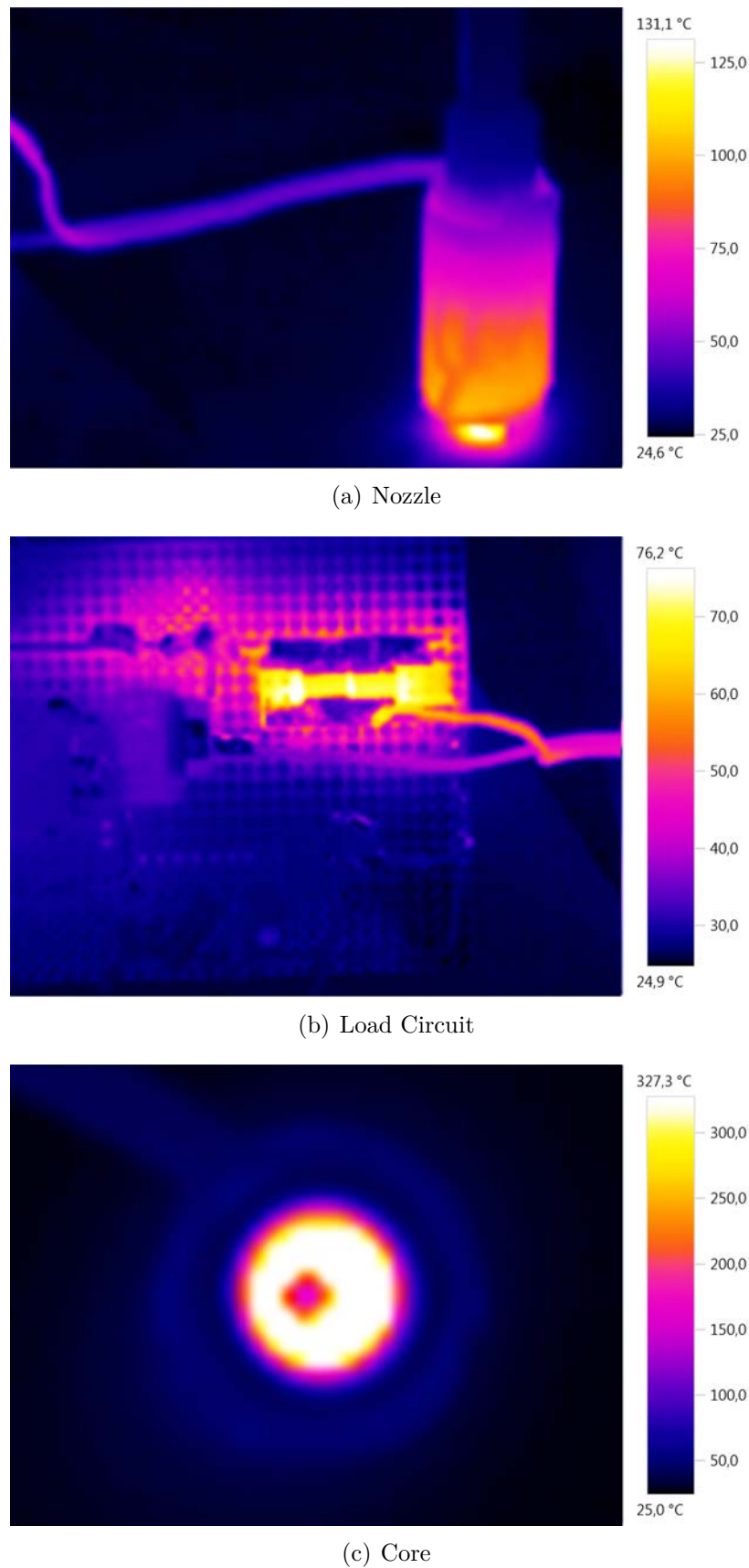
6 Test and measurement

Figure 6.9: Thermal images of the first test run after several minutes.

6 Test and measurement

The plot of the outer controller's frequency, temperature and PWM off-cycles (cf. figure 6.11) shows that the temperature adjusts to two different values in case different resonance frequencies are given as set points. The long-term test over 30 minutes in figure 6.11(b) shows that the controller keeps the temperature steady to some extent, but that there is still a ripple of at least 10 °C. But this also shows that at about $n=23000$ the controller takes a tumble. It seems like the controller got unstable after the resonance frequency first slightly rises and immediately afterwards drops to an relatively low value, due to the controller the PWM off-cycles are inversely following this signal change. Because of this interference the temperature totters and after the controller becomes level again the temperature has an offset to the level before that event of about 5 °C.

6.2.2.1 Extrusion test

Figure 6.12 shows the resonance frequency and the PWM off-cycles of the outer controller during a test extrusion. The filament was pushed in with different speeds. If the load rises (faster filament), the resonance frequency also rises due to the lower temperature and the off-cycles are reduced by the controller. If the filament is pushed too fast, as it happens above $n \approx 4000$, the outer controller switches the inductive heating to 100% of the time so that the resonance frequency rises even further. This means that the temperature still drops. Since the T2 core in this test run is almost entirely enclosed during testing, a direct temperature measurement with the thermistor wasn't possible. Therefore, the resonance frequency set point of the outer controller was simply reduced until the plastic filament started melting. This seemed to happen at 72 kHz which should be approximately the melting point of ABS (230 °C). If the measurements in table 6.1 are extrapolated linearly, a set point of 72 kHz corresponds to a temperature lower than 0 °C. Since these two measurement were carried out on different days, it is possible that some of the environment variables (e.g. environment temperature) have changed or that the introduced filament has changed the properties of the load, and by that the temperature/frequency characteristic.

6.2.3 Third test run

In the second test run, the connection wire of the primary coil (consisting of 6 parallel enameled copper wires with a diameter of 0.4 mm) had heated up. Therefore and in order to reduce the resistance of the copper wire, a third test run was performed with a coil consisting of 10 parallel wires of the same diameter. By that, the heat buildup due to resistive heating within the copper wire was to be reduced. This new coil has an inductance of about $6 \mu H$ (L_{load}), C_{tank} remained at 810 nF for this run.

6 Test and measurement

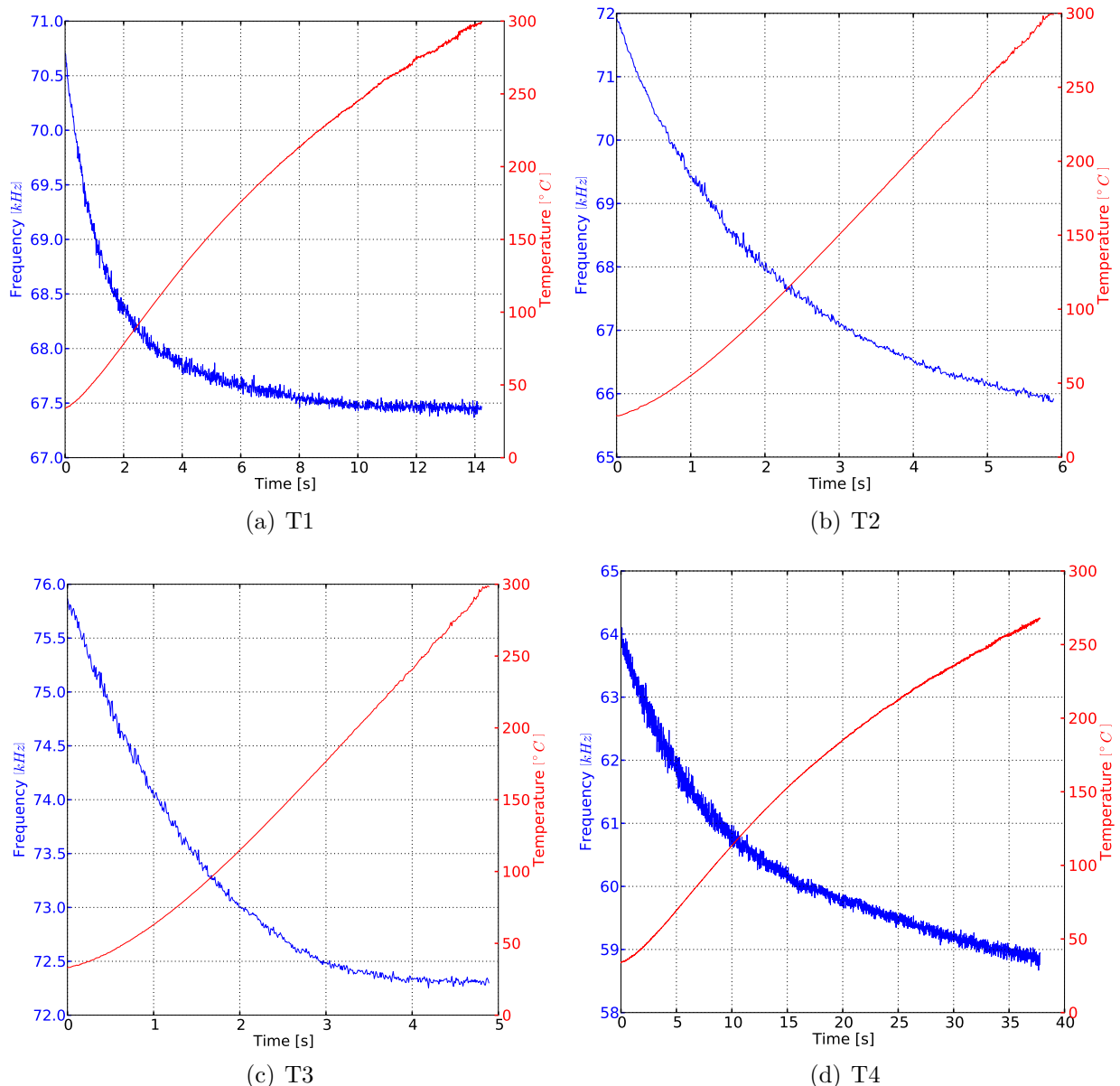


Figure 6.10: Temperature step response of the different cores, with inductive heating at 100% of the time. Resonance frequency and temperature against time.

6 Test and measurement

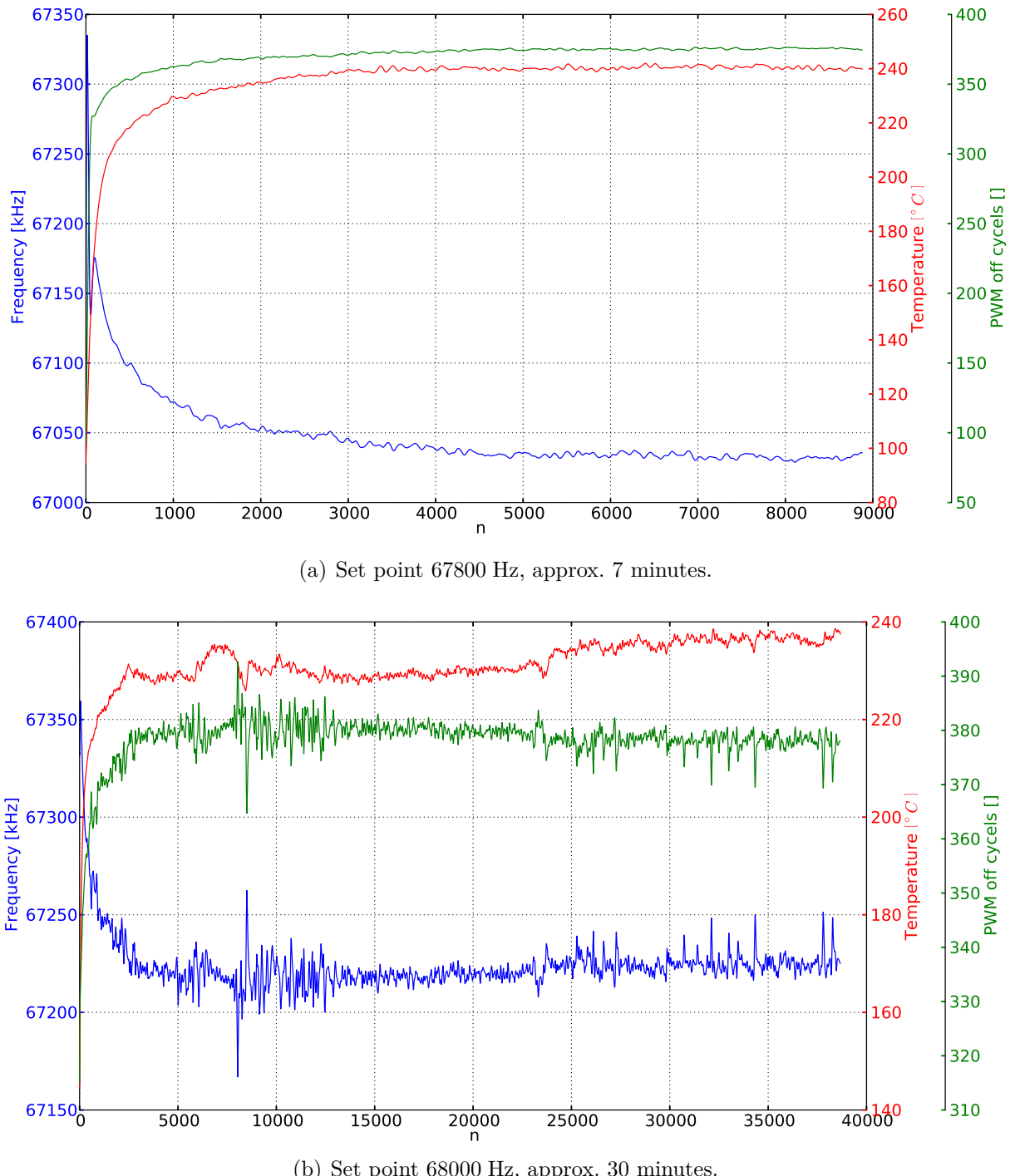


Figure 6.11: Plots at different set points, smoothed with a Gaussian filter ($\sigma = 25$). Measured with a T2 core. Red: core temperature, blue: resonance frequency, green: PWM off-cycles of the outer controller.

6 Test and measurement

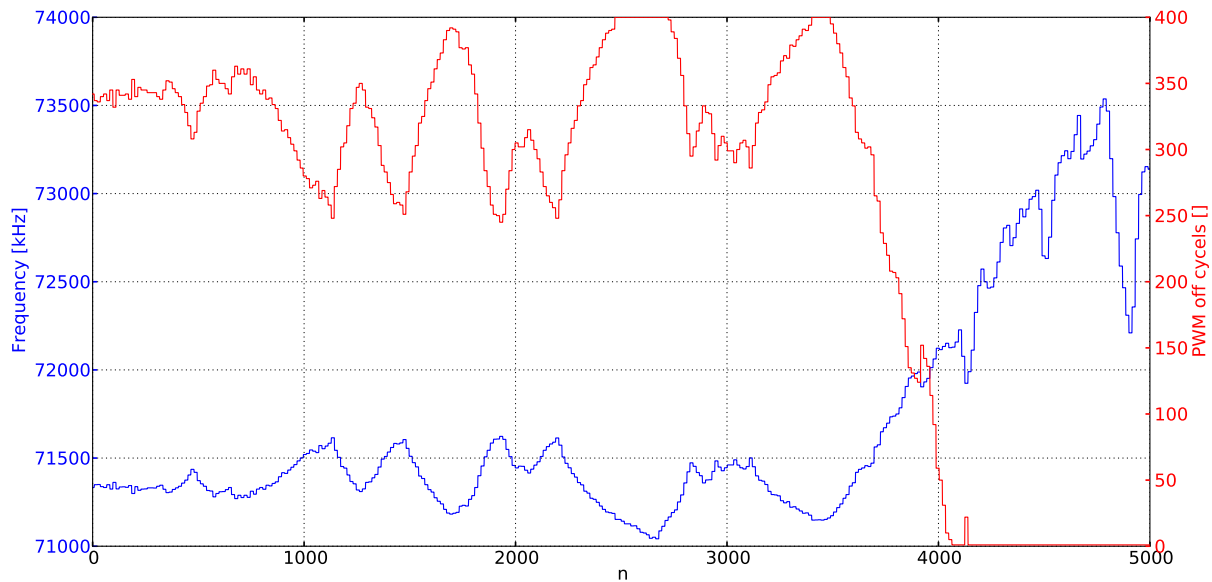


Figure 6.12: Resonance frequency (blue) and PWM off-cycles (red) of a T2 core during filament extrusion with a set point of 72000 Hz.

As the current and voltage measurement in figure 6.13 shows, the current (i_{load}) remains almost sinusoidal which corresponds with the simulation seen in figure 4.10 (x in this case is $\frac{6 \mu\text{H}}{810 \text{nF}} = 7.4 \text{ H/F}$). The figure also shows that current I_{load} increased in all three described iterations. In the first one, I_{load} was 4 A (see figure 6.4(c)), in the second it was 6.5 A (see table 6.1) and in the third one it was 7 A (see figure 6.13). All three were measured with a T3 core to make the results comparable. As opposed to the first test run, another capacitor was put in parallel. By that, the losses due to the ESR of the capacitors were reduced. By putting shorter wires (less loops) in parallel for the primary coil, the losses due to the resistance of the wire were reduced. Also, the tank voltage U_{tank} was reduced. Unlike the 37 V RMS value in the first described setup (see figure 6.4(d)), owing to the changed ratio of C_{tank} and L_{load} (see equation 4.13), the value is now 19.5 V (see figure 6.13). As described above in section 6.1, this is desirable due to the allowed contact voltage.

Another important thing to note is that the current I_{load} strongly increases if the setup is driven at full power for too much time because the core temperature exceeds the Curie point at which the core loses its ferromagnetic properties. By that, the hysteresis losses disappear, thereby reducing the losses (reduction of R_{load}). If this happens, the current I_{load} reaches values of approx. 9.5 A.

As the thermal images in figures 6.14 show, the temperature measured after less than one minute at full power are higher than in the first measurement (see figures 6.9). This is due to the higher current in comparison to the first measurement. It shows that the enameled copper wire reaches a temperature that is higher than its specifications allow

6 Test and measurement

for (maximum temperature ≈ 150 °C). The used capacitors are specified for an operating temperature of up to 125 °C. As seen in figure 6.14(b), the measured temperature at the surface is almost at the limit. Due to these facts it is absolutely essential that the setup is not driven at full power for too much time since in most cases the enameled copper wire would overheat and shorten. In order to reduce the temperature of the capacitors in later designs, thermal vias should be placed on or near the soldering pads and the opposite side should be a wide and continuous copper area covered with solder resist for better heat emission. If necessary, the capacitors could as well be equipped with heat sinks.

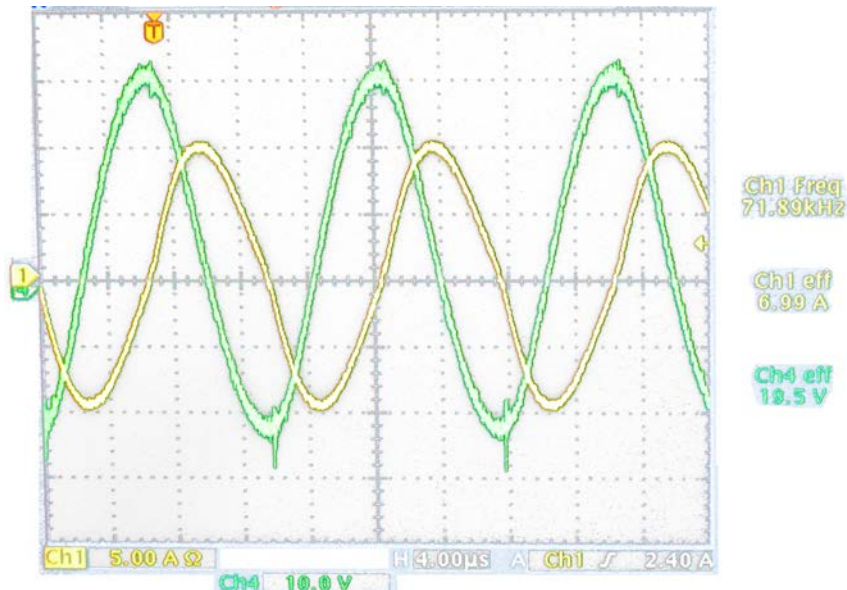


Figure 6.13: Current (i_{load} , yellow) and voltages. Tank voltage (u_{tank} , green), measured with the T3 core.

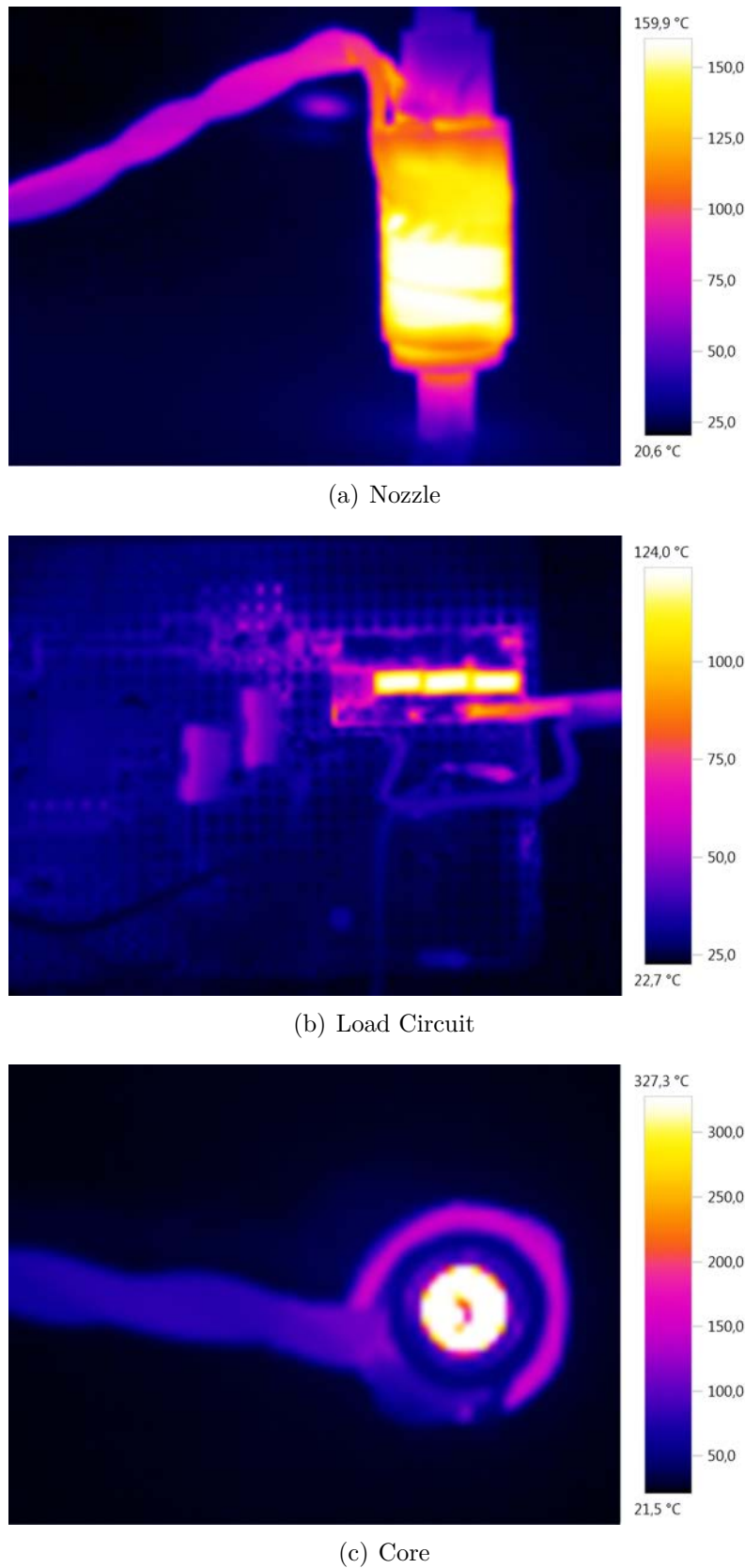
6 Test and measurement

Figure 6.14: Thermal images of the T3 core at full power applied for a short period of time (less than 1 min).

INDUCTIVE HEATING AND TEMPERATURE MEASURING SYSTEM

6 Test and measurement

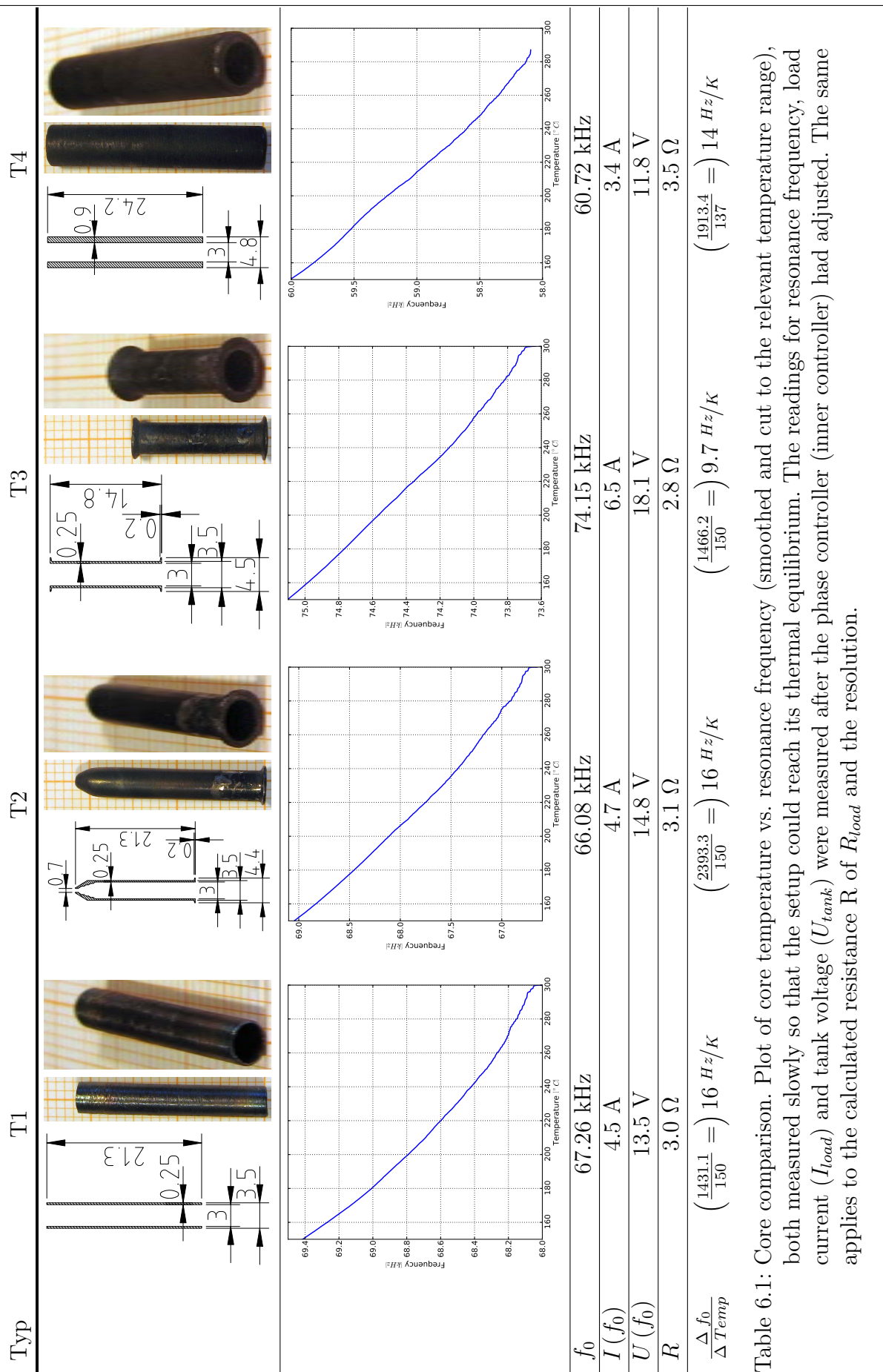


Table 6.1: Core comparison. Plot of core temperature vs. resonance frequency (smoothed and cut to the relevant temperature range), both measured slowly so that the setup could reach its thermal equilibrium. The readings for resonance frequency, load current (I_{load}) and tank voltage (U_{tank}) were measured after the phase controller (inner controller) had adjusted. The same applies to the calculated resistance R of R_{load} and the resolution.

7 End

7 End

7.1 Conclusions and prospects

As chapter 6 shows, it is possible to control and measure the temperature of the core without a temperature sensor and with a completely enclosed nozzle. For example it would be possible to use a temperature sensor to calibrate the setup and creating a look-up table correlating resonance frequency and temperature.

As shown in table 6.1, the necessary frequency resolution for 1 K lies between 9.7 Hz and 16 Hz for the different types of cores. At a resonance frequency of 60 kHz, the necessary accuracy for the frequency measurement would be about 167 ppm (0.0167%) ($\frac{10 \text{ Hz}}{60 \text{ kHz}}$) for a measurement resolution of 1 K. This would demand high standards of the components and the software. Since all electrical components age over time and also the environment variables such as the ambient temperature have an influence on the measurement, these factors need to be considered if the necessary high accuracy is to be reached.

If it is possible to reduce the necessary accuracy by increasing the frequency change, at the same temperature change, the influence of the described side effects would be reduced. A possible solution to this problem could be the usage of other core materials or a mixture of materials, such as a metal core coiled with a wire made of a different material that involves a greater change of properties in the desired temperature range.

To reduce costs and the complexity of the circuitry, the DDS IC could be replaced by a self-oscillating half bridge driver IC, e.g. the IR2153. To set the frequency at this IC, it is necessary to change the resistance between the GND and one I/O of the IC. This can be achieved with an RC low pass and a MOSFET which is driven by a PWM signal from the controller. Another possibility would be to directly generate the control signal for the actual driver IC with the controller, as shown in section 5.5. However, due to the fact that the accuracy decreases with rising frequency, this is only possible if the necessary frequency is low.

7.2 Used tools

Below, almost all tools used to create this thesis are listed. All webpages were last checked on August 28, 2012.

Hardware development

- LTspice IV (v. 4.15l)
www.linear.com/designtools/software
- Python (v. 2.7.2) with several third-party packages
www.python.org
- ParaView (v. 3.12.0)
www.paraview.org

Software development

- AVR Dragon
www.atmel.com/dyn/products/tools_card.asp?tool_id=3891&source=redirect
- Sublime Text (v. 2.0.1 Build 2217)
www.sublimetext.com
- HTerm (v. 0.8.1beta)
www.der-hammer.info/terminal/index.htm
- Doxygen (v. 1.7.3)
www.stack.nl/~dimitri/doxygen/index.html
- Atmel Studio 6 (v. 6.0.1843)
www.atmel.com/Microsite/atmel_studio6

Creation of this document

- L^AT_EX (MiK^TeX v. 2.9)
www.miktex.org
- JabRef (v. 2.6)
www.jabref.sourceforge.net
- QCad (v. 2.0.5.0 [Community Edition])
www.ribbonsoft.com

7 End

- yEd (v. 3.6.1.1)
www.yworks.com/de/index.html

7.3 Acknowledgments

I would like to thank the company Arcus-EDS [2] for granting me access to all necessary tools to create this thesis. Also, I want to thank all employees for their great support, especially Hjalmar Hevers for his great support during the development process.

Wolfgang Vogel of RepRap Fab (reprap-fab.org) provided material for the mechanical setup, Prof. Dr.-Ing. Alfred Rozek supervised my thesis and supported me while creating it. Many thanks also to them.

As well as Martin Schmucker for proofreading and his improvement suggestions.

Bibliography

Bibliography

- [1] *Analog Devices*. www.analog.com. Version: September 2012. – Building Three, Three Technology Way, Norwood 02062 4
- [2] *arcus-eds*. www.arcus-eds.de. Version: September 2012. – Rigaer Straße 88, 10247 BERLIN 4.7.1, 7.3
- [3] *Atmel*. www.atmel.com. Version: September 2012. – 2325 Orchard Parkway, San Jose, 95131 United States 1
- [4] *Deutsches Patent- und Markenamt*. www.dpma.de. Version: September 2012. – Zweibrückenstr. 12, 80331 München 1.5
- [5] *International Rectifier*. www.irf.com. Version: September 2012. – 101 N Sepulveda Blvd., El Segundo, CA 90245 USA 6
- [6] *United States Patent and Trademark Office*. www.uspto.gov. Version: September 2012. – USPTO MADISON BUILDING, 600 Dulany Street, Alexandria, VA 22314 1.5
- [7] ANALOG DEVICES: *AD9833, Low Power, 12.65 mW, 2.3 V to 5.5 V, Programmable Waveform Generator*. September 2010. – Rev. D 2.9, 2.10, 5.2
- [8] ATMEL: *ATmega 324P, 8-bit Microcontroller with 16K/32K/64K Bytes In-System Programmable Flash ATmega164P/V; ATmega324P/V; ATmega644P/V*. www.atmel.com/dyn/resources/prod_documents/8011S.pdf. Version: July 2010. – Rev. 8011O- 07/10 4.7.1, 4.19, 5.3
- [9] AVX: *High Voltage MLC Chips; For 600V to 5000V Applications* 4.3
- [10] BAYLESS, Jacob ; CHEN, Mo ; DAI, Bing: *Wire Embedding 3D Printer*. April 2010 1.1
- [11] BAYLESS, Jacob ; CHEN, Mo ; DAI, Bing: *SpoolHead*. Wikipedia. www.reprap.org/wiki/SpoolHead. Version: March 2012 1.1

INDUCTIVE HEATING AND TEMPERATURE MEASURING SYSTEM

Bibliography

- [12] BAYLESS, Jacob ; WANG, Vicky: *Induction Heating Extruder*. www.ubc-rapid.com/wiki/index.php?title=Induction_Heating_Extruder. Version: September 2012 1.5, 6.2.1.1, 6.2.2
- [13] BEUTH UNIVERSITY: *Beuth University of Applied Sciences*. Luxemburger Straße 10, 13353 Berlin, Germany, March 2012. www.beuth-hochschule.de 1.1
- [14] DEGGENDORF UNIVERSITY: *Deggendorf University of Applied Sciences*. Edlmairstraße 6 und 8, 94469 Deggendorf, Germany, March 2012. www.hdu-deggendorf.de 1.1
- [15] EDWARD ANTHONY SELLS: *Towards a Self-Manufacturing Rapid Prototyping Machine*. A thesis submitted for the degree of Doctor of Philosophy, January 2009 2.4
- [16] EPCOS: *Datasheet NTC B57560G104F*. September 2001. – Rev. a 5.6
- [17] H., Frohne ; K.H., Löcherer ; H., Müller ; T., Harriehausen ; D., Schwarzenau: *Moeller Grundlagen der Elektrotechnik*. Vieweg+Teubner Verlag, 2008 (21. Auflage) 4.2, 4.2.1
- [18] HENKE, Heino: *Elektromagnetische Felder: Theorie und Anwendung*. Springer Berlin Heidelberg, 2011 (4. Auflage) 2.1
- [19] IDA, Nathan: *Engineering Electromagnetics*. Springer, 2007 (2nd ed.) 2.1
- [20] INTEL CORPORATION: *ATX12V Power Supply Design Guide*. 2005. – Version 2.2 4.1
- [21] INTERNATIONAL RECTIFIER: *HALF-BRIDGE DRIVER, IR2184(4)(S) & (PbF); (Data Sheet No. PD60174)*. April 2006. – Rev. G 4.4.4, 4.14, 6.1
- [22] INTERNATIONAL RECTIFIER: *Application Note AN-978, HV Floating MOS-Gate Driver ICs*. March 2007. – Rev. D 4.4.4
- [23] MATSUMOTO, Isao ; FUSATO, Tetsuo ; KIMURA, Fumitoshi ; MATSUI, Fujio: *HIGH FREQUENCY INDUCTION AND METHOD WITH TEMPERATURE CONTROL*. Patent, December 1995. – Patent Number: 5,477,035 1.5
- [24] MENGES ; HABERSTROH ; MICHAELI ; SCHMACHTERBERG: *Werkstoffkunde Kunststoffe*. 5. Auflage. Carl Hanser Verlag GmbH & CO. KG, 2002 2.4.1.2, 2.7
- [25] NATIONAL INSTITUTE OF STANDARDS & TECHNOLOGY: *CRC Handbook of Chemistry and Physics*. Taylor & Francis, 2009 (90th revised edition) 2.1, 2.1, 2.2.3
- [26] RAINER OSE: *Elektrotechnik für Ingenieure: Bauelemente und Grundschaltungen mit PSPICE*. Carl Hanser Verlag GmbH & CO. KG, 2006 (Auflage 1) 4.2.1

INDUCTIVE HEATING AND TEMPERATURE MEASURING SYSTEM

Bibliography

- [27] REIBIGER, Küpfmüller M.: *Theoretische Elektrotechnik*. Springer, 2008 (18. Auflage) 2.2.3
- [28] REPRAP WIKIPEDIA: *RepRap Project*. www.en.wikipedia.org/wiki/RepRap_Project 2.4
- [29] TEXAS INSTRUMENTS: *ADC Oversampling Techniques for Stellaris Family Microcontrollers*. June 2009 2.5, 2.8
- [30] UNIVERSITY OF BRITISH COLUMBIA: *The University of British Columbia*. 2329 West Mall, Vancouver, B.C., Canada V6T 1Z4, March 2012. www.ubc.ca 1.1
- [31] VIRDEE, Bal S. ; VIRDEE, Avtar S. ; BANYAMIN, Ben Y.: *Broadband Microwave Amplifiers*. Artech House Inc, 2004 4.2
- [32] VOGEL, Wolfgang: *Reprap-Fab*. www.reprap-fab.org. Version: September 2012 2.4.1.1, 2.5(c), 2.6
- [33] WIMA: *Metallized Polyphenylene-Sulphide (PPS)*. www.wima.com/EN/temperatur.htm. Version: September 2012 4.11

A Appendix

A.1 Setup

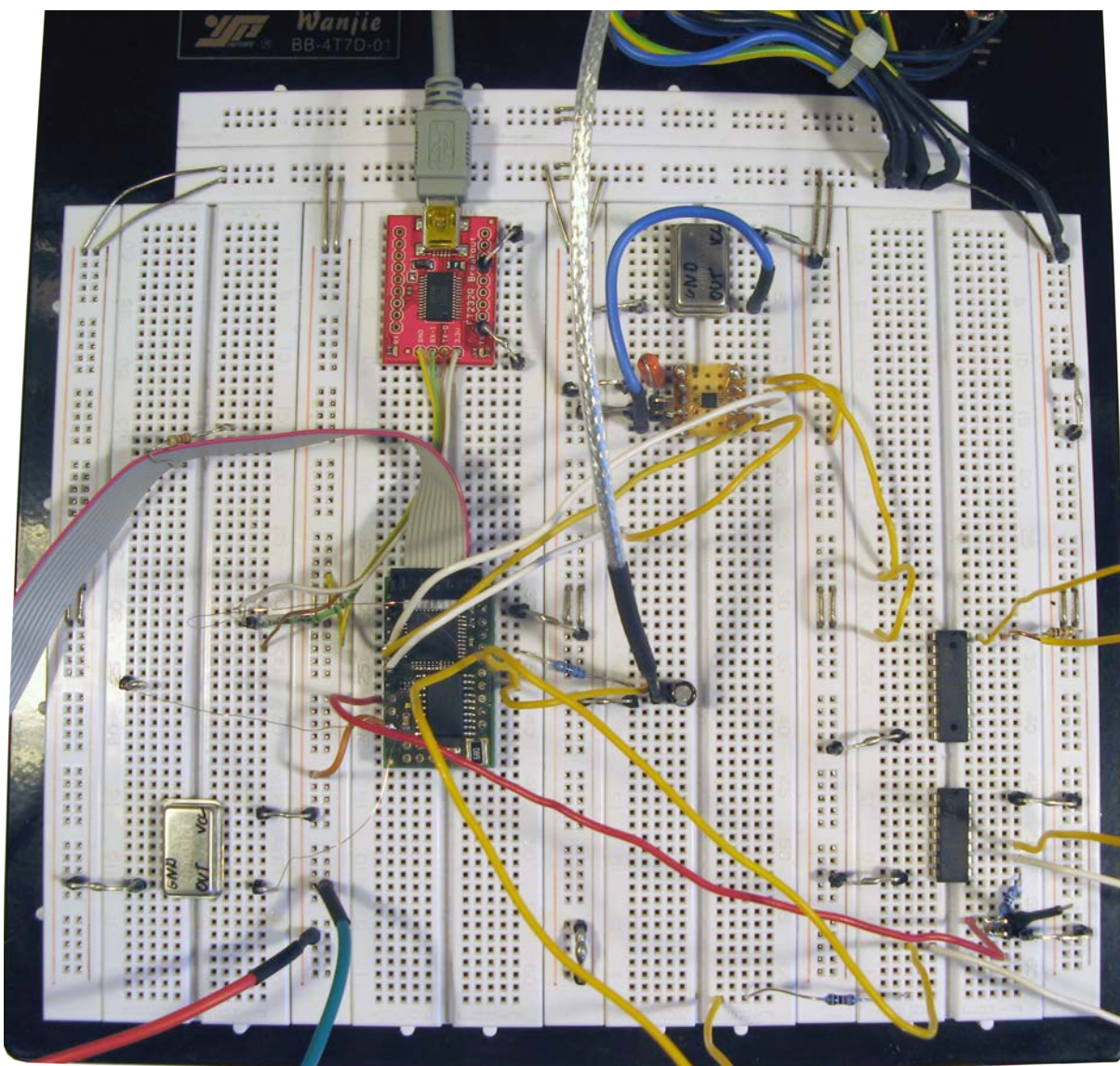


Figure A.1: Bread board setup

INDUCTIVE HEATING AND TEMPERATURE MEASURING SYSTEM

A Appendix

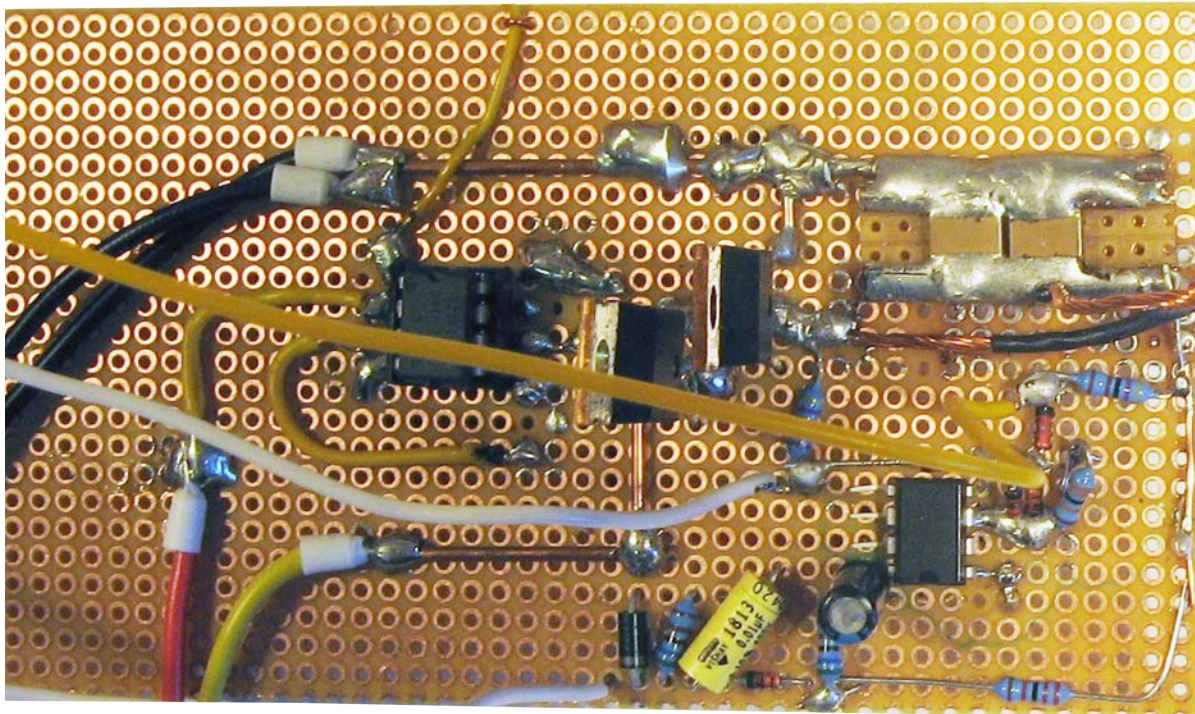


Figure A.2: Load perfboard setup (top)

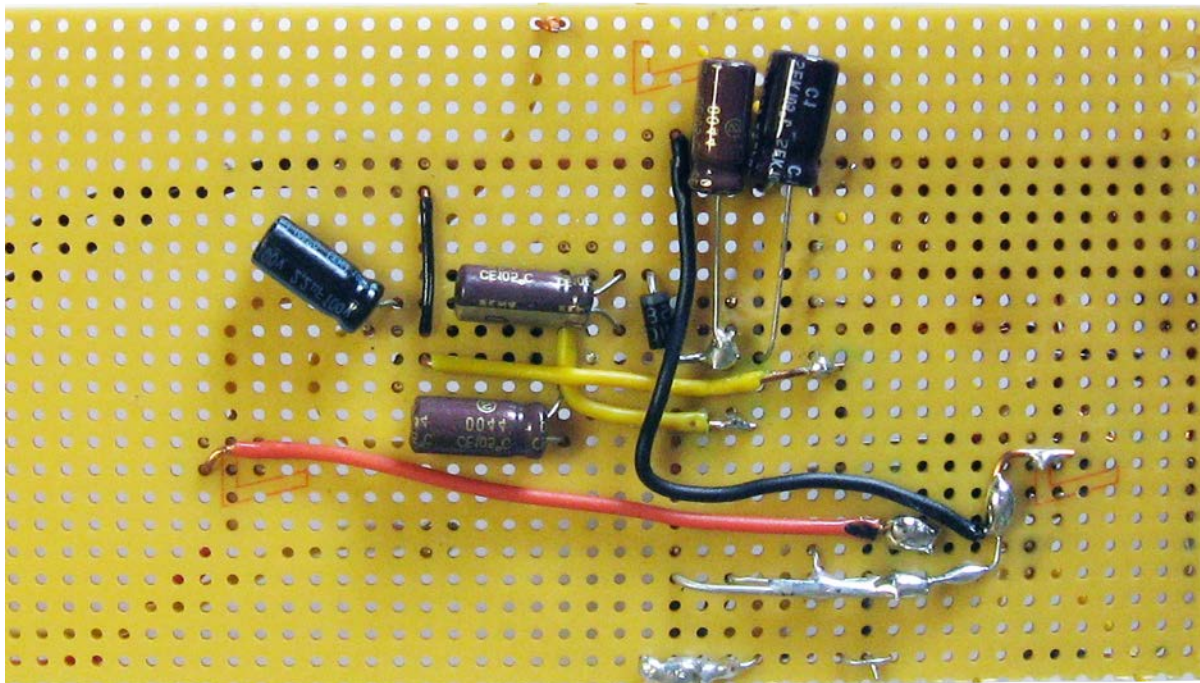
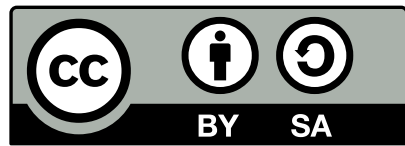


Figure A.3: Load perfboard setup (bottom)

INDUCTIVE HEATING AND TEMPERATURE MEASURING SYSTEM

A Appendix



Inductive Heating and Temperature Measuring
System for Small Metal Objects by Krallinger
Sebastian is licensed under a Creative Commons
Attribution-ShareAlike 3.0 Unported License.